INVESTIGATION OF HETEROGENEOUS REACTIONS OF TRIFLUOROMETHANE WITH SOME METAL OXIDES, HYDROXIDES AND CARBONATES

Andrii Vakulka

Doctoral Dissertation
Jožef Stefan International Postgraduate School
Ljubljana, Slovenia, September 2012

Evaluation Board:

Prof. Boris Žemva, Chairman, Department of Inorganic Chemistry and Technology, Jožef Stefan Institute and Jožef Stefan International Postgraduate School

Prof. Mihael Drofenik, Member, Faculty of Chemistry and Chemical Engineering, University of Maribor

Asst. Prof. Gašper Tavčar, Member, Department of Inorganic Chemistry and Technology, Jožef Stefan Institute and Jožef Stefan International Postgraduate School

MEDNARODNA PODIPLOMSKA ŠOLA JOŽEFA STEFANA
JOŽEF STEFAN INTERNATIONAL POSTGRADUATE SCHOOL

Andrii Vakulka

INVESTIGATION OF HETEROGENEOUS REACTIONS OF TRIFLUOROMETHANE WITH SOME METAL OXIDES, HYDROXIDES AND CARBONATES

Doctoral Dissertation

RAZISKAVE HETEROGENIH REAKCIJ TRIFLUOROMETANA Z NEKATERIMI KOVINSKIMI OKSIDI, HIDROKSIDI IN KARBONATI

Doktorska disertacija

Supervisor: Asst. Prof. Tomaž Skapin

Ljubljana, Slovenia, September 2012

Index

Abstract ..... **VII**

Povzetek ..... **IX**

Abbreviations ..... **XI**

1 Introduction **1**

2 Background **3**
2.1 Physical properties of CHF_3 3
2.2 CHF_3 – a potent greenhouse gas 4
2.3 Chemical properties of CHF_3 6
2.3.1 Conversion of CHF_3 to other C–F compounds 6
2.3.2 Fluorination of metal oxides with CHF_3 7
2.3.3 Reactivity and decomposition of CHF_3 under mild conditions 9
2.3.4 CHF_3 as a weak C–H acid 9

3 Materials and Methods **11**
3.1 General aspects 11
3.2 Materials and preparation of solid precursors 11
3.3 Experimental setups for gas-solid reactions under different regimes 12
3.4 Fluorination 14
3.5 Chemical analysis 15
3.6 Fourier Transformed Infrared (FTIR) spectroscopy 15
3.7 Pyridine adsorption tests 17
3.8 Mass Spectrometry (MS) 17
3.9 Powder X-ray Diffraction (XRD) 17
3.10 SEM imaging 18
3.11 Specific Surface Area (SSA) determination 18
3.12 X-ray Photoelectron Spectroscopy (XPS) 18
3.13 Catalytic tests 19
3.14 Thermal decomposition of CHF_3 over fluorinated alumina 19

4 Results and Discussion **21**
4.1 Fluorination of γ-Al_2O_3, γ-Ga_2O_3, and mixed γ-Al_2O_3/γ-Ga_2O_3 with CHF_3 21
4.1.1 Oxide precursors 21
4.1.2 Fluorination of oxide xerogels with CHF_3 22
4.1.2.1 Morphological transformations 26

4.1.2.2 Thermal behaviour of fluorinated products 26
4.1.2.3 Thermal decomposition of CHF_3 over fluorinated oxides 31
4.1.3 Surface effects of fluorination 34
4.1.3.1 PAS-py of oxide precursors 34
4.1.3.2 PAS-py of fluorinated products 39
4.1.3.3 XRD investigations 40
4.1.3.4 Surface hydroxyls 44
4.1.3.5 Catalytic behaviour in isomerisation of CCl_2FCClF_2 46
4.2 Interaction of CHF_3 with alkali hydroxides and alkali carbonates 49
4.2.1 Reaction under static conditions 49
4.2.1.1 Side reactions with hydroxides 58
4.2.1.2 Reactions with other halocarbons 60
4.2.2 Reactions under flow conditions 61
4.2.3 Comparison of CHF_3 reactions with hydroxides under static and dynamic conditions 64
4.2.4 Activation of CHF_3 by hydroxides or carbonates through acid-base interactions 64
4.2.5 Comparison between the activity of alkali hydroxides and carbonates 67
4.3 Possible technological and ecological implications of current findings 69

5 Conclusions 71

6 Acknowledgements 73

7 References 75

Index of Figures and Schemes 85

Index of Tables 87

Appendices 89
Appendix I 90
Appendix II 91
Appendix III 94
Appendix IV 96
Appendix V 98
Appendix VI 100

Abstract

Heterogeneous reactions of trifluoromethane CHF_3 with solid xerogel oxides, alkali hydroxides and carbonates were investigated under static and dynamic conditions and at moderate temperatures. In all cases, main reaction is fluorination characterised by a complete decomposition (mineralisation) of the fluorinating agent, CHF_3, and the formation of the solid metal fluorides. Extent of fluorination strongly depends on temperature and is dictated by the nature of the solid precursors. Alkali hydroxides, KOH, NaOH, or LiOH, are the most reactive solids that start to react with CHF_3 at relatively low temperatures, 100–210 °C. Onset temperatures for fluorination of corresponding carbonates are 100–150 °C higher. In the case of alumina-gallia xerogels the starting temperature of fluorination depends on the gallia content and varies from 125 to 180 °C. Reactivity of the solids towards CHF_3 is directly related to their basicity. The reactions are rationalised on the basis of the acid-base interactions between CHF_3 as a weak C–H acid, and basic oxygen species on the surface of the solids. These interactions apparently play a key role during the initial binding of CHF_3 molecule to the solid reactant, in this way enabling or facilitating other decomposition steps that finally lead to a complete destruction of the CHF_3 molecule. Total decomposition of CHF_3 with KOH or NaOH that is achievable at relatively low temperatures, could in some specific cases represent a possible alternative to the energy-demanding CHF_3 decomposition by incineration. On the other side, interaction of single γ-Al_2O_3 and γ-Ga_2O_3, and mixed γ-Al_2O_3/γ-Ga_2O_3 xerogels with CHF_3 at intermediate temperatures (from room temperature to 450 ºC) resulted in partial fluorination. Fluorinated oxides remain amorphous and retain a considerable part of the initial surface area; for the fluorinated Al-based materials surface areas in all cases exceed 100 $m^2\ g^{-1}$. Lewis acidity of mixed oxides, either before or after fluorination, is strongly influenced by the presence of surface Ga^{3+} ions, mainly due to their strong preference to replace highly acidic Al^{3+} ions in tetrahedral positions. Ion replacement leads to the formation of acidic sites with lower strengths what is confirmed by the model catalytic reaction, isomerisation of CCl_2FCClF_2. Activity of γ-Al_2O_3 and γ-Ga_2O_3, and mixed γ-Al_2O_3/γ-Ga_2O_3 can therefore be described in terms of coordination preferences of surface Al^{3+} and Ga^{3+} ions and the clear difference in the strength of related acid sites. XPS investigations indicate that fluorination of mixed oxides is accompanied by substantial surface reconstructions and preferential formation of Al–F based phases with Ga remaining mainly in O environments. Further segregation processes, such as slow crystallisation of $Al(F,OH)_3 \cdot nH_2O$ phases, are probably promoted by water adsorption.

Povzetek

Doktorsko delo zajema heterogene reakcije trifluorometana, CHF_3, s trdnimi oksidnimi kserogeli in alkalijskimi hidroksidi oziroma karbonati, ki sem jih preučeval pod statičnimi in dinamičnimi pogoji ter pri zmernih temperaturah. Osnovna reakcija je v vseh primerih fluoriranje trdnih prekurzorjev, ki je povezano s popolnim razpadom (mineralizacijo) fluorirnega sredstva, CHF_3, in tvorbo trdnih kovinskih fluoridov. Stopnja fluoriranja je močno odvisna od temperature in narave trdnih reaktantov. Alkalijski hidroksidi, KOH, NaOH ali LiOH, so najbolj aktivni trdni reagenti, ki reagirati s CHF_3 že pri relativno nizkih temperaturah, 100–210 °C. Začetne temperature fluoriranja ustreznih alkalijskih karbonatov so za 100–150 °C višje. V primeru mešanih kserogelov na osnovi aluminijevega in galijevega oksida so začetne temperature fluoriranja odvisne od vsebnosti galijevega oksida in ležijo v vmesnem temperaturnem območju, 125–180 °C. Reaktivnost trdnih reagentov s CHF_3 lahko direktno povežemo z njihovo bazičnostjo. Vse reakcije lahko tako pojasnimo na osnovi interakcij med kislino in bazo, pri čemer CHF_3, kot šibka C–H kislina, reagira z močno bazičnimi kisikovimi zvrstmi, ki so prisotne na površini trdih reaktantov. Te interakcije so odločilnega pomena pri začetni vezavi CHF_3 molekule na površino trdnega reagenta in omogočajo nadaljnje površinske reakcije, ki v končni fazi vodijo do popolnega razpada CHF_3. Popoln razpad CHF_3 s KOH ali NaOH dosežemo že pri relativno nizkih temperaturah, kar lahko v nekaterih specifičnih primerih predstavlja možno alternativo energetsko zelo zahtevni termični razgradnji CHF_3. Na drugi strani interakcije γ-Al_2O_3 in γ-Ga_2O_3 ter mešanih γ-Al_2O_3/γ-Ga_2O_3 kserogelov s CHF_3 pri zmernih temperaturah vodijo do delnega fluoriranja. Fluorirani oksidi ostajajo amorfni in ohranijo znaten del začetne specifične površine, ki za vse čiste in mešane fluorirane kserogele na osnovi γ-Al_2O_3 presega 100 $m^2\ g^{-1}$. Lewisova kislost mešanih oksidov, tako pred kot tudi po fluoriranju, je močno odvisna od prisotnosti površinskih Ga^{3+} ionov, predvsem zaradi preferenčne zamenjave močno kislih Al^{3+} ionov na tetraedrskih pozicijah z Ga^{3+} ioni. Zamenjava ionov vodi do tvorbe kislinskih centrov manjše jakosti, kar potrjujejo rezultati modelne katalitske reakcije izomerizacije CCl_2FCClF_2. Razlike v katalitski aktivnosti γ-Al_2O_3 in γ-Ga_2O_3 ter mešanih γ-Al_2O_3/γ-Ga_2O_3 kserogelov lahko pojasnimo s koordinacijskimi preferencami površinskih Al^{3+} in Ga^{3+} ionov ter jasno razliko v jakosti pripadajočih kislinskih centrov. XPS raziskave kažejo, da je fluoriranje mešanih oksidov povezano z znatno rekonstrukcijo površin in preferenčno tvorbo Al–F faz, medtem ko Ga ostaja predvsem v O okoljih. Nadaljnji procesi ločevanja faz, kot je npr. počasna kristalizacija $Al(F,OH)_3 \cdot nH_2O$ faz, so najverjetneje povezani z adsorpcijo vode.

Abbreviations

AC	=	Activated carbon
BE	=	Binding energy
BET	=	Brunauer, Emmet, and Teller method for surface area determination from adsorption isotherms
CFC	=	Chlorofluorocarbon
cus	=	Coordinatively unsaturated
DMF	=	Dimethylformamide
DMSO	=	Dimethylsulfoxide
FTIR	=	Fourier transform infrared spectroscopy
FWHM	=	Full Width at Half Maximum
GWP	=	Global warming potential
Hal	=	Halogen (F, Cl, Br, I)
HCFC	=	Hydrochlorofluorocarbon
HFC	=	Hydrofluorocarbon
i.d.	=	Internal diameter
IR	=	Infrared
M	=	Metal
MS	=	Mass spectrometry
NMP	=	N-methyl-2-pyrrolidone
PA-FTIR	=	Photo acoustic Fourier transform infrared spectroscopy
PAS-py	=	Photo acoustic FTIR spectroscopy of adsorbed pyridine
PFC	=	Perfluorocarbon
PTFE	=	Polytetrafluoroethylene
py	=	Pyridine
SSA	=	Specific surface area
XPS	=	X-ray photoelectron spectroscopy

1 Introduction

Trifluoromethane (CHF_3, fluoroform, HFC-23) is a very stable compound with exceptionally high global warming potential. Production and emissions of CHF_3 are closely related with the continuously expanding production of fluorocarbon polymers. Due to its very high stability, majority of the technically relevant chemical transformations of CHF_3 proceed at rather severe conditions, *e.g.* in the temperature range of 700–1200 °C. Relevant background of these aspects is given in Section 2.

In contrast to the broadly investigated CHF_3 reactions at high temperatures, the work included in this dissertation was focused on those CHF_3 transformations that could possibly be achieved at lower temperatures. In this context, heterogeneous reactions of CHF_3 with some reactive metal oxides, hydroxides and carbonates at temperatures below 400 °C were investigated. Main purpose of the work was to supplement the relatively limited knowledge on the chemistry of CHF_3 at lower temperatures and, by implication, to expand the possibilities for economical and ecologically sound exploitation of waste CHF_3 feedstocks.

Heterogeneous reactions of CHF_3 at mild conditions were investigated from two main aspects:

1) Fluorination capacity of CHF_3: Fluorination activity of CHF_3 was investigated in reactions with some model technically relevant oxides, Al_2O_3, Ga_2O_3 and mixed Al_2O_3-Ga_2O_3. In contrast to Al_2O_3, there were no reports on the fluorination of Ga_2O_3 and mixed Al_2O_3-Ga_2O_3 with CHF_3. Within this work, a new class of fluorinated gallium containing oxide materials was prepared and characterised, with the emphasis on changes in the structure, morphology and surface acidity that originate from the partial or complete O/F and Al/Ga exchanges. Related results are given in Section 4.1.

2) Total decomposition (mineralisation) of CHF_3: A systematic study of technically relevant alkali hydroxides and carbonates as possible mineralisation agents for CHF_3 was performed. It was found that with sufficiently active solid reactants total decomposition of CHF_3 can be accomplished at temperatures that are far below the temperatures used in current CHF_3 incineration processes. Results connected with this segment are presented in Section 4.2.

Common goal in both cases was to elucidate the underlying chemistry and to scrutinise both processes as a basis for possible future applications. Results included in this work open some new or alternative possibilities for the utilisation or decomposition of the environmentally problematic CHF_3.

2 Background

CHF_3 was firstly prepared in 1894 by Meslans who fluorinated iodoform, CHI_3, with an unspecified silver fluoride, AgF_x, in chloroform [1]. Product was however contaminated with difluoroiodomethane, CHF_2I, what has not allowed an accurate determination of the physical properties of the CHF_3. In 1936 Ruff improved the synthesis by using a mixture of mercury(II) and calcium fluorides, HgF_2 and CaF_2, as fluorinating agents [2]. Synthetic procedure was further improved in 1937 by Henne who used bromoform, $CHBr_3$, and a mixture of antimony(III) and mercury(II) fluorides, SbF_3 and HgF_2 [3]. Nowadays, production of chlorodifluoromethane, $CHClF_2$, is the most important source of CHF_3. In this process, CHF_3 is produced as an unwanted overfluorinated by-product. On the other side, decarboxylation of trifluoroacetic acid, CF_3COOH, by decarboxylase according to Eq. 1 was identified as a possible natural source of CHF_3. However, emissions from natural sources are estimated to be practically negligible in comparison with the anthropogenic emissions from the production of $CHClF_2$.

$$CF_3COOH \rightarrow CHF_3 + CO_2 \qquad (1)$$

Applications of CHF_3 are rather limited; in minor quantities it is used as a low-temperature refrigerant, as an etching agent in plasma treatment of silicon or silicon dioxide components, as a convenient source of CF_3 groups in organic and organometallic syntheses [4, 5], and as a fire suppressant (with the trade name FE-13, DuPont). Nevertheless, majority of the co-produced CHF_3 is still treated as a waste that is either released into the atmosphere or incinerated.

CHF_3 is therefore studied mainly in relation with its decomposition or conversion to other useful fluorinated products. A comprehensive overview of both areas appeared recently [6]. In the continuation, some of the key properties of CHF_3, most relevant for the current work, are shortly summarised.

2.1 Physical properties of CHF_3

Under normal conditions, CHF_3 is a colourless and odourless gas. CHF_3 is non-flammable, non-corrosive and non-toxic (the toxic effects or physiological changes associated with CHF_3 were not observed). Its molecular weight is 70.01. Density of liquid CHF_3 is 0.673 g cm^{-3} at 25 °C and 101.3 kPa. At normal pressure, CHF_3 boils at –82 °C and freezes at –155 °C. CHF_3 is more soluble in water than CF_4 and less soluble than CO_2. Critical temperature and pressure are 26 °C and 4.82 MPa, respectively. Key physical properties of CHF_3 are summarised in Table A-1 (Appendix I).

CHF_3 possesses high polarizability and hydrogen-bonding ability. It has a quite high dipole moment (Table A-1), comparable to that of methanol (1.70 C m) and, for example, higher than that of chloroform (1.04 C m) or bromoform (0.99 C m) [7]. The room temperature viscosity of liquid CHF_3 is very close to that of liquid CO_2. The geometry of CHF_3 molecule is well described by a "symmetric spinner" model comprising a third order axis L_3 and three mirror planes m (see Figure 1). For the CHF_3 molecule, one can

expect 9 normal vibration modes (calculated by using the formula, 3N–6, where N is the number of atoms in the molecule). CHF_3 molecule possesses four stretching vibration modes and 5 deformation modes; three of the stretching vibrations (C–F stretching) are degenerated. The number of infrared-active vibrations for CHF_3 is six [8]. The most remarkable are the C–H stretching vibration located at 3035 cm^{-1} and the C–F stretching vibration located at 1153 cm^{-1} (see Figure 2).

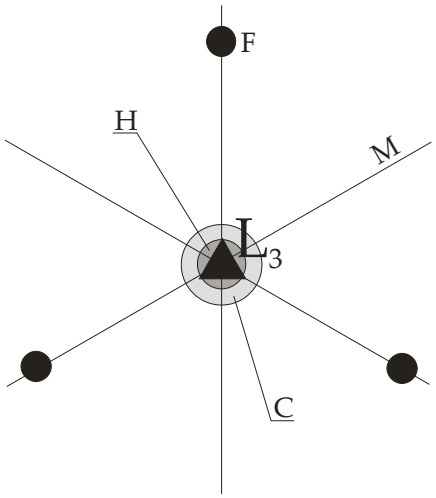

Figure 1: *Schematic representation of the symmetry (C_{3v}) of the CHF_3 molecule (a view along the third order axis).* L_3 – third order axis; M – mirror plane; C, H, and F – atoms in the CHF_3 molecule.

2.2 CHF_3 – a potent greenhouse gas

CHF_3 is a greenhouse gas with some distinctive features. In contrast to other hydrohalocarbons (HFCs and HCFCs) present in the atmosphere, it is remarkably persistent with the atmospheric lifetime of 270 years. Due to its very high stability and the strong infra-red adsorption of the CF_3 group, CHF_3 has a very high global warming potential (GWP) of 14,800 kg CO_2 kg^{-1} for a 100-year time horizon [9, 10]. The radiative forcing constant of CHF_3 is estimated to be 0.16 W m^{-2} $ppbv^{-1}$ [11–14]. Main source of CHF_3 is the production of chlorodifluoromethane ($CHClF_2$, HCFC-22), a precursor of tetrafluoroethylene, TFE, that is the key precursor for the production of fluorocarbon polymers, mainly polytetrafluoroethylene, PTFE. In the production of $CHClF_2$, CHF_3 is formed as an inevitable over-fluorinated by-product in amounts ranging from 1% to 4% of the $CHClF_2$ produced [10]. Amounts of the co-produced CHF_3 largely exceed the quantities consumed in rather limited applications (see below). Majority of the produced CHF_3 is therefore regarded as a waste that was in the past predominantly released to the atmosphere. Estimated global CHF_3 emissions peaked $1.5 \cdot 10^4$ tons in 2006 followed by a gradual decrease to $8.6 \cdot 10^3$ tons in 2009 [11]. Due to its long atmospheric lifetime, CHF_3 is persistently accumulating in the atmosphere, *i.e.* its global atmospheric abundance of 22.6 pmol mol^{-1} in 2009 was seven times higher than three decades ago [11]. In the nineties, $CHClF_2$ producers in the developed countries achieved a considerable reduction of CHF_3 emissions by the strict optimisation of the $CHClF_2$ production processes to reduce CHF_3 co-production and by the thermal oxidation (incineration) of the produced CHF_3 waste streams. It is estimated that consistent adoption of such practices by all major

$CHClF_2$ producers worldwide could result in a considerable drop of the global CHF_3 emissions to approximately one quarter of the emission recorded in 2009, despite the fact that a continued growth of the $CHClF_2$ production is expected in the next years [10, 11].

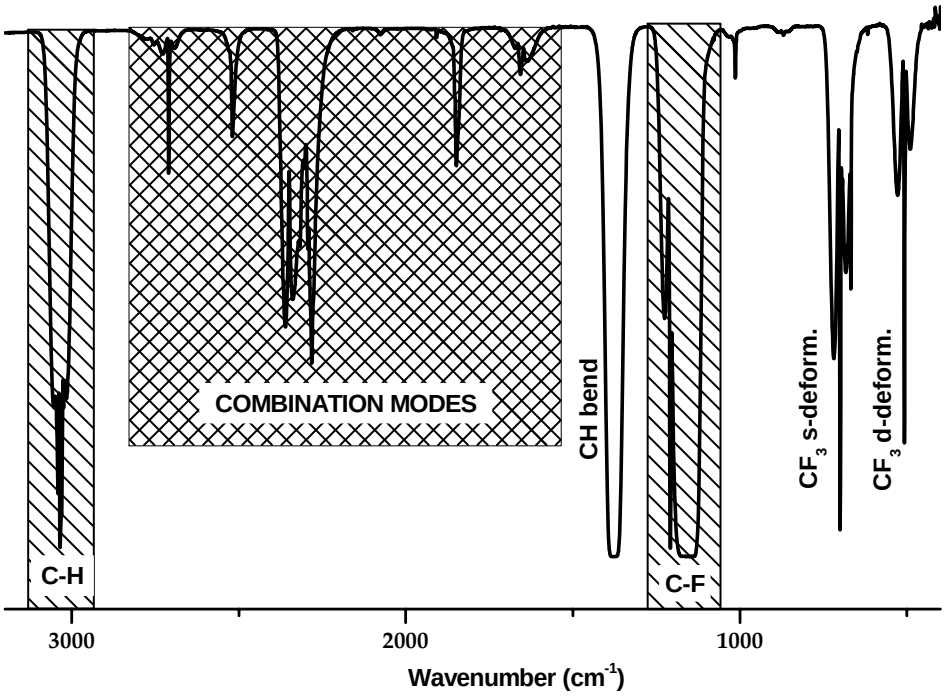

Figure 2: *Transmittance FTIR spectrum of gaseous CHF_3*; 133.3 kPa of CHF_3 in a 0.8 cm gas cell with KBr windows. Dashed areas mark the regions of C–H and C–F stretching vibration modes and combination modes.

In the last few decades, approximately 10^4 tons of CHF_3 were released into the atmosphere each year, corresponding to a yearly emission of $1.48 \cdot 10^8$ tons of a CO_2 equivalent. However, the overall climate impact of accumulated CHF_3 is still rather small, mainly due to the relatively low amounts released on a global scale. Its radiative forcing arising from 37.3 pmol mol^{-1}, expected in 2015, is expected to be 0.006 W m^{-2}. This amount represents only 0.18 % of the total radiative forcing from all other greenhouse gases having anthropogenic origins, like CO_2, CH_4, nitrous oxide, N_2O, other hydrofluorocarbons, HFCs, chlorofluorocarbons, CFCs, perfluorocarbons, PFCs, and sulphur hexafluoride, SF_6. For 2015, the predicted emission of all anthropogenic greenhouse gases will be in the range of $4.6–5.9 \cdot 10^{10}$ tons of a CO_2 equivalent [12, 13].

CHF_3, CF_3CH_2F and CH_3CHF_2 are the most abundant HFCs in the atmosphere. According to the 2007 IPCC climate report, CHF_3 was the most abundant HFC in the global atmosphere until around 2001, when the global mean concentration of CF_3CH_2F noticeably increased [9]. There is however a large difference in the atmospheric lifetimes of these HFCs. In clear contrast with the already mentioned 270 years for CHF_3, CF_3CH_2F has an atmospheric lifetime of 13.8 years while CH_3CHF_2 is a noticeably short-lived HFC with an atmospheric lifetime of 1.4 years. Although accumulation is less pronounced for the short-lived HFCs their atmospheric abundances are also increasing due to the progressive replacement of the ozone harmful CFCs, especially with the two mentioned fluoroethanes.

FTIR spectrum of gaseous CHF_3 is shown in Figure 2 and demonstrates the strong absorption of this compound in the IR region. Spectrum is characterised by strong absorption bands that corresponds to the C–H and C–F stretching vibration modes. The later are especially important since they coincide with the so called infrared atmospheric window that lies in the region between 1250 and 700 cm^{-1}.

2.3 Chemical properties of CHF_3

In the earlier investigations of CHF_3 its remarkable inertness was noticed [1–3]. As reported at that time, CHF_3 was inactive towards alkali metals and concentrated solutions of alkali hydroxides. Reaction of CHF_3 with calcium oxide, CaO, was, for example, observed only at red hot temperature [3]. However, further investigations of the CHF_3 chemistry clearly demonstrated that the claimed very high inertness of this compound was rather overestimated.

In the 1950s Hine et al. performed a series of fundamental investigations on the chemical behaviour of various haloforms [15–22]. These investigations showed that chemical behaviour of CHF_3 is distinctively different from that of other haloforms; CHF_3 usually exhibited the lowest reactivity among the haloforms. An important finding of these investigations was that all haloforms behave as weak acids. For example, in alkali hydroxide solutions chloroform, $CHCl_3$, easily forms CCl_3^- anions that dissociate to Cl^- and CCl_2. The reaction between CCl_2 and OH results in the formation of CO and formate anions. On the other side, CHF_3 was found to be very resistant to hydrolysis in strong alkaline solutions without appreciable dissociation to CF_2 and HF. However, when contacted with concentrated $NaOD/D_2O$ solutions at 105 °C it readily underwent H/D isotope exchange that was accompanied by an almost negligible extent of hydrolysis [23, 24]. This indicates that the hydrogen atom attached to the CF_3 radical can be easily exchanged. This also indicates that C–H acidity may have a detrimental effect on the specific chemical properties of CHF_3 at low and moderate temperatures.

More recently, direct cupration of CHF_3 was achieved at room temperature in nearly quantitative yields by reacting CHF_3 with a mixture of copper(I) halides, CuX (X = Cl, Br or I), and alkali alkoxides, MOR (M = K or Na), in DMF or NMP [4]. It is possible that the high basicity of the mixed CuX/MOR/DMF systems provides conditions for the outstanding room temperature reactivity of CHF_3. The CHF_3 derived $CuCF_3$ was proved to be a convenient reagent for the trifluoromethylation of organic and inorganic electrophiles. These findings opened an important new route for the direct application of CHF_3 as a very convenient source for the introduction of CF_3 groups into organic molecules [4, 5].

Despite the promising examples given above, reports on reactions of CHF_3 at low temperatures are still rather scarce [5]. Due its relatively high stability, majority of the technologically relevant reactions of CHF_3 is performed at considerably higher temperatures, usually in the temperature range 300–1200 °C. These reactions comprise pyrolytic and related reactions, fluorinations with CHF_3, and CHF_3 decomposition. Some representative examples of these reaction classes are given in the following sections.

2.3.1 Conversion of CHF_3 to other C–F compounds

Pyrolytic and related reactions of CHF_3, usually performed at temperatures 500–1000 °C, received considerable attention, especially as possible routes for the conversion of CHF_3

to commercially more interesting products. In the initial studies on CHF_3 pyrolysis it was proposed that the first step in pyrolytic decomposition is dehydrofluorination of CHF_3 to difluorocarbene, CF_2 (Eq. 2) [25]; in general, the data acquired afterwards are largely consistent with this mechanism. CF_2 is a very reactive species; its respective half-lives in solution and in the gas phase are 0.5 and 20 ms [26]. Under homogeneous gas phase conditions, discernible thermal decomposition (pyrolysis) of a pure CHF_3 starts above 750 °C [25].

$$CHF_3 \rightarrow HF + CF_2 \qquad E_a = 264 \text{ kJ mol}^{-1} \text{ [25]} \qquad (2)$$

Romelaer *et al.* pyrolised CHF_3 at 775 °C in the presence of hydrogen and obtained CF_3CH_2F, CH_2F_2 and CHF_2CHF_2 as the main fluorinated products [27]. Moon *et al.* investigated the pyrolysis of a mixture of CHF_3 and $CF_2=CF_2$ at 700–1000 °C in order to obtain $CF_3CF=CF_2$ [28]. Quan *et al.* pyrolised CHF_3 at 550 °C in the presence of iodine and oxygen on a KF-impregnated activated charcoal (AC) catalyst to prepare CF_3I [29]. Similar AC-based catalysts doped with K_2O greatly increased the conversion of CHF_3 to $CF_2=CF_2$ and $CF_3CF=CF_2$ at 600–900 °C [30]. Kennedy *et al.* performed a series of detailed investigations on the reaction of CHF_3 and CH_4 at 400–900 °C in order to obtain a highly valuable product, $CH_2=CF_2$ [31–33].

2.3.2 Fluorination of metal oxides with CHF_3

Fluorination of metal oxides is a well-known procedure to modify, *i.e.* mainly increase, their Lewis acidity and to achieve catalytic activity in reactions that require acid sites of higher strengths [34]. For these purposes, oxide precursors with high surface areas are usually treated with gaseous fluorinating agents, among them, hydrogen fluoride, HF, is most commonly used [35–37]. Besides surface modification, fluorination also induces some structural and morphological changes [35, 36]. Extent of these changes strongly depends on the level of fluorination. For example, in highly fluorinated active aluminium(III) oxide, γ-Al_2O_3, bulk conversion to fluoride is observed with the formation of crystalline AlF_3 phases with strongly reduced specific surface areas [36].

Due to the nontoxic and noncorrosive nature together with its availability, CHF_3 was proposed as an alternative fluorinating agent for the conversion of a variety of metal oxides to the corresponding fluorides or oxyfluorides. Due to its technical relevance, special attention was paid to the fluorination of γ-Al_2O_3 to relatively pure AlF_3 [38]. Although temperature programmed desorption (TPD) experiments of CHF_3, adsorbed on partially fluorinated γ-Al_2O_3 at room temperature, showed that CHF_3 dissociation starts already above 175 °C [39], quantitative conversion of bulk γ-Al_2O_3 to AlF_3 required much higher fluorination temperatures, usually 400–500 °C [38, 39]. In some earlier studies, fluorination with CHF_3 at 300–480 °C was used for the preparation of a number of partially or fully fluorinated Al_2O_3 [35–37] or Cr_2O_3 based [35, 40] xerogels or aerogels for catalytic purposes. In addition, commercial γ-Al_2O_3 fluorinated with CHF_3 at 350 °C was used as a partially fluorinated benchmark to compare catalytic activity of diverse AlF_3-based materials [35, 41].

Investigations mentioned above proved that CHF_3 is a safe and convenient alternative fluorinating agent with the fluorinating capability comparable to HF [35, 36, 38]. Comparative studies also showed that fluorination of oxides; mainly Al_2O_3 and Cr_2O_3, with either HF or CHF_3 resulted in very similar levels of fluorine incorporation. At medium and high temperatures the fluorination activity of CHF_3 is comparable to that of HF. Fluorination activity of CHF_3 can therefore be estimated as moderate at medium

temperatures and high at temperatures above 400–450 ºC. Nearly all basic oxides can be fluorinated with CHF_3. Comparison of stoichiometries of fluorination reactions, exemplified for Al_2O_3 in Eqs. 3 and 4, shows that fluorination with CHF_3 results in considerably lower H_2O formation what may reduce the extent of unwanted hydration and hydrolysis processes that may impair some properties of the fluorinated products. Another distinction between the two reactions is in the reductive character of the reaction with CHF_3. This aspect was apparently not of greater relevance in the above mentioned fluorinations of Al_2O_3 and Cr_2O_3 based materials, however, it may become important in systems with easily reducible metal cations.

$$Al_2O_3 + 2CHF_3 \rightarrow 2AlF_3 + 2CO + H_2O \quad (3)$$
$$Al_2O_3 + 6HF \rightarrow 2AlF_3 + 3H_2O \quad (4)$$

From the technical standpoint, some important differences between the two fluorinating agents must be mentioned. HF is highly corrosive and toxic and must be handled with great precaution in specially designed corrosion-resistant equipment. In fluorinations under flow conditions, exact dosing of gaseous HF usually represents a serious technical problem. On the other side, CHF_3 is non-toxic and non-corrosive what greatly facilitates all manipulations, including flow regulation that can be carried out with conventional regulators for non-aggressive gases. As a result, fluorination with CHF_3 in flow systems can be performed under precisely controlled conditions.

CHF_3 contains strong C–F bonds (552 kJ mol^{-1}) and a relatively weak C–H bond (338 kJ mol^{-1}) [7]. This can explain the higher fluorination activity of the CHF_3 molecule in comparison with some other fluorocarbons, like the very stable tetrafluoromethane, CF_4, where possible interactions with reactive species are in addition sterically hindered [42, 43].

In contrast to alumina, Al_2O_3, which is one of the most intensively studied oxides, research of gallia, Ga_2O_3, received much less attention. Due to some distinctive structural and other similarities between the two families of oxides, Ga_2O_3 polymorphs are frequently studied in comparison with the respective Al_2O_3 analogues [44, 45]. Although Ga_2O_3-based or Ga-containing materials are known catalysts for some applications, see for example related references in [45], it appears that current interest is oriented mainly towards mixed Al_2O_3/Ga_2O_3 catalysts. Good catalytic performance of the mixed materials was observed in selective catalytic reduction (SCR) of nitrogen oxides by hydrocarbons [46–49], in dehydration of alkanes [50], and in cracking reactions [51]. As noted in several reports, improved catalytic behaviour of the mixed oxides was, besides other factors, associated with higher Lewis acidity that originates from the unique arrangements of Ga^{3+} ions found only on the surfaces of mixed Al_2O_3/Ga_2O_3 [47, 50, 51].

Systematic studies of the fluorination of Ga_2O_3-based materials were apparently not undertaken to a greater extent. In an earlier study, fluoride doped Al_2O_3/Ga_2O_3 catalysts were prepared and the promoting effect of the added fluoride was demonstrated in some cracking and hydrocracking reactions [52]. Mixed Al_2O_3/Ga_2O_3 catalysts were also found to be highly active in hydrolytic decomposition of the very stable CF_4 in the temperature range of 530–630 °C. Catalytic activity was correlated with the amount of Lewis acid sites that was increasing with the increasing Ga_2O_3 content up to the optimal value of 20 mol.%. It was also found that the addition of Ga_2O_3 stabilised the surface area during the hydrolytic reactions [42, 43].

2.3.3 Reactivity and decomposition of CHF_3 under mild conditions

As it appears, the only relevant chemical process involving CHF_3 that currently operates on larger scale is thermal oxidation of CHF_3 to CO_2 and HF as a key element of the current strategies to reduce CHF_3 emissions. Besides its beneficial environmental effects, the process has some disadvantages: it is an energy intensive process that operates at about 1200 °C, fossil fuels are consumed for incineration and it converts a potentially useful fluorinated product (CHF_3) into metal fluorides, mainly NaF or CaF_2, of low value that are usually disposed of as waste [53]. Total decomposition of CHF_3 is achievable also through catalysed hydrolysis reactions in the presence of zirconia or sulphated zirconia at 300–500 °C [54], or on phosphate-based catalysts at 500–700 °C [55]. As can be seen, the operational temperatures of the catalysed hydrolyses are considerably lower than those used in the non-catalysed incineration. These processes are however suitable for the destruction of CHF_3 at lower concentrations and are therefore not convenient for the decomposition of bulk CHF_3 streams [6].

Majority of chemical reactions with CHF_3 mentioned so far take place at relatively high temperatures that can be associated with the high energy required to activate the very stable CHF_3 molecule. Very little is known about the chemical behaviour of CHF_3 below the 300–400 °C temperature range and there are apparently no reports about the interactions of CHF_3 with some reactive solids that might serve as possible mineralisers for complete CHF_3 decomposition, like alkali hydroxides or carbonates, or some metal salts. In some related systems it was demonstrated that compounds with very strong C–F bonds can be quantitatively decomposed at relatively mild conditions by adequate mineralising agents. Burdeniuc and Crabtree demonstrated that very inert CFCs can be completely decomposed (mineralised) by sodium oxalate, $Na_2C_2O_4$, already at 270 °C, to yield a mixture of solid NaF and NaCl [56]. Similarly, a relatively stable graphite fluoride, CF_x ($x<1$), was completely defluorinated in a melted NaOH-KOH eutectic at 250 °C to yield graphitised carbon particles that contained residual hydroxyl groups [57]. Hydroxylation was most probably the result of F/OH exchange between surface fluorine and OH groups in alkali hydroxides. It was also found that some of the broadly used volatile anaesthetics based on fluorine-containing ethers, *i.e.* desflurane, enflurane or isoflurane, may decompose already at room temperature to yield detrimental levels of CO when contacted with some commonly used CO_2 absorbents that contain strong metal hydroxides, *i.e.* barium hydroxide lime or soda lime. It was proposed that decomposition starts with the base-catalysed deprotonation of the ether followed by the formation of the reactive CF_2 intermediate that reacts further with water or hydroxide to yield CO. In these systems, CHF_3 was however one of the possible gaseous decomposition products [58].

2.3.4 CHF_3 as a weak C–H acid

As mentioned above, extensive investigations of numerous haloforms [15–22] confirmed the weak acidic character of these compounds. Among them, CHF_3 was found to be the least acidic [59] and the least reactive what could be correlated with its specific chemical behaviour in comparison to other members of the haloform family.

Classical approach, based on a high negative induction effect, –I, of fluorine does not give an adequate explanation for the acidity trends observed among the related haloforms. As noted in [59], d-orbitals of heavier halogens delocalise the negative charge of $CH(Hal)_3$ (Hal = Cl, Br or I). The absence of d-electrons in fluorine does not enable the formation of a 10-electron resonance structure (Scheme 1) in CF_3. In other words, higher polarizability of the $C(Hal)_3$ radical results in its higher nucleophilicity. Thus high

nucleophilicity as well as high polarizability result in more pronounced acidic properties of the corresponding C–H acid. As a result, one can expect that CHI_3 is the strongest C–H acid among the haloforms. The acidity of the relative haloform is responsible for its low- and middle-temperature reactivity. The data about pK_a values of some related fluorocarbons are listed in Appendix IV Table A-10. At moderate conditions, a relatively high strength of the C–H bond does not allow reversible dissociation processes of the CHF_3 molecule, like those represented in Eqs. 5 and 6:

$$F_3C–H \rightleftharpoons F_3C^- + H^+ \qquad \text{(heterolytic dissociation)} \qquad (5)$$

$$F_3C–H \rightleftharpoons F_3C^\bullet + H^\bullet \qquad \text{(homolytic dissociation)} \qquad (6)$$

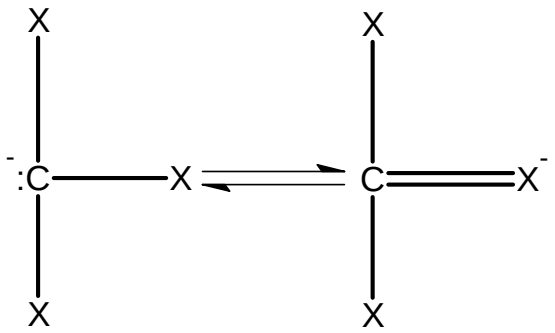

Scheme 1: *Resonance structures of the haloform radicals* (X = Cl, Br or I).

Considerable dissociation of CHF_3 takes place for example at higher temperatures or in plasma. This does not allow direct measurements of the acid strength of the CHF_3. Nevertheless, there are some indirect methods for the experimental determination of the acidic strength of different weak C–H acids. For example, the acidity of CH_4 can be evaluated through the following reaction (Eq. 7) [60]:

$$(CH_3)_2Hg + 2H^+ + 2e \rightarrow 2CH_4 + Hg^0 \qquad (7)$$

Polarographic measurements of the standard potential of this reaction in DMSO indicated that pK_a of CH_4 is 56, classifying CH_4 as an extremely weak acid.

In similar polarographic measurements (Eq. 8), pK_a of CHF_3 was determined to be 26 [60] what indicates that CHF_3 is much stronger acid than CH_4.

$$(CF_3)_2Hg + 2H^+ + 2e \rightarrow 2CF_3H + Hg^0 \qquad (8)$$

In addition to the polarographic measurements, pK_a values for CHF_3 were determined from the H/D exchange rate constants for reactions in $CDF_3/NaOH/H_2O$ and $CHF_3/NaOD/D_2O$ systems [23, 24], and in $CDF_3/NaOCH_3/CH_3OH$ and $CHF_3/NaOCH_3/CH_3OD$ systems [61]. Overview of this subject, given in [23, 24], indicates that the pK_a values for CHF_3 obtained by different approaches are congruent and fall in a relatively narrow range of 26–28. These studies also show that other haloforms and some other fluorocarbons exhibit higher acidities than CHF_3. For example, the rate of isotope exchange grows from $CHCl_3$ to CHI_3, though acidities of $CHBr_3$ and CHI_3 are nearly the same [62].

3 Materials and Methods

3.1 General aspects

This section gives an overview of experimental techniques used within this work to follow the heterogeneous reactions of CHF_3 with various oxides, hydroxides and carbonates. It refers mainly to a standard set of techniques used for the characterisation of bulk and surface properties of solid precursors and their fluorinated products, and for the characterisation of gaseous effluents. Among them, chemical analyses, BET specific surface area measurements, PA-FTIR and FTIR spectroscopy, XPS measurements, XRD of powdered samples, mass spectrometry etc. Some of techniques were modified and/or combined to meet the specific requirements of the current experiments, *e.g.* fluorination under flow conditions combined with a continuous FTIR monitoring of the effluent gases. For the sake of clarity, some of the less relevant experimental details, like the calibration data of the static gas IR cell with different gases, are presented in Appendix II.

3.2 Materials and preparation of solid precursors

All commercial chemicals used within this work were of reagent purity and were used as received. CHF_3, purity min. 98 %, was purchased from Matheson, Europe. Purity of CHF_3 was additionally checked with FTIR and MS. Other halocarbons used in this work (trichlorofluoromethane CCl_3F (ALDRICH, Germany), dichlorodifluoromethane CCl_2F_2 (Merck, Germany), perfluoromethylcyclohexane $C_6F_{11}CF_3$ (AlfaAesar, Germany), chlorodifluoromethane $CHClF_2$ (Merck, Germany), 1,1,2-trichlorotrifluoroethane CCl_2FCClF_2 (ALDRICH, Germany), and chloroform $CHCl_3$ (Kemika, Croatia)) were also commercial chemicals of reagent purity, minimum 99 %. Nitrogen and helium, both of high purity, min. 99.999 vol.%, were supplied by Messer. Methane, CH_4, for the calibration of a static gas IR cell (min. 99.995 vol.%) was also purchased from Messer. Pyridine C_5H_5N, purity min. 99.5 %, Kemika, was additionally dried by granulated solid potassium hydroxide, KOH.

Alkali hydroxides and carbonates, and alkaline earth carbonates were commercial chemicals of high purity, min. 99.99 wt.%. Before experiments, all solids were ground and sieved through a 1 mm sieve. All manipulations with these solid reactants were performed in a glove box to avoid hydration and, in the case of hydroxides, also carbonate formation.

Some of the solid precursors were prepared by the following procedures:

Preparation of oxide xerogels: Single γ-Al_2O_3 and γ-Ga_2O_3, and mixed γ-Al_2O_3/γ-Ga_2O_3 xerogels were prepared from inorganic precursors following the procedures from previous reports [63, 64]. Commercial aluminium nitrate, $Al(NO_3)_3 \cdot 9H_2O$, (Merck, p. a., min. 98.5 %) was used; aqueous solution of gallium nitrate, $Ga(NO_3)_3$, was prepared by dissolving metallic gallium (Alfa Aesar, 99.9 %) at about 70 °C in nitric acid (AppliChem, p. a., 65 %) diluted to ~30 vol.%. For the preparation of mixed xerogels, aqueous solutions of both nitrates were premixed in proportions corresponding to the

Al/Ga ratios given in Table 1. Gelatinous hydroxide hydrogels were prepared from 0.5 molar solutions of single or mixed nitrate(s) by the addition of aqueous ammonia solution (AppliChem, p. a., 25 %) under vigorous stirring. Final pH was adjusted to 6–7. Due to the reported difficulties in the preparation of γ-Ga_2O_3 from systems containing excessive water [44, 65], all hydrogels were filtered, thoroughly washed with distilled water, and immediately transferred into a preheated muffle furnace where they were dried at 450 °C for 24 h. Single Al_2O_3 and Ga_2O_3 xerogels are denoted as Al#0 and Ga#0, respectively. Mixed Al_2O_3/Ga_2O_3 xerogels are denoted as Al/Ga-x where x represents the nominal Al/Ga atomic ratio, *e.g.* sample with the nominal molar ratio of Al_2O_3:Ga_2O_3 = 100:1 is denoted as Al/Ga-100. Compositions of mixed xerogels prepared within this work are given in Table 1.

Preparation of sodium deuteroxide, NaOD: NaOD was prepared by the reaction between metallic sodium (purity min. 99.99 %, Aldrich) and deuterated water (purity 99.9 % D_2O, Aldrich) in argon atmosphere. Solution of NaOD was evaporated to dryness at 90 °C. Solid product was afterwards dried at 400 °C under dynamic vacuum for 20 hours. Dried NaOD was ground and sieved through a 1 mm sieve and stored under dry argon.

3.3 Experimental setups for gas-solid reactions under different regimes

Heterogeneous reactions of CHF_3 with solid reactants were investigated under different operational regimes. Reactions with oxides were performed under flow conditions while the reactions with hydroxides/carbonates were performed under flow and static conditions. Experimental setups for both regimes are shortly described below. All reactions of CHF_3 with solid reactants resulted in fluorination of the latter; details about diverse fluorination reactions investigated are given in Section 3.4.

Flow reactor: Flow reactor combined with an IR gas flow cell used within this work is schematically represented in Figure 3. Reactor was a tube with 5 mm i.d. made of pure nickel (purity min. 99 %). Layer of the reactive solid substrate was held in the tube with a plug made of pressed silver wool (purity min. 99.9 %, 0.05 mm fibres, Alfa Aesar). Reactor was heated by an external oven equipped with a temperature programmable regulator and a K-type thermocouple. Flow of the reactive gas, CHF_3, was balanced with the flow of nitrogen that simultaneously acted as an inert gas carrier and diluent. Flows of both gases were controlled by mass flow controllers. In order to remove potentially corrosive HF from the effluent gasses from some reactions at higher temperatures, gaseous products were directed through an absorption column filled with granulated KOH. Composition of the effluent gasses was usually monitored on-line with FTIR spectroscopy (see Section 3.6). All gas connections were made of PTFE tube with 2 mm i.d. Two types of the flow reactors were used; (i) reactor with the length of 50 cm was used for reactions at temperatures above 450 ºC to prevent thermal damages to the plastic connectors and (ii) reactor with the length of 35 cm that was used for all reactions performed below 450 °C. It should be noted that same flow reactor set-up was used also in catalytic tests (Section 3.13) and for pyridine adsorption (Section 3.7).

Taking into consideration the geometry of the flow reactor and the dimensions of particles in solid reactants as well as quantities of the solid reactants and flows of gases applied, it can be assumed that in majority of cases flow reactor operated in quasi-differential mode. This mode is characterised by very low temperature and concentration gradients along the reactor. A distinguishing feature of the flow reactor operating under such conditions is therefore in relatively uniform and constant concentration profiles of the gaseous species. This is true when the rate of gas reactant consumption is much lower

than its total flow. This was verified with the on-line FTIR spectroscopy of effluent gases that showed that the ratio between the incoming CHF_3 and that consumed in the fluorination reaction was always much higher than 1.

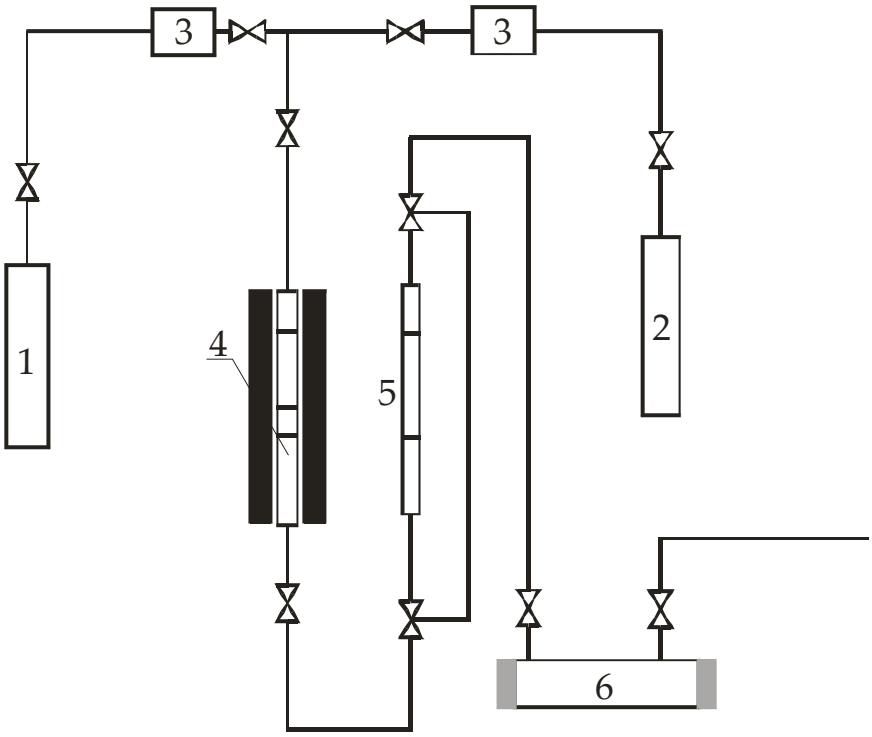

Figure 3: *Scheme of the flow reactor combined with the FTIR monitoring of the effluent gases*; 1 and 2 – cylinders with CHF_3 and nitrogen, 3 – mass flow controllers, 4 – flow reactor equipped with a controllable tubular heater (marked with black colour), 5 – absorption column filled with granulated KOH, 6 – 10-cm gas IR cell.

Batch reactor: Reactions under static conditions were performed in a batch reactor that consisted of a high pressure vessel with a volume of 112 cm^3. Vessel was made of nickel and was equipped with a valve made from the same material and an inlet for solid reactant dosing. During the reaction vessel was closed; its body part allowed heating up to 500–550 °C. Before each reaction, vessel was washed with diluted nitric acid (~30 vol. %), doubly distilled water and ethanol. During the reaction, reactor was positioned in an oven. Temperature of the oven was regulated by a temperature controller equipped with a K-type thermocouple. Gaseous reactants and products were dosed/manipulated on a vacuum system where an average dynamic vacuum of 0.667 Pa could be obtained. Scheme of the batch reactor is shown in Figure 4.

In contrast to the flow reactor, the concentration of CHF_3 in the static reactor is decreasing with time down to the point when the quasi-equilibrium state is achieved, *i.e.* when the velocity of the fluorination becomes negligibly small. Problems with the possible non-homogeneity of the fluorinated products were reduced by grinding and mixing of the whole batch after fluorination.

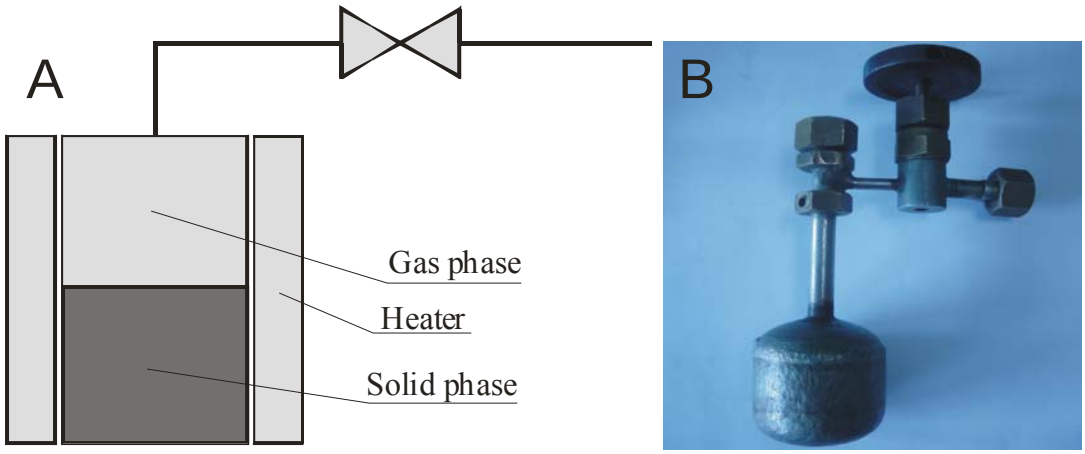

Figure 4: *Batch reactor*: A – schematic representation of the batch reactor equipped with a heater, B – image of a batch reactor made of nickel.

3.4 Fluorination

Fluorinations were carried out with pure CHF_3 (static conditions) or with CHF_3 that was diluted with nitrogen, N_2, to various extents (flow conditions). Fluorination runs under flow conditions were usually monitored on-line by FTIR spectroscopy, as described in Section 3.6.

Fluorination of oxide xerogels under flow conditions: Oxide xerogels were fluorinated with CHF_3 under dynamic conditions in the flow reactor described above. Batches of oxides were usually fluorinated to prepare materials for further investigations. In a typical preparative fluorination, oxide xerogel, 1–1.2 g, was fluorinated under a steady flow of CHF_3 diluted to 20 vol. % with N_2 for 2 h at constant temperatures specified in Table 1. Fluorinated oxides are marked with the extension -F. Total flow of CHF_3/N_2 was 30 cm^3 min^{-1}.

Fluorination of hydroxides under flow conditions: Alkali hydroxides were fluorinated in a flow of pure CHF_3 at 200–250 °C. Flow of CHF_3 was 1 cm^3 min^{-1} that, depending on the amount of the solid reactant, corresponded to contact times of 2–20 s.

Temperature programmed fluorinations (TPF): Different series of TPF experiments were conducted to determine the fluorination onset temperatures and, consequently, to compare reactivities of diverse solid reactants towards CHF_3. TPF experiments were performed with approximately 100 mg of the solid that were pre-treated *in situ* at 400 ºC (oxides and carbonates) or at 300 °C (hydroxides) in a flow of N_2. After cooling to room temperature, a constant flow of CHF_3, 33 vol.% (for oxides) and 9.1 vol.% (for hydroxides and carbonates) in N_2, was applied and the temperature of the reactor was raised linearly with a heating rate of 1.8 ºC min^{-1} until a distinctive fluorination onset was recorded. Fluorination onset temperatures were determined arbitrarily and correspond to the points where a clear shift from the background could be observed.

Fluorination of hydroxides/carbonates under static conditions: Reactions between CHF_3 and various hydroxides and carbonates were performed in a closed batch reactor described above. In a typical static experiment, solids were heated in the batch reactor filled with CHF_3 or some other gaseous reactants for 20 hours. Possible catalytic effects of the reactor material (nickel) on the methanation reaction (Eq. 18) was verified by heating a mixture of CO and H_2, molar ratio of 2.5:1, at 350 °C for 20 hours in the nickel

reactor normally used in batch experiments. Formation of CH_4 was confirmed by FTIR. In a replicated test performed in a glass reactor formation of CH_4 was not observed.

3.5 Chemical analysis

Total content of fluorine in the solid fluorinated products was determined by chemical analysis. Fluorinated solids were decomposed in a melted mixture of sodium potassium carbonate, $NaKCO_3$. Melt was dissolved in water and the total fluoride content was determined by direct potentiometry using a fluoride ion selective electrode [66, 67].

3.6 Fourier Transformed Infrared (FTIR) spectroscopy

FTIR spectroscopy was one of the key characterisation methods used within this work. It was used for the characterisation of some solid precursors and fluorinated products, and gaseous effluents. All spectra were recorded on a Perkin Elmer GX spectrometer, usually at 2 and 4 cm^{-1} resolution. The latter resolution was preferentially used in photo acoustic FTIR (PA-FTIR) measurements of solids.

FTIR spectroscopy of solids: Photoacoustic spectra of the solids were recorded on the above mentioned FTIR spectrometer equipped with a MTEC Model 300 photoacoustic detector. Photoacoustic cell was continuously purged with a flow of 10 cm^3 min^{-1} of high purity helium (min. 99.999 vol. %). Spectra were recorded in a sealed photoacoustic cell under a static helium atmosphere. During the transfer to the photoacoustic cell, samples were for a short time in contact with ambient air. Spectra obtained in this way are denoted as PA-FTIR spectra. A considerable part of PA-FTIR spectra was recorded for solids on which pyridine was adsorbed. Details about this procedure are given in Section 3.7.

FTIR spectroscopy of gases: FTIR spectra of gaseous products from different reactions with CHF_3 were recorded under static or dynamic (flow) conditions. Gaseous products from the batch reactor were analysed in a static gas IR cell with the optical path of 8 mm. Cell consists of a brass frame and body, two KBr windows, and a brass valve. Scheme of the cell is shown in Figure 5. Cell evacuation and filling were carried out on the vacuum system. For quantitative analyses, cell was calibrated with the key components found in the gaseous products, unconverted CHF_3, carbon monoxide, CO, and methane, CH_4, at different relative pressures. Intensities of lines at 2519 cm^{-1} for CHF_3, 2120 cm^{-1} for CO, and 2958 cm^{-1} for CH_4 were used for calibration. Further details about the calibration procedure are given in Appendix II. FTIR spectroscopy of gases performed under flow conditions was used in the on-line IR-monitoring of gaseous effluents, as described below.

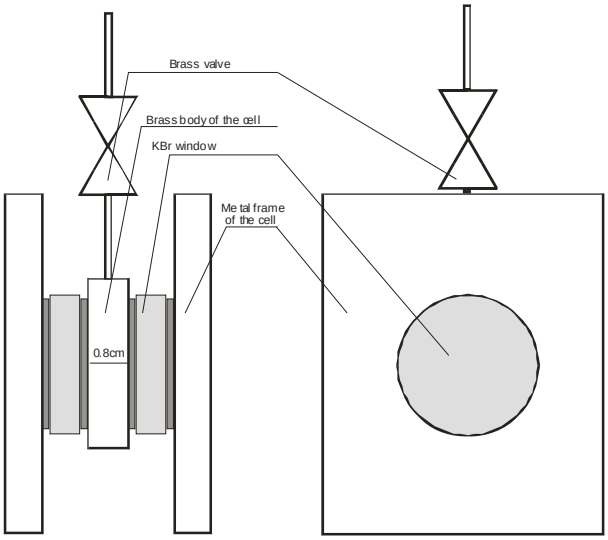

Figure 5: *Static gas IR cell* (optical path 8 mm).

On-line IR-monitoring of gaseous effluents: Gaseous products from the reactions with CHF_3 performed under flow conditions were monitored with a 10 cm gas flow IR cell. Cell consists of a PTFE body, two NaCl windows, and an inlet and outlet valve made of PTFE. Scheme of the gas flow cell is presented in Figure 6. Design of the cell allows measurements at normal pressure and at room temperature. During the runs, spectra of the gaseous effluents were recorded continuously with predetermined scanning rates; usual rate was 5 scans min^{-1}. After run completion, component-specific evolution profiles were constructed from the batch data using the capabilities of the Spectrum TimeBase (PerkinElmer) software. Carbon monoxide, CO, was identified as a suitable marker for following reactions between CHF_3 and various oxygen-containing solids since it allows a clear and unhindered distinction from other components in the IR-spectra of bulk gaseous effluents. CO evolution profiles were constructed from the line at 2120 cm^{-1}. In some temperature programmed experiments, profiles for H_2O were constructed from the line at 3845 cm^{-1} and those for HF from the line at 4075 cm^{-1}.

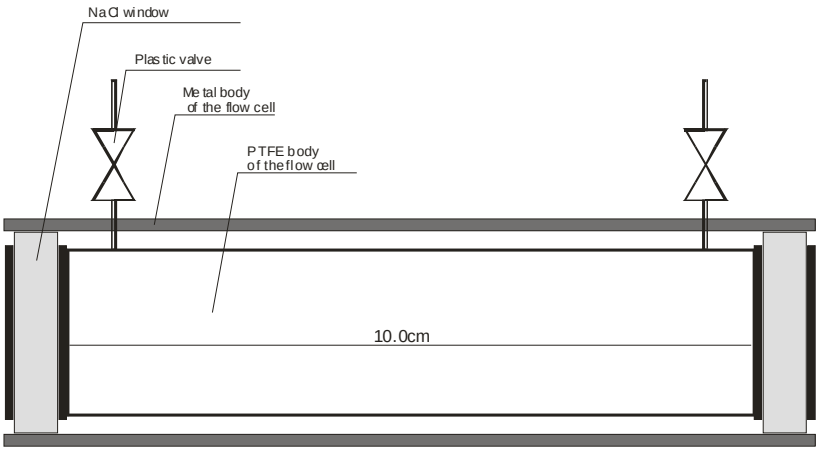

Figure 6: *Gas flow IR cell* (optical path 10 cm).

3.7 Pyridine adsorption tests

Adsorption of probe molecules is commonly used to detect and characterize various acid sites found on the surfaces of inorganic solids. Among different possible probe molecules, pyridine (py) is most frequently employed. Namely, FTIR spectrum of adsorbed py clearly indicates the presence of either Lewis or Brønsted acid sites and gives important information on their relative strengths. Py is a base that can interact with both Lewis acid sites or acidic protons to give either a coordination complex or pyridinium species (see Scheme A-1 in Appendix V). In both cases the interaction is via the lone pair of electrons on nitrogen. Most indicative IR bands of adsorbed py are located in the region between 1400 and 1700 cm^{-1}. Adsorption of py was found to be a valuable tool for the qualitative evaluation of changes in acidity during the fluorination of a variety of metal oxides [68–70]. Analytically most relevant interactions between py and surface acidic sites are summarised in Appendix V.

Pyridine adsorption followed by PA-FTIR spectroscopy of chemisorbed pyridine (PAS-py) was performed according to the procedure reported earlier [68]. Before pyridine adsorption, samples were conditioned in a flow of N_2, 30 cm^3 min^{-1}, at 250 °C for 1 h. Afterwards, reactor was cooled to 150 °C and 3 μl of liquid pyridine were injected directly into the reactor inlet where they were immediately evaporated. After pyridine injection, reactor was flushed with N_2 for additional 15 min to remove excessive and physically adsorbed pyridine from the system.

In another set of experiments, thermal stability of pyridine adsorbed on oxides and fluorinated products was investigated by pre-adsorbing pyridine at room temperature followed by linear heating of the pyridine-loaded materials under flow of N_2 to 400 °C (oxides) or 350 °C (fluorides) with a heating rate of 2 K min^{-1}. Evolution of pyridine was monitored by on-line FTIR spectroscopy; thermally treated solid materials were examined by PA-FTIR spectroscopy.

3.8 Mass Spectrometry (MS)

This technique was used for the analysis of gaseous products from some reactions, mainly from the reactions between NaOH or NaOD and CHF_3. Products from these reactions were analysed by the low resolution 60 degree Nier Type mass spectrometer. The samples were introduced into the spectrometer through a 0.5 m long nickel capillary with 0.1 mm i.d. from a reservoir kept at 1.33 kPa. The samples were ionised by electrons at 35 eV and 10 μA trap current intensity. For ion detection an ETP electron multiplier (ATF151H) operating at 1.8 kV in analogue mode was used. Scheme of the mass spectrometer used in the current research is presented in the Figure 7.

3.9 Powder X-ray Diffraction (XRD)

Powder diffractograms of oxide precursors and fluorinated products were recorded on AXS D4 Endeavor diffractometer (Bruker) using Cu K_α radiation. Before analysis, each sample was slightly ground to obtain a sufficiently uniform and compact layer on the sample holder.

Powder diffractograms of solid precursors and products of alkali hydroxides fluorination were recorded on ItalStructures IPD 3000 diffractometer equipped with an image plate detector by using the Cu K_α radiation. Each sample was ground and filled in a 0.3 mm i.d. quartz capillary.

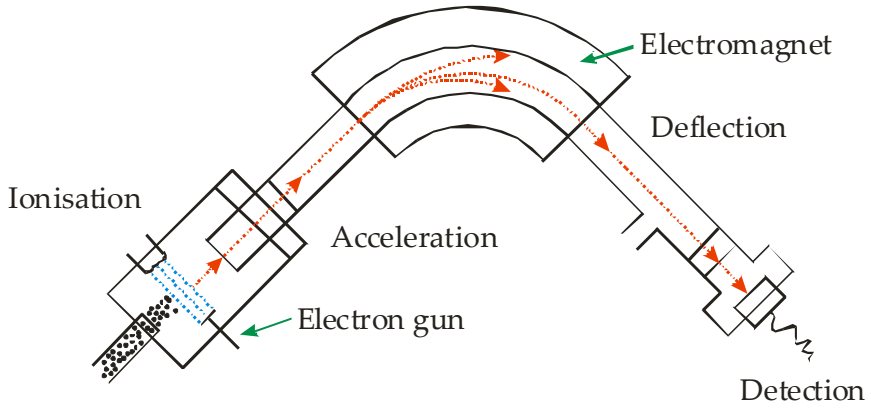

Figure 7: *Scheme of the applied mass spectrometer.*

3.10 SEM imaging

Scanning electron microscopy (SEM) is a type of microscopy that images the sample surface by scanning it with a high-energy beam of electrons in a raster scan pattern. The electrons interact with the atoms that make up the sample producing signal that contains information about the surface topography, composition and other properties, such as electrical conductivity. In this work SEM pictures were recorded by using SEM Jeol 5800. Before analysis, surface of each powdered sample was covered with a layer of gold to improve its conductivity.

3.11 Specific Surface Area (SSA) determination

Surface areas of oxides and their fluorinated products were determined with a single-point Brunauer, Emmet, and Teller (BET) method of monolayer N_2 adsorption. Analyses were performed with a dynamic method of N_2 adsorption from a 30:70 vol. % mixture of N_2 in He at –196 °C on a FlowSorb II 2300 instrument (Micromeritics). Before each analysis, solid samples were evacuated at 250 °C for several hours and additionally conditioned at the same temperature under flow of N_2 for 1 h in the test tube of the FlowSorb instrument.

3.12 X-ray Photoelectron Spectroscopy (XPS)

XPS is an analytical technique for the qualitative and quantitative investigation of surfaces. Detection limit for most elements is lying between 0.1 and 1.0 at.%. Elements with the atomic number lower than 3, *i.e.* hydrogen and helium, can not be detected by XPS. The reason for this is in the diameter of their orbitals which are too small to catch the X-ray quants.

Within this work XPS analyses were carried out on the PHI-TFA XPS spectrometer exiting a sample surface by using X-ray radiation from Al monochromatic source. The samples were in the form of 1 mm thick pressed pellets. The analysed area was 0.4 mm in diameter and the analysed depth was 2–5 nm. The XPS survey and narrow scan spectra of emitted photoelectrons were taken with pass energies of 187 eV and 29 eV, respectively. With pass energy of 29 eV energy resolution of 0.6 eV was obtained on the Ag $3d_{5/2}$ peak. During analysis, XPS spectra were shifted due to sample charging; neutralizer gun for

low energy electrons was used to reduce this effect. The binding energy 284.8 eV for C 1s peak was used as reference energy for spectra alignment. The spectra of Al 2p, Ga 2p, Ga 3d, O 1s, C 1s and F 1s were acquired during XPS analyses. Relative sensitivity factors provided by instrument producer were used to calculate surface concentrations. The composition was calculated in the model of homogeneous matrix. It was estimated that the relative error for calculated concentrations is about 20 % of reported values. Error in binding energy was 0.3 eV.

3.13 Catalytic tests

Catalytic behaviour of some representative fluorinated oxide xerogels in isomerisation of 1,1,2-trichlorotrifluoroethane, CCl_2FCClF_2, and subsequent dismutations was investigated under steady flow conditions. Catalytic line and basic test conditions were similar to those used in some of the previous comparative investigations using various AlF_3-based materials as catalysts [35, 41, 71]. Each catalytic test consisted of two consecutive stages: firstly the temperature was steeply increased to 350 °C (activation stage), active materials were afterwards tested at steeply reduced temperatures, down to 250 °C. Analyses of the gaseous effluents were performed by using on-line gas chromatography after 1 h stabilisation period at each temperature ramp.

3.14 Thermal decomposition of CHF_3 over fluorinated alumina

Alumina fluorinated with CHF_3 at 400–550 ºC was applied as a catalyst for thermal decomposition of CHF_3. Tests were performed in the flow reactor at 400–550 ºC. Gaseous products were analysed continuously by on-line FTIR spectroscopy (see Section 3.6). HF in the effluent gases was adsorbed in a column filled with granular solid KOH. CHF_3 was diluted with dry nitrogen to 25 vol.%, maximum flow of the CHF_3/N_2 mixture was 30 cm^3 min^{-1}.

4 Results and Discussion

Fluorination of γ-Al_2O_3/γ-Ga_2O_3 with CHF_3 at intermediate temperatures was demonstrated to be a versatile approach for the preparation of solid materials with tailored properties. This can conveniently be achieved by proper combination of the Al/Ga ratio and the extent of fluorination.

Alkali hydroxides and carbonates investigated within the present work react with CHF_3 at moderate temperatures. In these heterogeneous reactions, CHF_3 undergoes complete decomposition (mineralisation) at temperatures lower than 300 ºC with the formation of gaseous CO and H_2O, and solid alkali fluorides.

4.1 Fluorination of γ-Al_2O_3, γ-Ga_2O_3, and mixed γ-Al_2O_3/γ-Ga_2O_3 with CHF_3

4.1.1 Oxide precursors

Surface areas and denomination of single and mixed oxide xerogels used as precursors within the present work are presented in Table 1. Surface areas of single oxides differ considerably, 235 $m^2\ g^{-1}$ for Al_2O_3 (Al#0) *vs.* 87 $m^2\ g^{-1}$ for Ga_2O_3 (Ga#0). In general, this divergence is consistent with previous comparative studies where it was found that surface areas of γ-Ga_2O_3 are always considerably lower, usually up to two times, as those of similarly prepared γ-Al_2O_3 analogues, *e.g.* respective ranges reported for γ-Ga_2O_3 and γ-Al_2O_3 are 100–160 $m^2\ g^{-1}$ and 170–300 $m^2\ g^{-1}$ [45–48, 50]. Surface area of Al#0 is within the typical values for γ-Al_2O_3, while that of Ga#0 is somehow lower as reported for γ-Ga_2O_3. In previous studies, Ga_2O_3 materials with surface areas below 100 $m^2\ g^{-1}$ were found to be at least partially crystallised [46, 49, 72]; *e.g.* inorganic preparation route, similar to that used in the present work, yielded crystalline α-Ga_2O_3 with surface area of 77 $m^2\ g^{-1}$ [72]. According to these precedents, relatively low surface area of Ga#0 could be possibly associated with the formation of crystalline Ga_2O_3 phases. XRD measurements do however not give any evidence for that and show that single oxides, Al#0 and Ga#0, are of very low crystallinity and consist only of metastable γ-Al_2O_3 and γ-Ga_2O_3 phases.

Mixed oxides investigated within this work comprise a series of Al_2O_3/Ga_2O_3 xerogels with Al_2O_3:Ga_2O_3 ratios ranging from 100:1 (Al/Ga-100) to 1:1 (Al/Ga-1). Nominal compositions, denomination and surface areas of mixed xerogels are given in Table 1. Surface areas of the mixed xerogels with lower Ga_2O_3 contents, up to the sample Al/Ga-2, are within the range typically observed for γ-Al_2O_3 (Al#0). Only the xerogel with the highest Ga_2O_3 content, Al/Ga-1, exhibits a somehow lower surface area of 164 $m^2\ g^{-1}$. Reported surface areas of mixed γ-Al_2O_3/γ-Ga_2O_3 are not consisted steadily with increasing of γ-Ga_2O_3 content [46, 47, 50, 73]; there is however also a number of reports where no distinctive trends were observed [48, 51, 52, 64]. XRD patterns of representative mixed Al_2O_3/Ga_2O_3 xerogels are shown in Figure 8 (traces a, c and e). Corresponding patterns are very similar to those of single oxides, γ-Al_2O_3 and γ-Ga_2O_3

(not shown). Broadness and low intensity of diffraction lines indicate that crystallinity is low what is in line with the observed high surface area of all mixed xerogels. Mixed γ-Al_2O_3/γ-Ga_2O_3 xerogels are commonly described as solid solutions with spinel-type structure [46–48, 50, 73]. Most indicative feature of these solutions is the enlargement of the unit cell parameter of γ-Al_2O_3 when Al^{3+} ions are isomorphically substituted by larger Ga^{3+} ions. This is manifested by the shift of characteristic diffraction lines to lower diffraction angles. Such shifts with increasing Ga_2O_3 contents were clearly observed also for current mixed oxides as seen in Figure 8 for two typical lines of γ-Al_2O_3 at 45.6 and 66.6 ° what indicates the formation of γ-Al_2O_3/γ-Ga_2O_3 solid solutions.

4.1.2 Fluorination of oxide xerogels with CHF_3

Fluorination of single oxides with CHF_3 under flow conditions was studied in the temperature range of 200–450 ºC (Table 1). For both single oxides, extent of fluorination deduced from the fluorine content of fluorinated products strongly depends on the temperature and is considerably higher for the γ-Al_2O_3-based Al#0 than for the γ-Ga_2O_3-based Ga#0, *e.g.* after fluorination at 450 °C the respective molar conversions of the two oxides to the corresponding fluorides are 56.1 and 19.0%. Different behaviour of γ-Al_2O_3 and γ-Ga_2O_3 towards fluorination can be partially ascribed to thermodynamic reasons. Namely, formation of crystalline aluminium(III) fluoride ($\Delta G^{298}_{f,AlF_3}$ = –1431 kJ mol^{-1}) is more favourable than formation of crystalline gallium(III) fluoride ($\Delta G^{298}_{f,GaF_3}$ = –1085 kJ mol^{-1}) [7]. In the current work, γ-oxide phases were only partially fluorinated and were not transformed to pure crystalline fluoride phases. Formed Al- and Ga-fluoride phases remained amorphous and highly dispersed. Another factor that may influence the reactivity of the oxide is its initial surface area that was considerably higher for γ-Al_2O_3 than for γ-Ga_2O_3. For both oxides, temperature of fluorination had a strong effect on the extent of fluorination. As can be seen from Table 1, in both cases content of fluorine in the fluorinated samples was increasing exponentially with temperature. This is in line with a trend given by the Arrhenius expression; where the reaction rate is proportional to $e^{\left(-\frac{E_a}{RT}\right)}$.

Fluorination of a series of mixed oxides was carried out at intermediate temperature of 350 ºC. Extent of fluorination for the mixed xerogels is close to the value found for the γ-Al_2O_3-based Al#0 treated at the same temperature (Table 1, sample Al#04-F). Within mixed xerogels, distinctively lower fluorine content was observed only for the Ga_2O_3-rich sample, Al/Ga-1. This implies that fluorination processes were not affected by intermediate levels of Ga. Another noticeable effect of fluorination was the decrease of surface area observed for all fluorinated oxide precursors. Corresponding reductions in surface areas were proportional to the extent of fluorination, as evidenced by the Al#0 and Ga#0 fluorination experiments performed at different temperatures (Table 1). Similar effects of fluorination were observed for a number of γ-Al_2O_3 and related materials and were usually associated with the expansion and crystallisation processes that take place during the conversion of the oxide matrix to bulk fluoride phase(s) [36–39].

Table 1: *Denomination and properties of single and mixed oxide precursors, and corresponding fluorinated products after treatment with CHF_3.*

Oxide precursors			Fluorinated products			
Sample	**Al/Ga ratio**	**BET SSA, $m^2 \cdot g^{-1}$**	**Sample**	**Fluorin. temp., °C**	**BET SSA, $m^2\ g^{-1}$**	**Fluorine content, wt.% F^-**
Al#0	/	235	Al#01-F	200	190	1.9
			Al#02-F	250	192	3.4
			Al#03-F	300	170	7.4
			Al#04-F	350	130	19
			Al#05-F	400	58	34
			Al#06-F	450	21	46
			Al#07-F	500	17	43
Ga#0	/	87	Ga#01-F	200	89	0.52
			Ga#02-F	250	86	1.1
			Ga#03-F	300	82	2.1
			Ga#04-F	350	79	3.6
			Ga#05-F	400	74	4.7
			Ga#06-F	450	55	11
			Ga#07-F	500	18	24
Al/Ga-100	100	200	Al/Ga-100-F	350	120	16
Al/Ga-50	50	207	Al/Ga-50-F	350	108	15
Al/Ga-25	25	220	Al/Ga-25-F	350	119	15
Al/Ga-15	15	250	Al/Ga-15-F	350	147	22
Al/Ga-5	5	210	Al/Ga-5-F	350	171	20
Al/Ga-2	2	296	Al/Ga-2-F	350	155	17
Al/Ga-1	1	164	Al/Ga-1-F	350	139	9.8

Chemical analysis indicates that all oxide xerogels underwent fluorination, although to different extents, *e.g.* Al#0 and Ga#0 fluorinated at 350 ºC contain, respectively, an equivalent of 27.7 wt. % of AlF_3 (Al#04-F) and 8.0 wt. % of GaF_3 (Ga#04-F). XRD investigations of fluorinated materials, performed shortly (within few days) after fluorination, do not reveal any crystalline phase(s), as exemplified on Figure 8 (trace f) for the Al/Ga-1-F sample. Recorded XRD patterns remain practically identical to those of

the γ-Al_2O_3 and/or γ-Ga_2O_3 precursors. In an earlier study, no crystalline phases were detected in fluorinated γ-Al_2O_3 containing up to 68 wt.% of AlF_3 [36]. It was concluded that even at such high AlF_3 contents fluoride remains strongly dispersed and of very low crystallinity that can not be detected by XRD. It is very likely that similar fluoride phases, amorphous to X-rays, were formed also here, especially in Ga-rich materials where the extent of fluorination is considerably lower. Further XRD investigations, performed within several months after preparation, showed however that the initial amorphous fluoride phases are not stable. Although the materials were stored and manipulated under dry conditions, noticeable crystallisation occurred, as shown in Figure 8 (traces b, d and g) for the three representative fluorinated mixed xerogels. Besides the unconverted oxide phase, XRD indicates the formation of a crystalline hydrated aluminium hydroxyfluoride with general formula, $Al(F,OH)_3 \cdot nH_2O$, having a pyrochlore structure and not well-specified composition [74]. Comparison with the XRD data from a previous study of Al-hydroxyfluorides [75] indicates that the crystallised product closely matches the compound with the reported composition of $AlF_{1.7}(OH)_{1.3} \cdot H_2O$ that however consists of two phases with different cell parameters. Crystallisation of hydrated AlF_3 or hydroxyfluoride phases after exposure to ambient air was also noticed in some previous reports dealing with amorphous AlF_3 with unusually high surface areas [76–78]. These findings gave clear evidence that H_2O uptake in these materials can be substantial, as anticipated from their strong Lewis acidity and high surface area. Recent *ab initio* and XPS investigations of AlF_3 with high surface areas [78], substantiated by computed phase diagrams for AlF_3 surfaces [79], strongly suggest that at room temperature H_2O adsorption followed by surface hydroxylation, hydration and hydrolysis can be very significant, and, more importantly, that these processes may take place already at H_2O levels that are orders of magnitude lower than those practically achievable in the laboratory, even if all operations are carried out at thoroughly controlled dry conditions. It is therefore very likely that formation of crystalline hydrated phases observed for the current partially fluorinated oxides is the result of H_2O adsorption during manipulation and storage that can practically not be avoided, as mentioned above. For the fluorinated mixed oxides, shown in Figure 8, it is clear that the extent of crystallisation of the $Al(F,OH)_3 \cdot nH_2O$ phase is inversely proportional to the Ga content. It should be noted that for the fluorinated single Ga_2O_3 (sample Ga#06-F, not shown) post-crystallisation was also observed. In fluorinated mixed oxides, behaviour of Ga is therefore different; preferential crystallisation of Al-hydroxyfluoride indicates that Ga-phases are not involved in the bulk crystallisation processes. Contrarily, they apparently retard the crystallisation of Al-rich phases, probably by lowering the concentration of available Al-species. On the other side, preferential formation of crystalline $Al(F,OH)_3 \cdot nH_2O$ phases may lead to the formation of segregated Al- and Ga-rich regions that may considerably increase the heterogeneity of these materials on a macro scale.

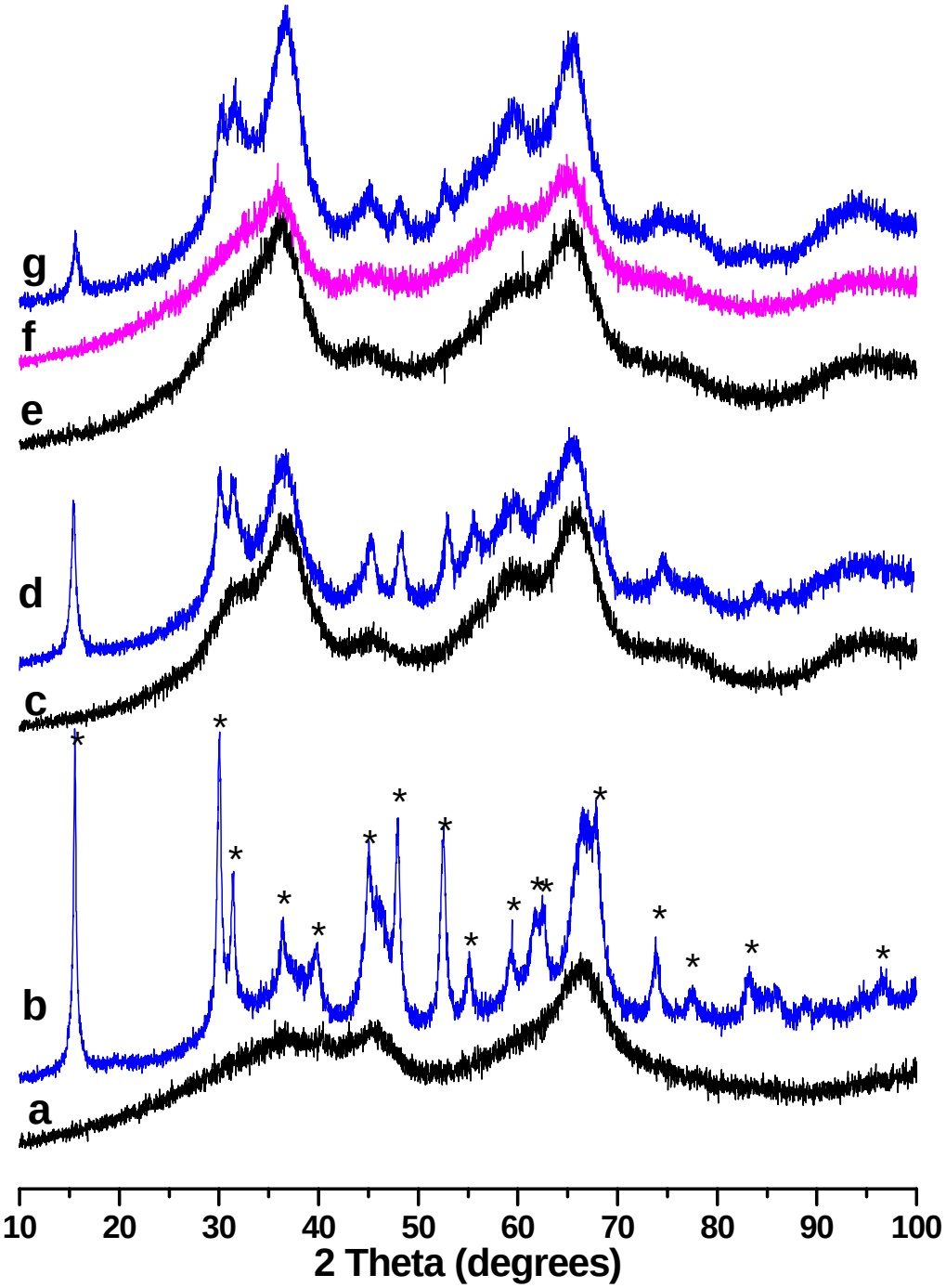

Figure 8: *Representative powder diffractograms (offset) for mixed oxide precursors and products of fluorination with CHF_3 at 350 °C;* Oxide precursors: (a) Al/Ga-100/1, (c) Al/Ga-2/1, and (e) Al/Ga-1/1; Fluorinated products: (b) Al/Ga-100/1/F (aged), (d) Al/Ga-2/1/F (aged), (f) Al/Ga-1/1/F (fresh), and (g) Al/Ga-1/1/F (aged). Corresponding compositions are given in Table 2. * - $Al(F,OH)_3 \cdot nH_2O$ [74].

4.1.2.1 Morphological transformations

SEM images were recorded in order to observe the morphological changes induced by fluorination with CHF_3. Representative SEM images for the mixed Al/Ga-2 xerogel are shown in Figure 9. As seen in Figure 9A, mixed Al/Ga-oxide xerogel precursors consist of large particles that are composed of smaller primary particles with prevalently spherical geometry. These primary particles with a diameter of approximately 100 nm form densely packed agglomerates. After treatment with CHF_3 the basic morphology remains practically unaltered; fluorinated oxides are also composed of globular primary particles (Figure 9B) with similar dimensions as those in oxide precursors. SEM does not reveal any crystallisation and therefore supports results obtained with chemical analysis and XRD that indicate only partial conversion of the oxide to fluoride with the fluoride phase being highly dispersed and amorphous.

4.1.2.2 Thermal behaviour of fluorinated products

Thermal behaviour of fluorinated products was verified with temperature programmed (TP) experiments, performed up to 500 ºC in flow of N_2. Effluent gases were monitored by on-line FTIR spectroscopy; representative evolution profiles for HF and H_2O for the Al/Ga-100-F sample are shown in Figure 10. It should be mentioned that very similar HF evolution profiles were recorded for the $MF_{3-x}(OH)_x \cdot nH_2O$ (M=Al or Ga) type of compounds [80] and for fluorinated Ga-doped Al_2O_3 [42]. Current TP experiments show that H_2O desorption from the fluorinated products is substantial. As can be observed, H_2O is evolving in three distinctive steps: (i) large amount of weakly bonded H_2O is desorbed up to 200 °C, (ii) within the temperature interval of 200–330 °C, desorption of H_2O is lower and decreases slowly, (iii) above 330 °C, a rapid decline in H_2O desorption is observed. On the other side, HF evolves in two stages: (i) evolution of HF starts at approximately 230 °C and increases slowly up to 380 °C, (ii) above 380 °C, intense evolution of HF takes place. Distinctive inverse course of H_2O and HF evolution at higher temperatures is a clear indication that both processes coincide what could be associated with the hydrolysis of the fluoride phase in which H_2O is consumed and HF is formed. According to TP experiments, current fluorinated oxides are relatively stable towards hydrolysis only at temperatures below 230 ºC, above this temperature, and especially above 380 ºC, all treatments performed under non-fluorinating conditions will led to some defluorination. As found for very active AlF_3-based materials, their surface and bulk properties may be strongly altered by hydration and hydrolysis [78, 81]. Such effects are however expected to be less pronounced for current partially fluorinated oxides that already consist of mixed bulk oxide/hydroxyfluoride phases, *i.e.* phases that are formed during the hydrolysis of stoichiometric fluorides.

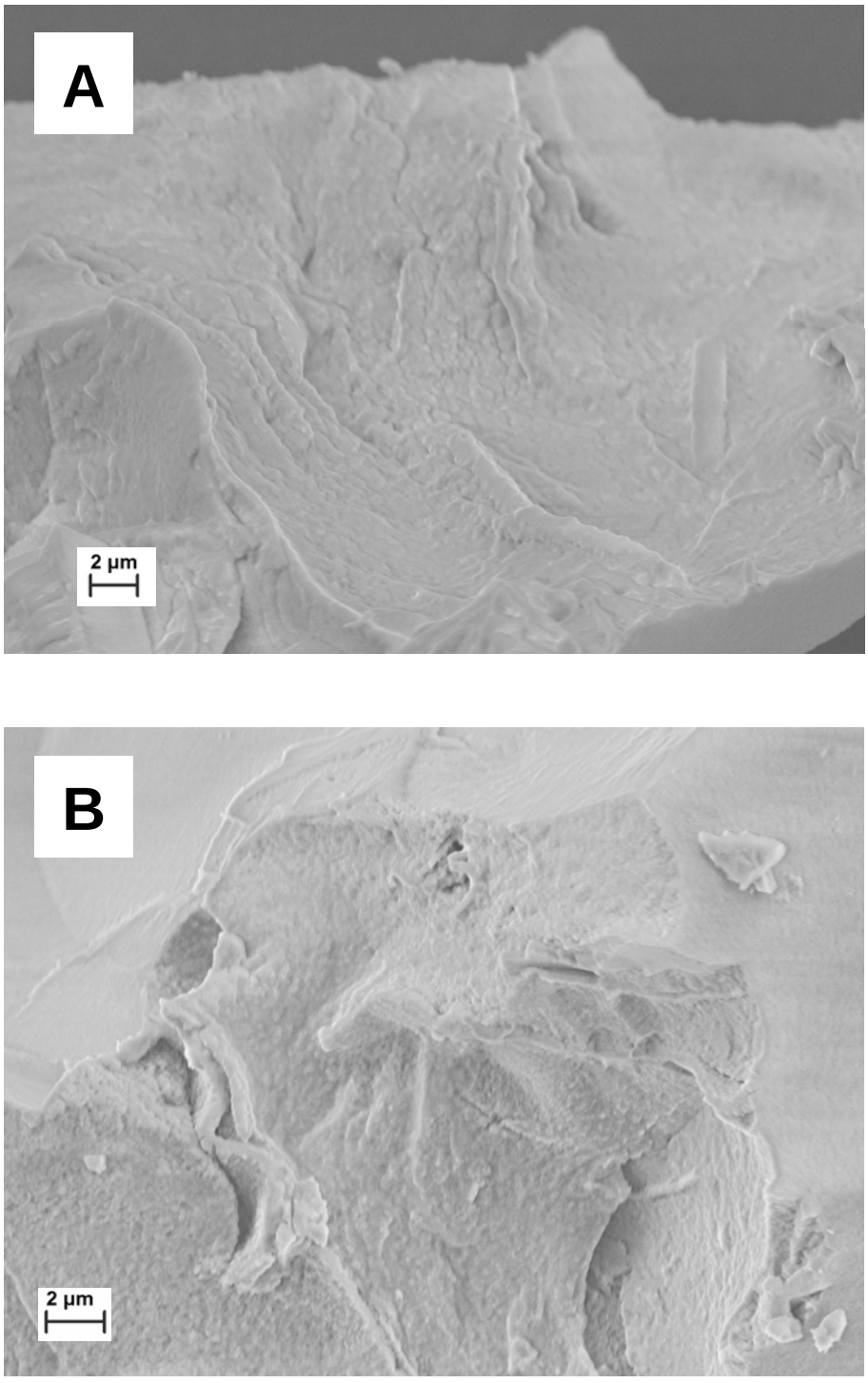

Figure 9: *SEM images of oxide precursor Al/Ga-2 (A), and its fluorinated product Al/Ga-2-F (B).*

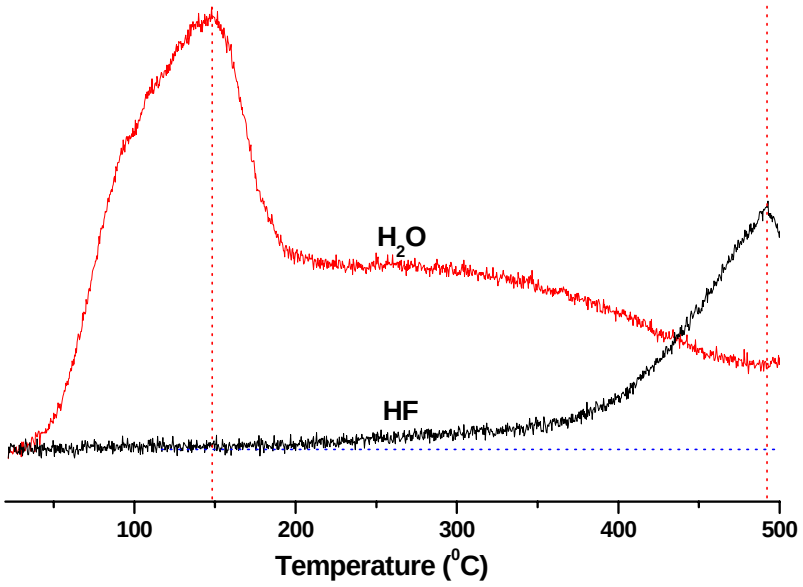

Figure 10: *H_2O and HF evolution profiles obtained with a temperature programmed heating of Al/Ga-100-F in a flow of N_2.*

A series of TPF experiments up to 400 ºC were performed to compare reactivities of single and mixed oxide towards CHF_3 in the initial stages of fluorination, *i.e.* when the reaction is limited mainly to the surface. Progress of fluorination was monitored by using FTIR spectroscopy; corresponding CO evolution profiles are presented in Figure 11. The two single oxides, samples Al#0 and Ga#0, start to react with CHF_3 at approximately 180 and 230 ºC, respectively. For the mixed oxides, onset of fluorinated is similar to Al#0, reaction starts at approximately 180 ºC; sample with highest Ga-content (Al/Ga-1) being a clear exemption reacting already at 130 ºC. Most notable difference between single and mixed oxides is exhibited in the intermediate temperature region, 130–330 ºC, where mixed oxides show a higher and graduated CO evolution that roughly increases with increasing Ga-content. Intense CO evolution, observed for all investigated materials above 310–350 ºC, can be associated with the beginning of bulk fluorination processes. There is however no clear correlation between these temperatures and fluorine contents obtained in preparative fluorination runs at 350 ºC (see Table 1). This suggests that bulk fluorination of the oxide matrix above 310–350 ºC is very likely controlled by diffusion. As mentioned before, fluorination of oxides is usually accompanied by a considerable decrease of internal porosity what may have a very strong effect on diffusion processes within the particles of reacting solids [36–38].

TPF experiments clearly demonstrate that mixed oxides exhibit higher surface reactivity towards CHF_3 than the single oxides and that the reactivity is increasing with increasing Ga content. Very reactive surface sites in mixed oxides, capable to react with CHF_3 at 130–330 ºC, seem to be more abundant and differ from those present on single oxides. This is in good correlation with current PAS-py and XPS results (see below) that suggest a higher surface heterogeneity in mixed oxides, especially those with higher Ga contents. Surfaces with higher degree of heterogeneity are expected to exhibit higher concentration and broader variety of reactive surface sites. Within this work, the exact nature of these reactive sites could not be unequivocally determined. However, as found within this work, relatively stable CHF_3 molecule starts to react with solid alkali

hydroxides at moderate temperatures, *i.e.* with KOH at 100 ºC and with NaOH at 150 ºC. As detailed in Section 4.2.4, reactivity of these solids towards CHF_3 is, at least in the initial stages, ascribed to acid-base type of interactions between CHF_3 acting as a weak C–H acid and strongly basic oxygen species on the solid hydroxides. In addition, in a previous study of γ-Al_2O_3 fluorination it was clearly demonstrated that fluorination starts on basic OH groups [82]. Initial reactivity of current oxides towards CHF_3 can be therefore tentatively ascribed to similar interactions, probably involving different types of strongly basic surface sites, *e.g.* basic OH groups and possibly surface O^{2-} anions. In additions, observed higher reactivity of mixed oxide is consistent with earlier studies that demonstrated a higher basic character of γ-Ga_2O_3 w.r.t. γ-Al_2O_3 [45], and an increase of basicity for Ga_2O_3 supported on Al_2O_3 in comparison with individual oxide components [83, 84]. It can be therefore speculated that graded CO evolution is an indication of CHF_3 reactions with different types of strongly basic sites that are characteristic only for mixed γ-Al_2O_3/γ-Ga_2O_3 surfaces. Strong basic sites on such materials could possibly be probed by means of TPF with CHF_3. Further investigations are however required to verify these possibilities.

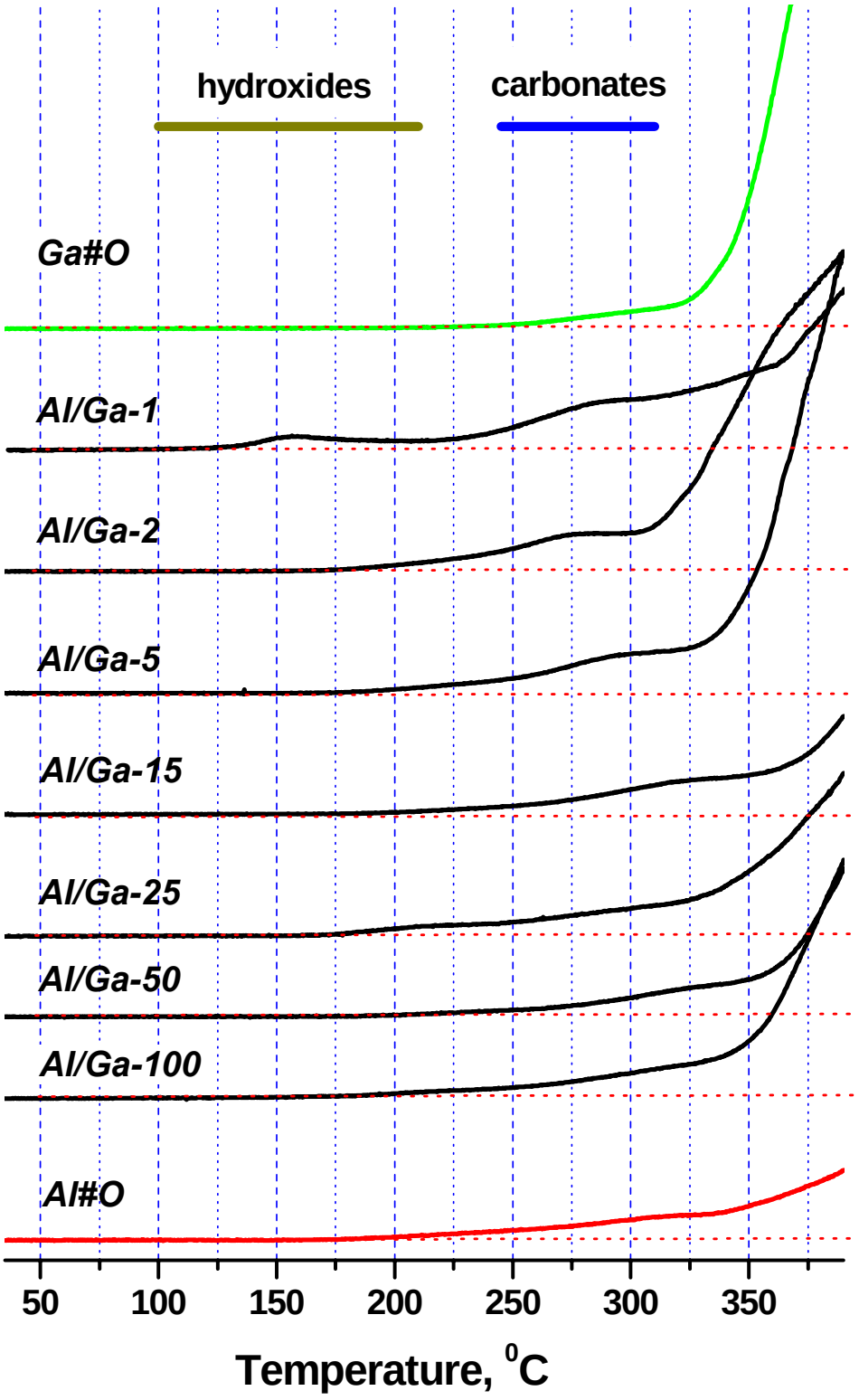

Figure 11: *Temperature programmed reaction of single and mixed oxides with CHF_3 under flow conditions*; corresponding CO-evolution profiles (offset) are shown. Inset horizontal lines show the range of fluorination onset temperatures for alkali hydroxides and carbonates (see Figure 28).

4.1.2.3 Thermal decomposition of CHF_3 over fluorinated oxides

Fluorinations with CHF_3, described so far, were conducted at moderate temperatures what leads to partial fluorination in which bulk of the oxide remains largely unconverted. As seen on Figure 11, temperature of 350 °C, that was used for the fluorination of the majority of materials investigated within this work, represents approximately the transition between the surface and bulk fluorination. This explains moderate fluorine incorporation and the retention of some characteristics of the starting oxides, like high surface area and amorphous structure.

In general, fluorination of oxides, especially for catalytic purposes, is rarely performed above 400–500 °C. Products obtained at these temperatures are usually highly fluorinated, crystalline and have low surface areas. In addition, they consist of the catalytically inactive α-AlF_3 phase [34].

Within this work a series of experiments was performed to obtain some comparative information about the behaviour of CHF_3 in contact with single oxides above 450 °C. A typical course of such reaction is shown in Figure 12 for γ-Ga_2O_3 at 450 °C. After the introduction of CHF_3, an abrupt evolution of CO is observed what can be associated with very intense fluorination of the oxide. This reactive stage probably includes surface and subsurface fluorination and is completed within the first 30–40 min on stream. Slow evolution of CO after this stage can be associated with slow fluorination of the interior of the particles that is controlled by diffusion that in turn becomes more and more difficult due to the formation of fluoride products.

Fluorination reaction is consistent with the stoichiometry given for the γ-Al_2O_3 precursor in Eq. 3', leading to the complete decomposition of the CHF_3 molecule. For the reactions above 450 °C, and especially above 500 °C, it was found that fluorination of γ-Al_2O_3 is accompanied and/or followed by some additional reactions of CHF_3 that are evidently promoted by the fluorinated surfaces formed. In Figures 13 and 14, evolution profiles for CO and CF_4 are shown for the fluorination of γ-Al_2O_3 xerogel at 500 and 550 °C, respectively. In both cases the bulk fluorination reaction is finished within the first 30–40 min after the introduction of the CHF_3/N_2 mixture. It can be seen that CF_4 evolution starts when the main fluorination process is virtually finished and is considerably higher at 550 °C than at 500 °C (compare corresponding traces in Figs. 13 and 14). It should be noted that CF_4 formation could not be detected by FTIR when the reaction was conducted at 450 °C. High temperature fluorination with CHF_3 is also accompanied by carbonisation of the fluorinated solid product. Extent of carbonisation depends on the temperature and is higher at 550 °C. It should also be noted that effluent gases are acidic due to HF formation. Evolution of HF was confirmed by FTIR, it was however not monitored on-line in order to avoid the destruction of NaCl windows of the flow IR cell. In contrast to the reactions observed with γ-Al_2O_3, similar high temperature runs performed on γ-Ga_2O_3 and In_2O_3 xerogels showed that on these oxides CF_4 was not formed and no carbonisation was observed.

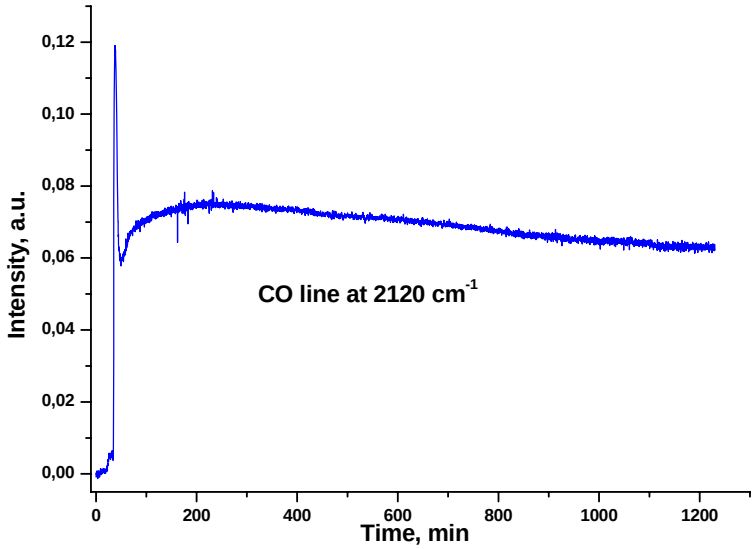

Figure 12: *Typical CO-evolution profile for the reaction of oxide precursors with CHF_3 under flow conditions*; graph shows the reaction of γ-Ga_2O_3 with CHF_3 at 450 °C.

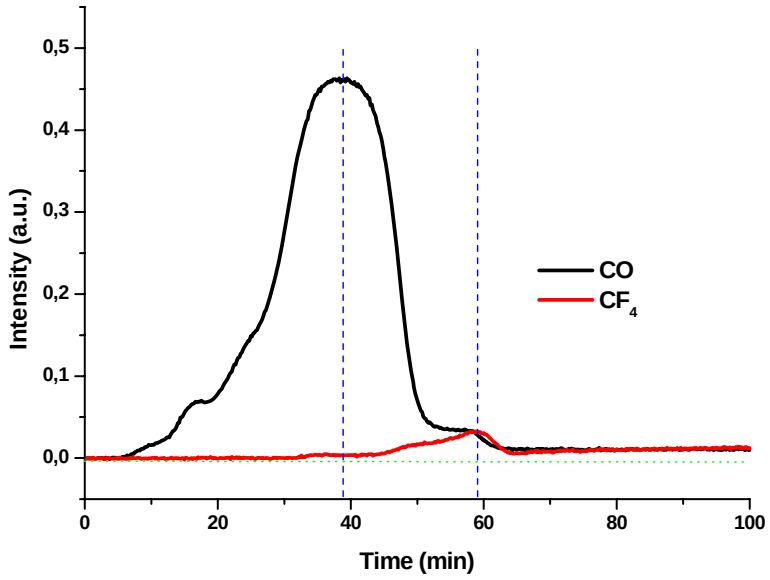

Figure 13: *Evolution of CF_4 and CO during the fluorination of the γ-Al_2O_3 xerogel with CHF_3 at 500 °C in the flow reactor.*

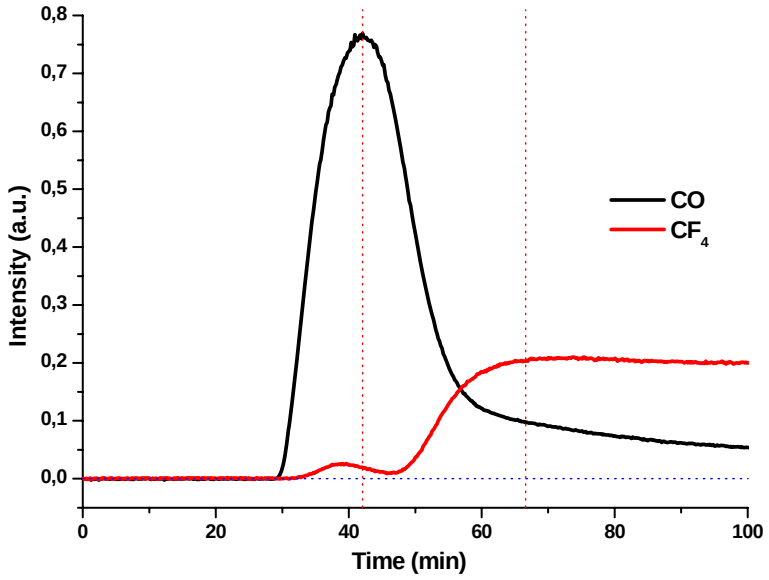

Figure 14: *Evolution of CF_4 and CO during the fluorination of the γ-Al_2O_3 xerogel with CHF_3 at 550 °C in the flow reactor.*

Based on these observations it can be concluded that at temperatures above 500 °C fluorination of γ-Al_2O_3 forms AlF_3-like surfaces with very low amounts of residual O-containing species (Eq. 3'). On such surfaces decomposition of CHF_3 to HF and CF_2 (Eqs. 2 and 2') may take place already at 500 °C. This reaction can therefore be regarded as a surface mediated low temperature pyrolysis in contrast to the classical homogeneous pyrolytic decomposition of CHF_3 that is observed at temperatures above 750 °C. Both products detected, CF_4 and carbon, originate from reactions of CF_2 adsorbed on the surface that can be tentatively represented by a simplified reaction (see Eq. 9) [85]. In this respect it must be noted that some recent reports [30] suggest that CF_2 on the surfaces of activated carbons, AC, or fluorides very likely reacts through a number of surface intermediates that besides CF_2 may also include CF_3, CF, and F species. Formation of intermediate CF_3 species is usually evidenced by the formation of both CF_4 and C_2F_6. Within the current work, formation of the latter was not observed. Although the applied FTIR monitoring of the gaseous products in the presence of the bulk CHF_3 matrix does not allow the detection of minor components it is clear that under the current reaction conditions CF_4 is the main side product. C_2F_6, if formed, is present only in negligible amounts.

$$Al_2O_3 + 2CHF_3 \rightarrow 2AlF_{3(s)} + 2CO_{(g)} + H_2O_{(g)} \quad (3')$$

$$CHF_{3(surf)} + \mathbf{Q} \rightarrow CF_{2(surf)} + HF \quad (2')$$

$$2CF_{2(surf)} \rightarrow CF_4 + C_{(surf)} \quad (9)$$

("surf" indicates surface species and **Q** indicates thermal energy)

The role of fluorinated alumina surfaces and the nature of active sites responsible for the decomposition of CHF_3 remain unresolved. For example, PAS-py investigation of fluorinated γ-Al_2O_3 used in CHF_3 decomposition at 550 °C does not reveal any considerable Lewis acidy. In addition, fluorination at 550 °C led to the formation of the α-AlF_3 phase that is usually regarded as catalytically inactive. However, current results indicate that decomposition of CHF_3 is promoted by both temperature and the surface of

highly fluorinated γ-Al_2O_3 which is qualitatively different from those in fluorinated γ-Ga_2O_3 and In_2O_3 xerogels.

4.1.3 Surface effects of fluorination

Pyridine, a relatively hard Lewis base with rather high chemical stability, is a classical IR probe for determination of the acidity of Al_2O_3-based materials [86] as well as that of their fluorinated analogues with largely different AlF_3 contents [68, 87]. In this work, spectroscopic investigations of adsorbed pyridine were used to follow the changes in acidity within the series of mixed oxides, and the corresponding changes induced by fluorination. Indicative PAS-py spectra of oxide precursors and related fluorinated products are presented in Figures 15A and 15B, respectively.

4.1.3.1 PAS-py of oxide precursors

PAS-py spectra of the two single oxides, Al#O and Ga#0 in Figure 15A, are characterised by the bands at about 1450, 1491, 1579 and 1615 cm^{-1}, that are typically assigned to pyridine coordinatively bonded to Lewis acid sites [68], see also Table A-11 in Appendix V. Absence of any significant bands at around 1545 and 1640 cm^{-1} indicates that strong Brønsted acid sites, capable to protonate pyridine to pyridinium species, are not present. In general, these results are consistent with previous reports on the acidity of amorphous γ-Al_2O_3 and γ-Ga_2O_3 where pyridine adsorption revealed only the presence of relatively strong Lewis acid sites [45, 50, 68, 72]. Slight fluctuations in the positions of the above bands, observed within these studies, can be ascribed to differences in the preparation and in the thermal treatment procedures used. As reported, position and intensity of relevant bands of adsorbed pyridine can depend strongly on the specific temperature regime employed [45].

PAS-py spectra of some representative mixed oxides are shown in Figure 15A. Main bands of adsorbed pyridine remain at approximately the same positions as in single oxides, at 1493, 1579 and 1615 cm^{-1}; only the band at 1447 cm^{-1} in Al#0 is blueshifted to 1450 cm^{-1}. However, intensity of all bands associated with Lewis acid sites is increasing with increasing Ga content. In addition, appearance of two new bands, observed as shoulders at 1458 and 1621 cm^{-1}, is evident for mixed oxides with higher Ga contents, starting from Al/Ga-5 upwards (see Figure 15A). All these findings suggest that acidity of current γ-Al_2O_3/γ-Ga_2O_3 xerogels is higher than that exhibited by individual oxides, as noted in a number of previous studies [47, 50, 51, 83, 88]. Current results suggest that although the strength of the Lewis acid sites remains apparently the same, their number is increasing with increasing Ga content and at the highest Ga contents studied (Al/Ga ratios from 5 to 1) additional Lewis acid sites, presumably with higher strength, are formed. The latter presumption is supported by PAS-py spectra recorded after heating the mixed oxides with pre-adsorbed pyridine to 400 °C. As shown in Figure 16, at 400 °C pyridine is retained only on samples with higher Ga contents, *i.e.* samples Al/Ga-(1–5). Corresponding spectra are characterised by a doublet at 1451/1456 cm^{-1} and a single band at 1620 cm^{-1} suggesting the presence of Lewis acid sites with higher strength, such sites are evidently not present in mixed oxides with lower Ga contents, *e.g.* sample Al/Ga-100 in Figure 16, which, after heating to 400 °C, do not show any pyridine retention. According to the classical Tanabe model for oxides [89], acidities of solid solutions consisting of isovalent cations should not deviate considerably from the sum of the acidities of individual components. It is obvious that current mixed oxides, consisting of isovalent Al^{3+} and Ga^{3+} cations, do not fit in this model, Figure 15A.

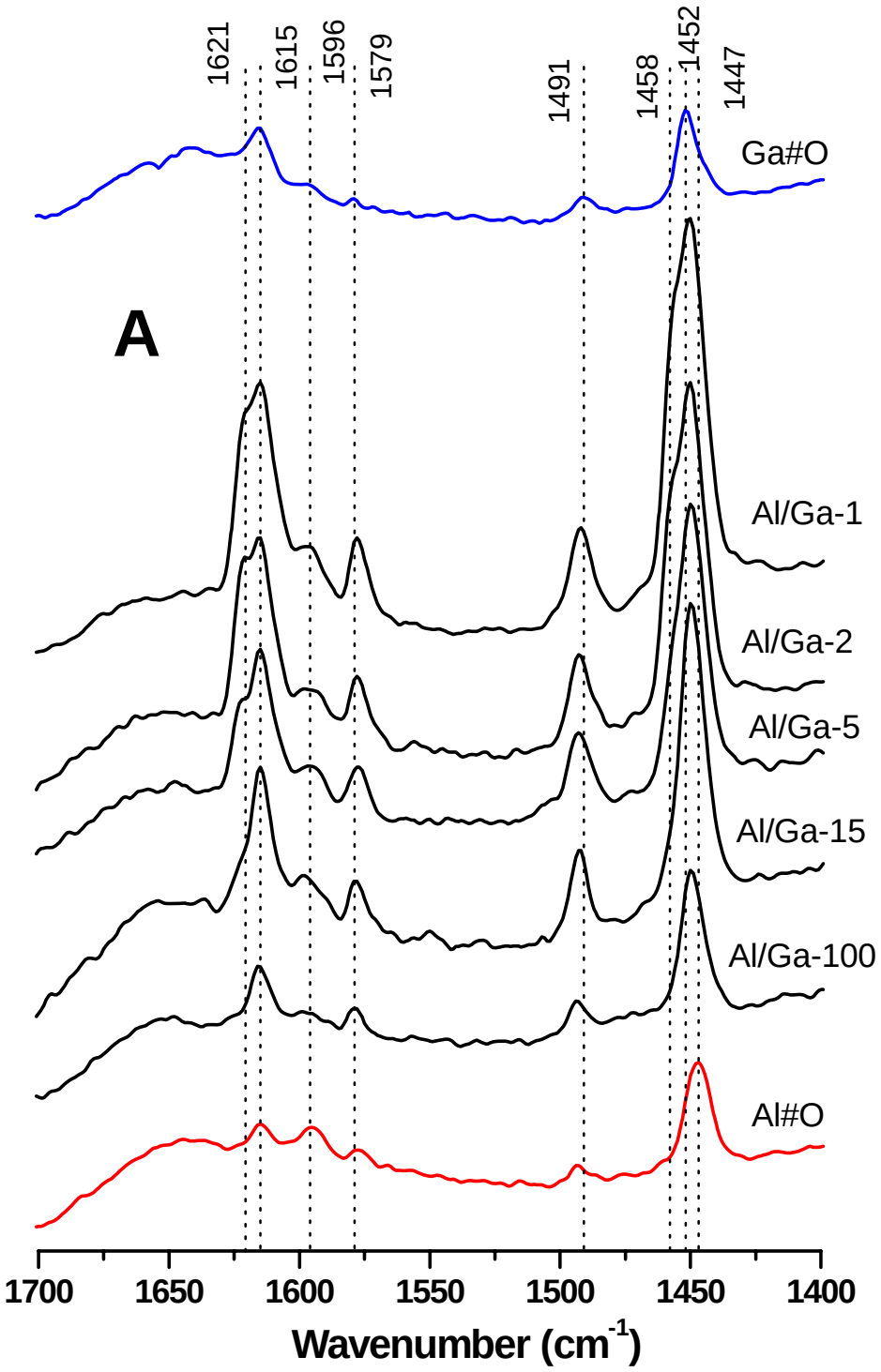
1621
1615
1596
1579
1491
1458
1452
1447
Ga#O
A
Al/Ga-1
Al/Ga-2
Al/Ga-5
Al/Ga-15
Al/Ga-100
Al#O
1700
1650
1600
1550
1500
1450
1400
Wavenumber (cm-1)

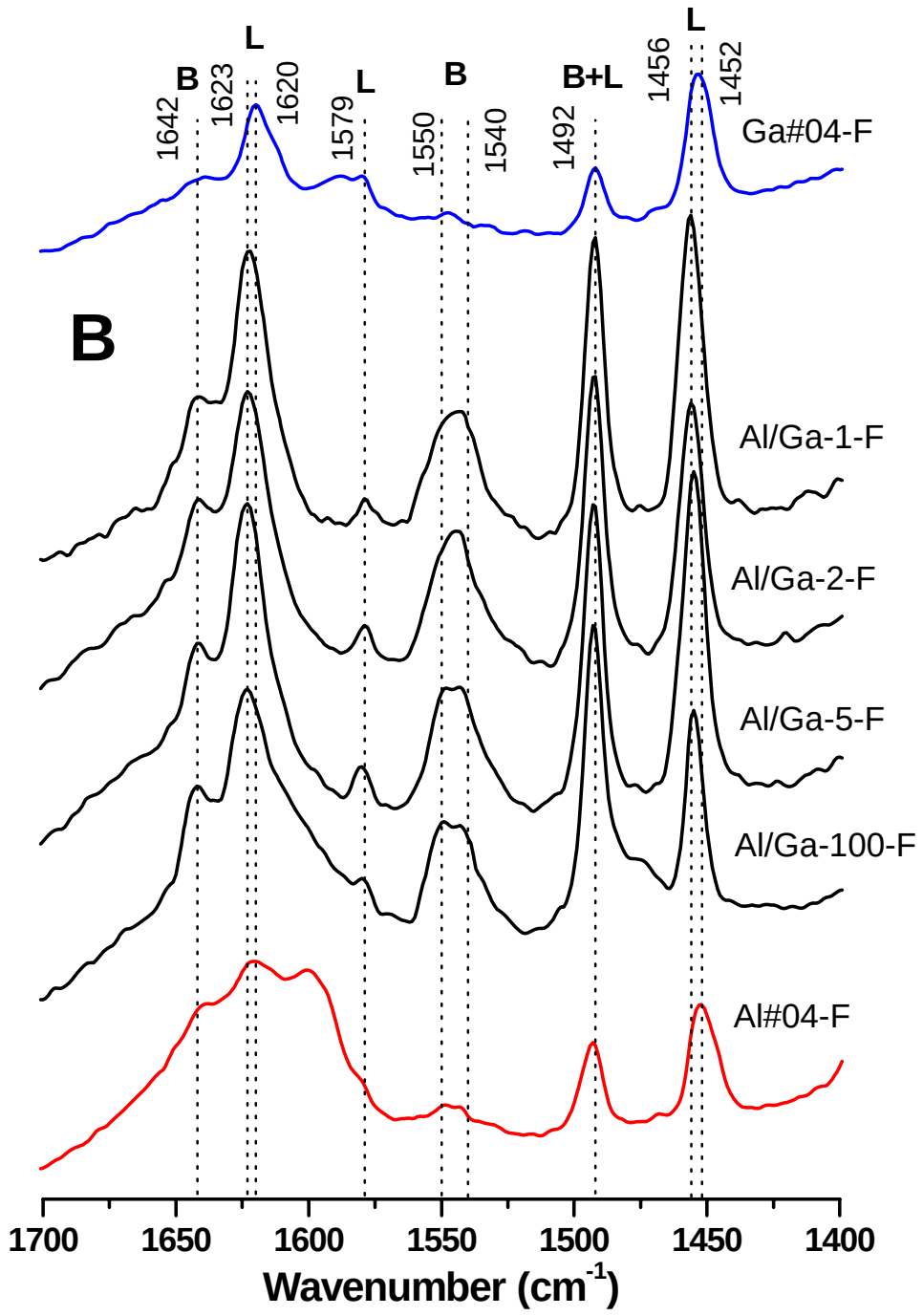

Figure 15: *Normalized PAS-py absorbance spectra (offset) of oxide precursors (A) and products after fluorination with CHF_3 at 350 °C (B)*; pyridine was adsorbed at 150 °C. In (B), bands of pyridine adsorbed on Lewis and Brønsted acid sites are marked with L and B, respectively.

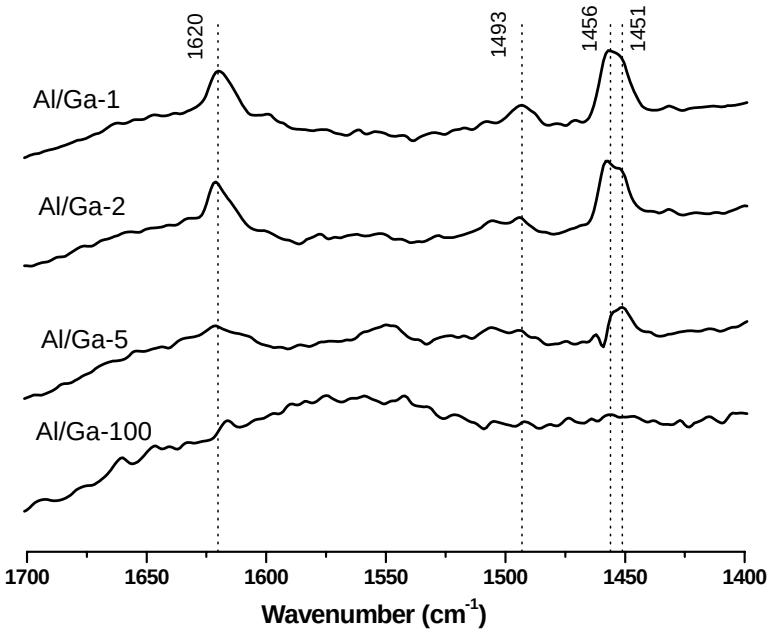

Figure 16: *Normalized PAS-py absorbance spectra (offset) of representative mixed oxide precursors*; pyridine was adsorbed at room temperature and desorbed in flow of N_2 at 400 °C.

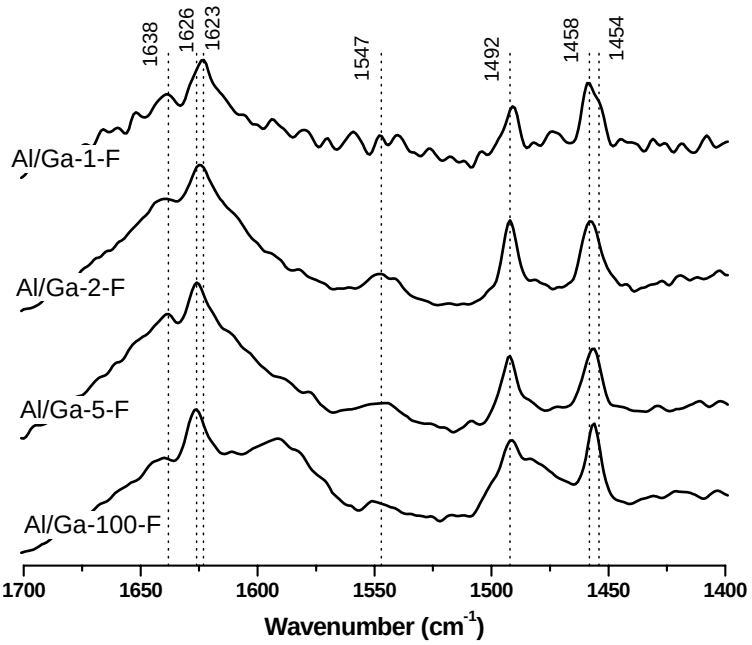

Figure 17: *Normalized PAS-py absorbance spectra (offset) of representative mixed oxides fluorinated with CHF_3 at 350 °C*; pyridine was adsorbed at room temperature and desorbed in flow of N_2 at 350 °C.

Lewis acidity of Al_2O_3 and Ga_2O_3 is in general associated with the presence of coordinatively unsaturated (cus) Al^{3+} or Ga^{3+} cations on the surface; the strongest acid sites being those originating from tetrahedral cus cations, cus-Al^{IV} and cus-Ga^{IV} [45, 72, 73, 86]. Lewis acidity of surface cus-Ga^{IV} sites in γ-Ga_2O_3 was found to be weaker than

that of the corresponding cus-Al^{IV} in γ-Al_2O_3 [45]. In the same study, density of acid sites on γ-Ga_2O_3 was higher than that on γ-Al_2O_3, presumably due to a higher tetrahedral preference of Ga^{3+} vs. Al^{3+} resulting in a higher concentration of strongly acidic cus-Ga^{IV} on γ-Ga_2O_3. In analogy with single oxides, Lewis acidity of mixed γ-Al_2O_3/γ-Ga_2O_3 is related to the presence of both types of acidic sites, cus-Al^{IV} and cus-Ga^{IV} [50, 73, 88]. However, due to the already mentioned preference of Ga^{3+} ions to occupy tetrahedral positions, there are no direct correlations between actual Al^{IV}/Ga^{IV} ratios and nominal Al/Ga ratios derived from the composition of γ-Al_2O_3/γ-Ga_2O_3 solid solutions. NMR [50, 73] and EXAFS/XANES [47, 49] investigations gave strong evidence that in these solid solutions majority of available tetrahedral positions is occupied by Ga^{3+} ions while Al^{3+} ions prevalently reside in octahedral positions. According to NMR investigations, in a solid solution with the nominal Al/Ga ratio of 1/1 (a direct equivalent to the current Al/Ga-1 sample) the Al^{IV}/Ga^{IV} ratio in the bulk is 1/2.88 vs. Al^{VI}/Ga^{VI} of 1/0.73 [73]. On the other side, IR spectroscopy of adsorbed probe molecules, like CO or pyridine, that can give a reliable information on the type and number of surface acid sites, cannot make a clear distinction between surface sites specific for cus-Al^{IV} or cus-Ga^{IV} [73, 83], as noted for CO adsorption on mixed γ-Al_2O_3/γ-Ga_2O_3 [73] and for pyridine adsorption on γ-Al_2O_3-supported Ga_2O_3 [83]. Similar low selectivity could therefore be expected also for current γ-Al_2O_3/γ-Ga_2O_3, *e.g.* spectra of pyridine adsorbed on individual γ-Al_2O_3 and γ-Ga_2O_3 are very similar with the relevant bands of adsorbed pyridine being shifted only for few cm^{-1} [45]. In amorphous or poorly crystalline mixed oxides bands of adsorbed species are additionally broadened what can lead to a considerable overlap of individual components. This may result in partially resolved or completely non-resolved composite bands.

For γ-Al_2O_3, the band at ca. 1625 cm^{-1} is assigned to pyridine being adsorbed on cus-Al^{IV} sites that are considered to be the strongest Lewis acid sites found on the surface of transition aluminas [86, 90]. By analogy, band at ca. 1622 cm^{-1} observed in current mixed oxides with higher Ga contents could tentatively be attributed to the appearance of cus-Ga^{IV} sites [90]. The reasons for the formation of such strongly acid sites only in Ga-rich samples are however not entirely clear. As reported before, strongly acidic cus-Al^{IV} sites are formed after γ-Al_2O_3 dehydration at relatively high temperatures, *e.g.* 500 °C [86]. Absence of these sites in current oxides, clearly seen in Al-rich samples, can therefore be ascribed to the lower dehydration temperature, 450 °C, used within this work. The fact that at the same treatment temperature strongly acidic cus-Ga^{IV} sites are readily formed in Ga-rich samples can be, in part, attributed to the high preference of Ga for tetrahedral vs. octahedral coordination [45, 72]. Probably more important, it appears that the preferentially formed cus-Ga^{IV} sites are efficiently stabilised within the mixed Al/Ga environments when Ga content is increasing. This assumption is somehow in line with a previous study of Ga_2O_3 supported on γ-Al_2O_3 where it was found that presence of the Al_2O_3 phase favours the formation of cus-Ga^{3+} sites [88]. In addition, increased Lewis acidity observed in Ga/Al-oxides was attributed to the formation of mixed Ga-O-Al linkages [42]. On the other side, it is known that observed concentration of the strongest cus-Al^{IV} sites on γ-Al_2O_3 is much lower than expected from its structural features, very likely due to surface reconstruction and ion-shielding effects [86]; in addition, DFT calculations suggest a spontaneous conversion of surface cus-Al^{IV} sites to quasi-bulk Al^{VI} sites with concomitant reduction in Lewis acidity [91]. It can be speculated that such reconstruction processes are apparently less effective for cus-Ga^{IV} sites in mixed Al/Ga environments what results in their higher retention on the surface. In contrast to the present results, spectra of adsorbed pyridine on a series of single and mixed Al_2O_3/Ga_2O_3 catalysts prepared by precipitation from alcoholic solutions do not exhibit any explicit double bands [50]. This indicates that composition and especially the structure of mixed

γ-Al_2O_3/γ-Ga_2O_3 surfaces may strongly depend on specific preparation and post-treatment conditions employed in different preparative approaches.

Observed increase of overall acidity in mixed oxides strongly suggests that the structure of mixed γ-Al_2O_3/γ-Ga_2O_3 surfaces is much more heterogeneous than that of the single oxides, γ-Al_2O_3 and γ-Ga_2O_3. This is also supported by TPF experiments (see Section 4.1.2.2). Mixed γ-Al_2O_3/γ-Ga_2O_3 are not typical homogeneous solid solutions. Namely, due to the preferential occupation of tetrahedral positions by Ga, they already include some structural heterogeneity. In addition, bulk structure is rather complex and includes different possible environments, M–O–M (M=Al, Ga), and coordinations, $Al^{IV+V+VI}$ and Ga^{IV+VI} [73], that all depend on the specific Al/Ga ratio. Diversity of these bulk structural features is reflected on the surface increasing its complexity and heterogeneity in comparison with single oxides. Real structures of mixed surfaces are however not known, especially with respect to possible surface reconstruction processes. Reliable modelling of surface relaxation and reconstruction processes was apparently accomplished only for γ-Al_2O_3 [91], similar calculations for mixed γ-Al_2O_3/γ-Ga_2O_3 surfaces are still missing.

4.1.3.2 PAS-py of fluorinated products

PAS-py spectra of single and mixed oxides fluorinated with CHF_3 at 350 are shown in Figure 15B. In addition to bands associated with Lewis acid sites, located at 1453–1456, 1492, 1579 and 1620–1623 cm^{-1}, spectra also reveal bands at 1492, 1540–1550 and 1642 cm^{-1} that are characteristic for pyridine interacting with strong Brønsted acid sites. Close similarity of current spectra with those reported earlier for $CHClF_2$-fluorinated γ-Al_2O_3 [68] indicates that both fluorinating agents, CHF_3 and $CHClF_2$, yield fluorinated products with very similar surface characteristics. This is somehow consistent with previous XPS investigations, where comparable fluorinating capabilities of both fluorocarbons towards γ-Al_2O_3 were observed; CHF_3 was however found to be more efficient than $CHClF_2$ in fluorinating a model γ-Al_2O_3 catalyst [92]. For the current fluorinated products, comparison of PAS-py spectra with those of corresponding oxide precursors (Figures 15A and 15B) demonstrates that after fluorination all relevant bands associated with Lewis acidity, *e.g.* bands at around 1450 and 1615 cm^{-1}, are blue-shifted. This is commonly explained by strengthening of Lewis acid sites through inductive effects due to the replacement of O- and OH-species with strongly electronegative F [68]. As is the case for mixed oxide precursors, bands of adsorbed pyridine in fluorinated mixed oxides are more intense and blue-shifted, for approximately 3 cm^{-1}, with respect to fluorinated single oxides. This suggests that both the number and the strength of Lewis acid sites of fluorinated mixed oxides are higher. In addition, double bands observed in Ga-rich mixed oxides disappear after fluorination, suggesting a partial reduction in heterogeneity of the Lewis acid sites. Increased acidity after fluorination is confirmed also by PAS-py spectra after pyridine desorption at 350 °C. Related spectra are shown on Figure 17. As expected, such treatment considerably reduces the Brønsted acidity and reveals the presence of strong Lewis acid sites with corresponding bands positioned at 1456–1458 and 1623–1626 cm^{-1}. In comparison with the similarly treated mixed oxides (see Figure 16), fluorinated Ga-rich mixed oxides exhibit only a slight blueshift of 1–2 cm^{-1}, indicating a relatively low effect of fluorination on acidity. On the other side, Al-rich samples, which as oxides do not show any considerable Lewis acidity, in their fluorinated form exhibit the presence of strong Lewis acid sites; most notable is the occurrence of the band at 1626 cm^{-1}. Position of this band is close to the band at 1628 cm^{-1} found in $AlF_{2.6}(OH)_{0.4}{\cdot}nH_2O$ (n=0.1–0.2) [93] and band at 1627 cm^{-1} for the $AlF_{3-x}(OH)_x$-type of compounds [94]. For these compounds with hexagonal tungsten bronze (HTB) structure the indicated bands

were associated with the presence of very strong Lewis acid sites related to cus-Al^{3+} ions. It is therefore reasonable to conclude that in the current fluorinated Al-rich samples strong Lewis acid sites originate prevalently from cus-Al^{3+} ions in various O/F environments. In Ga-rich samples, concentration of strong cus-Al^{3+} sites is lower due to the preferential formation of cus-Ga^{3+} ions which in turn exhibit lower Lewis acidity [45]. In addition, pyridine adsorption on HTB hydroxyfluorides of the type, $MF_{3-x}(OH)_x \cdot nH_2O$ (M=Al or Ga), revealed a higher Lewis acid strength of the Al-containing compound [80].

It should also be mentioned that besides the observed increase of Lewis acid strength, fluorination apparently lowers the heterogeneity of these surface sites, as suggested by the disappearance of double bands and by band narrowing. PAS-py spectra of mixed oxides (see Figure 15A) show that the width of the bands related to Lewis acid sites is increasing with increasing Ga-content, *i.e.* full width at half maximum (FWHM) of the band at ca. 1452 cm^{-1} is increasing from 10 cm^{-1} for Al/Ga-100 to 15 cm^{-1} for Al/Ga-1. This can be correlated with the formation of various new acid sites in Ga-rich oxides, as mentioned above. Observed FWHM of the corresponding bands in fluorinated oxides is lower, *i.e.* 7 cm^{-1} for Al/Ga-100-F and 10 cm^{-1} for Al/Ga-1F. Relative narrowing of these bands after fluorination indicates that some structure reconstruction and ordering is probably taking place, although at levels that are, at least in the initial stages, not detectable by XRD (see Figure 8, trace f). Namely, a recent TEM study clearly demonstrated that AlF_3-based materials, despite being completely amorphous to X-rays, may contain well-ordered regions consisting of nanocrystalline fluoride phases [77].

In summary, fluorination of mixed γ-Al_2O_3/γ-Ga_2O_3 increases the strength of Lewis acid sites due to the partial replacement of O/OH with F, and apparently reduces the heterogeneity of these sites due to some structural ordering. Similarly to the situation encountered with mixed oxides (Section 4.1.3.1), acidity of fluorinated mixed oxides is considerably higher than that exhibited by fluorinated single oxides, Figure 15B. Also in this case, such synergetic effects in mixed materials seem to contradict the Tanabe model [89]. Namely, validity of the Tanabe model was confirmed for a number of mixed metal fluorides; accordingly, no synergetic effects on acidity were observed for solid solutions of diverse isovalent M^{3+} fluorides [95].

4.1.3.3 XRD investigations

XPS was applied in order to get insights into surface chemistry of samples Ga#0, Al/Ga-1 and Al/Ga-2 before and after treatment with CHF_3. The sample Al/Ga-15 was measured by XPS only after treatment with CHF_3 (Al/Ga-15-F). Surface concentrations were calculated from the XPS spectra and are given in Table 2. As it can be seen carbon is present on the surface of all samples probably due to adventitious carbon species related with the exposure of samples to air atmosphere. Surface composition of the oxide precursors is roughly consistent with their nominal composition, *i.e.* concentration of Al on Al/Ga-2 is approximately two times higher than on sample Al/Ga-1. After treatment with CHF_3 all samples contain F. The highest concentration of F, ~35 at.%, was found on the Ga#4-F sample. Treatment of mixed Al/Ga-oxides with CHF_3 resulted in lower F concentrations which were about 13 at.%. Incorporation of F is accompanied by a clear decrease of surface O concentrations. This reflects the reaction of substitution of oxygen atoms by fluorine atoms.

Interesting parameter which was changing during CHF_3 treatment is the ratio between surface Al and Ga atoms (see Table 2). As expected, the Al/Ga ratio for the mixed oxide Al/Ga-2 is about two times higher than for Al/Ga-1. However, comparison of nominal and measured Al/Ga ratios shows that surfaces of mixed oxides are enriched with Al. Similar results were also obtained in some related studies [50, 64]. This suggests that in

mixed Al/Ga-oxides surface relaxation and reconstruction processes are very likely cation-specific. Inverse process was observed after treatment with CHF_3; the Al/Ga ratio decreased nearly by factor of two with respect to the un-treated mixed oxides. This means that surfaces of CHF_3-treated oxides are enriched by Ga with respect to Al. At the same time the F/Al ratios (see Table 2) remain very similar for all three samples analysed. These observations can be interpreted as formation of the Al–F based phases in the subsurface region what lefts Ga–O phases enriched on the surface.

Table 2: *Surface concentration (in at.%) determined by XPS for the analysed oxide precursors and fluorinated products*

Sample	Surface concentration, at.%					Al/Ga (nominal / measured)	F/Al
	C	O	Ga	Al	F		
Ga#0	37.4	45.5	17.2	-	-	-	-
Ga#04-F	27.6	20.6	17.1	-	34.9	-	-
Al/Ga-1	31.2	48.3	7.8	12.7	-	1 / 1.6	-
Al/Ga-1-F	15.1	40.0	16.7	15.7	12.7	1 / 0.9	0.81
Al/Ga-2	19.2	55.9	7.0	20.3	-	2 / 2.9	-
Al/Ga-2-F	20.6	41.5	9.1	16.2	12.7	2 / 1.8	0.78
Al/Ga-15-F	18.9	43.5	2.1	17.6	13.4	15 / 8.6	0.76

In order to understand chemical bonding at sample surfaces before and after CHF_3 treatment, high resolution XPS spectra were acquired which are presented in Figure 18 for Ga#0 and Ga#04-F, and in Figure 19 for Al/Ga-1 and Al/Ga-1-F. XPS results show that fluorination of pure Ga_2O_3, Ga#0 sample, leads to two types of Ga chemical environments; Ga_2O_3 and Ga–F (see Figure 19). This was recognized from the Ga 2p and Ga 3d spectra. On pure Ga_2O_3 sample Ga 2p is at 1118.0 eV and Ga 3d is at 20.0 eV. Energy of 20.0 eV for the Ga 3d peak is characteristic of Ga^{3+} oxidation state, what can be expected for Ga_2O_3 [96, 97]. After fluorination new peaks appear in addition to previous ones: in Ga 3d spectrum at 22.0 eV and in Ga $2p_{3/2}$ spectrum at 1119.5 eV. These new peaks can be related with the formation of Ga–F bonds, as suggested in literature [97, 98]. This shows that partial fluorination of Ga_2O_3 occurred, what follows also from appearance of F at the surface (see Table 2). On fluorinated Ga#04-F, F 1s spectrum (see Figure 19) is asymmetric towards low binding energy side. This can be interpreted as a presence of two peaks at 686.5 eV and 684.0 eV indicating two types of F-sites. In literature the main peak is attributed to fluoride species and the second peak to different F/O environments, where the presence of O causes redistribution of electron density [41]. Oxygen O 1s spectra show broad structure with a maximum at around 531.8 eV. This is related with oxygen atoms bound in oxide matrix. The O 1s spectra are also asymmetric towards higher binding energy (532–533 eV), what is characteristic for hydroxides and adsorbed water.

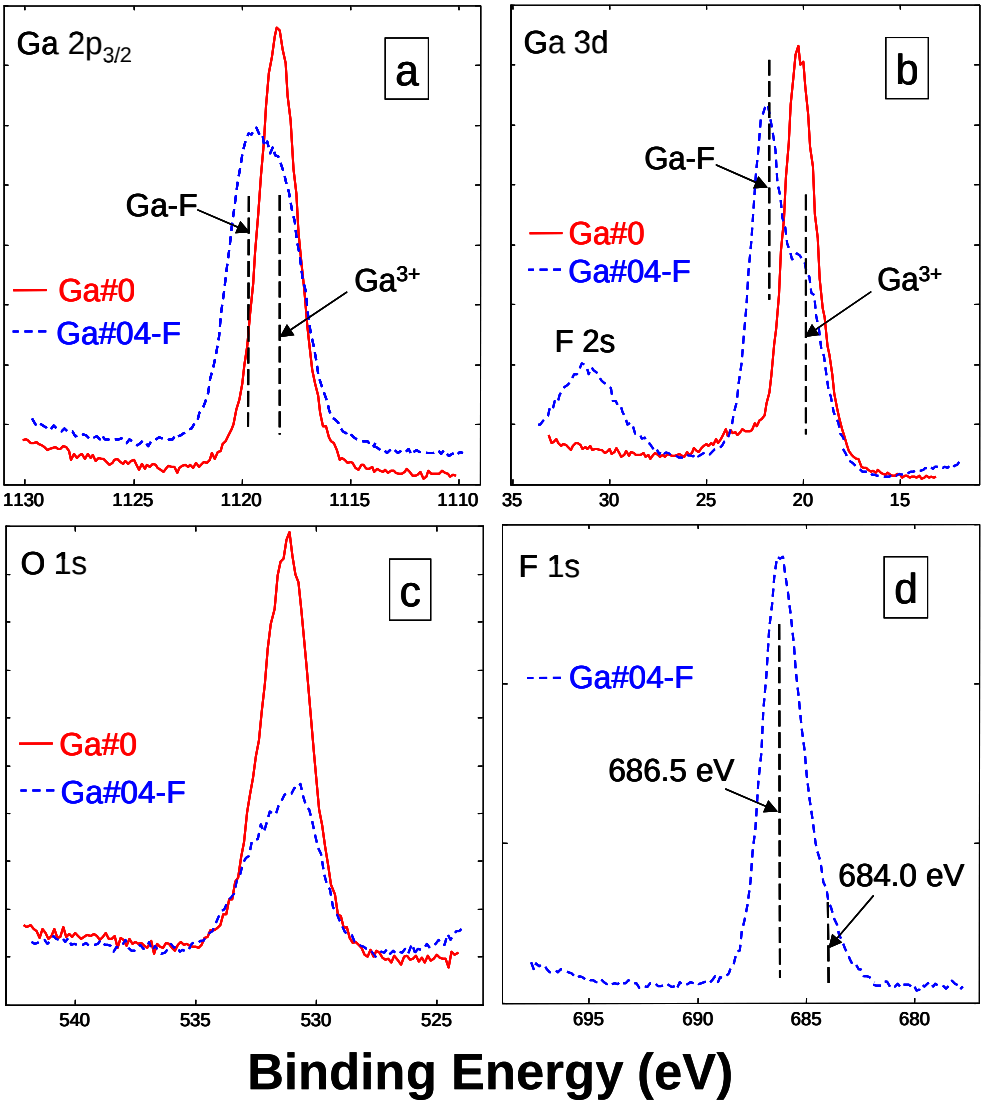

Figure 18: *XPS spectra of Ga 2p (a), Ga 3d (b), O 1s (c) and F 1s (d) for γ-Ga_2O_3 (Ga#0) and its fluorinated product (Ga#04-F)*. Y-axes present photoemission intensities.

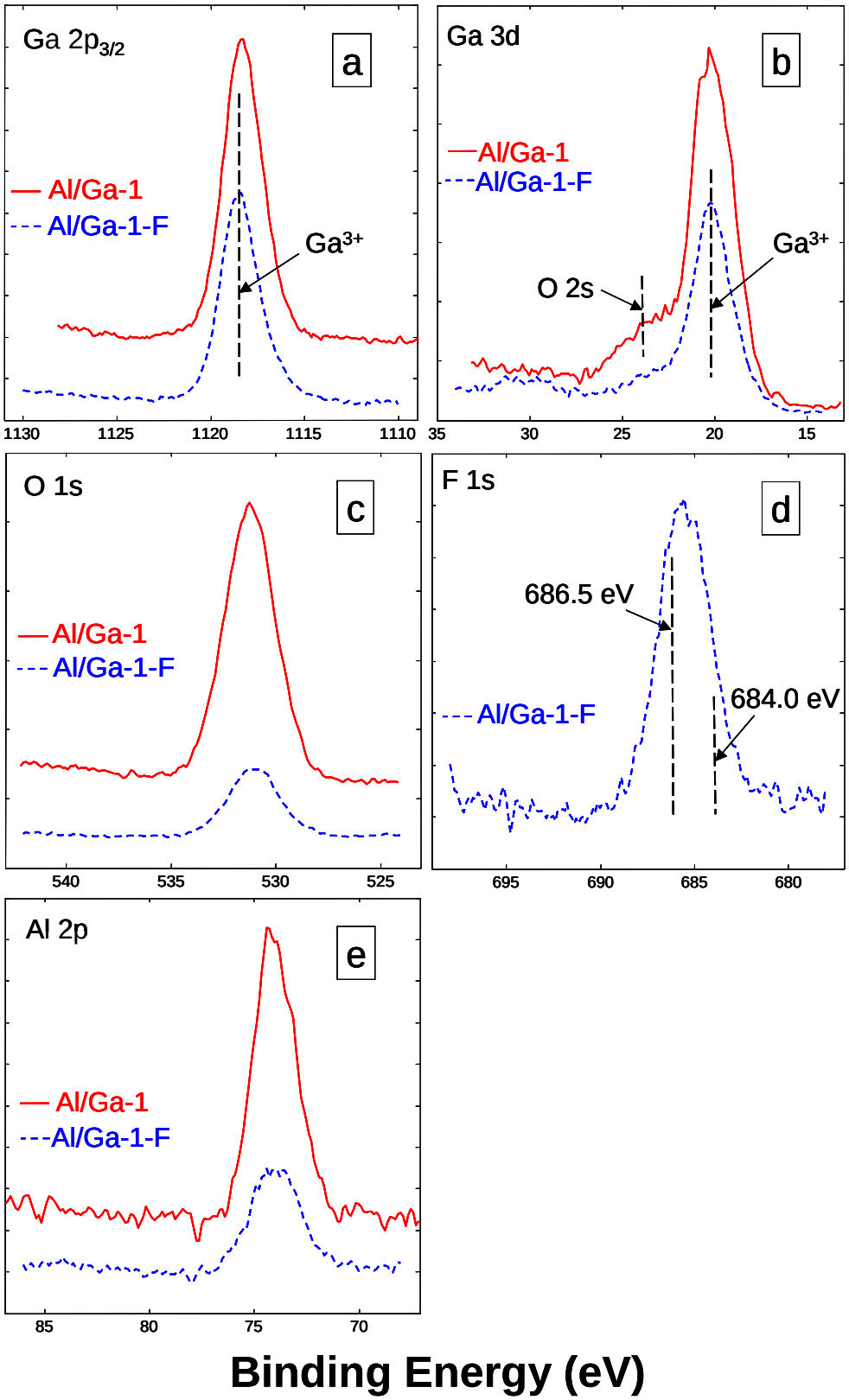

Figure 19: *XPS spectra of Ga 2p (a), Ga 3d (b), O 1s (c), F 1s (d) and Al 2p (e) for mixed oxide (Al/Ga-1) and its fluorinated product (Al/Ga-1-F).* Y-axes present photoemission intensities.

Similar XPS characterisation was performed on representative mixed oxides. XPS spectra of Al/Ga-1 and Al/Ga-2 were quite similar. Only XPS spectra of Al/Ga-1 before and after fluorination with CHF_3 are therefore shown in Figure 18. The most noticeable feature of these spectra is that peaks at 22.0 eV and at 1119.5 eV, observed in Ga 2p and Ga 3d spectra of the CHF_3-treated Ga_2O_3 (Ga#04-F in Figure 18), are not present. This indicates that Ga-atoms in mixed oxides are not involved to a greater extent in direct interactions with F. Ga 3d peak at 20.0 eV is characteristic for the Ga^{3+} oxidation state in oxides. In addition, XPS does not reveal any reduction to $Ga^{<3+}$ states, presence of the latter should be recognized as a shift in XPS spectra towards lower binding energies [96, 97]. XPS spectrum of Al 2p is shown in Figure 19. The main peak Al 2p is at 74.0 eV what is characteristic for Al^{3+} in oxides [96]. Small shift towards higher binding energy of Al 2p peak of 0.5 eV was only observed after fluorination which may be related with an AlF_3-like environment as observed in literature [41]. XPS spectrum of F 1s for fluorinated mixed Al/Ga-oxides is broader than on fluorinated Ga_2O_3 (see Figures 18 and 19). This may be due to presence of two peaks at 686.5 eV and 684.0 eV that can be related to fluoride species and mixed F/O environments, respectively. Additional reason for peak broadening could be a larger degree of disorder in the structure of fluorinated mixed oxides. Our XPS results discussed above show that during the treatment of mixed Al/Ga-oxides with CHF_3 mainly Al-atoms form bonds with F-atoms while Ga-atoms remain prevalently in O environments. XPS results also suggest that fluorinated mixed oxides are more disordered as fluorinated single oxides what is in line with IR results discussed below. Similar features of O 1s spectra as described above are present also in O 1s spectra for mixed oxides.

4.1.3.4 Surface hydroxyls

PA-FTIR spectra of γ-Al_2O_3/γ-Ga_2O_3 xerogel precursors and their fluorinated products are shown in Figures 20A and 20B, respectively. All spectra are characterised by a very broad band in the 3800–2700 cm^{-1} region that is characteristic for different O–H stretching vibrations. This suggests the presence of a large variety of surface and bulk hydroxyl groups. For oxides, maximum of this band is located at 3520 cm^{-1} for the Al-rich oxide xerogel (Al/Ga-100) and is gradually shifted to 3370 cm^{-1} for the Ga-rich xerogel (Al/Ga-1). Intensity of this band is somewhat lower for the fluorinated materials what can be ascribed to partial OH/F replacement as a result of fluorination. In this case the maxima are less pronounced and are located at around 3480 cm^{-1}. Another and relatively sharp band, located at about 1640 cm^{-1} for oxides and 1635 cm^{-1} for fluorinated products, can be assigned to the deformation mode of molecular water. It is remarkable that the position of this mode shows a relatively low dependence on the gallium content in the γ-Al_2O_3/γ-Ga_2O_3 samples as well as on fluorination. These findings indicate that hydration and hydroxylation in oxide precursors and in fluorinated products may be substantial. For the fluorinated products this is in line with chemical analysis that shows partial fluorination as well as with XPS and XRD investigations that both confirm the presence of OH groups and discrete H_2O. At relatively low fluorination temperatures employed within this work part of the H_2O formed is very likely retained within the solid products. Additional source of H_2O, although quantitatively probably much less important, is adsorption during the transfers required to obtain FTIR spectra. A clear differentiation between the oxygen species originating from these two sources and their relative quantification is therefore not possible.

As mentioned in Section 4.1.2, aged fluorinated γ-Al_2O_3/γ-Ga_2O_3 crystallise in the form of a pyrochlore type $Al(F,OH)_3 \cdot nH_2O$ (Figure 8). This process is very likely promoted by adventitious water adsorption during storage and manipulation. Comparison

of the PA-FTIR spectra of the as-prepared and aged Al/Ga-100-F is given in Figure 21 (traces A and B). Spectrum of the aged Al/Ga-100-F differs from that of the as-prepared Al/Ga-100-F by the appearance of two relatively very sharp and intense bands located at 3679 and 1102 cm^{-1}. Similar sharp bands were observed for $Al(F,OH)_3$ with a hexagonal tungsten bronze (HTB) structure derived from a HTB β-AlF_3 [45, 93]. For this class of hydroxyfluorides, sharp bands at 4772, 3669, and 1130 cm^{-1} were ascribed to combination, stretching, and deformation modes of bridging (isolated) OH groups located in the channels of the HTB $Al(F,OH)_3$ structure. Sharp bands observed within the current work can be assigned to similar type of specific isolated bridging OH groups. Observed shifts from the bands found for the HTB $Al(F,OH)_3$, *i.e.* 3669 vs. 3679 and 1130 vs. 1102 cm^{-1}, can be associated with the pyrochlore structure of the current $Al(F,OH)_3 \cdot nH_2O$ phases as well as with the presence of Ga^{3+} ions that can replace some of the Al^{3+} ions in the crystal lattice altering slightly their structures.

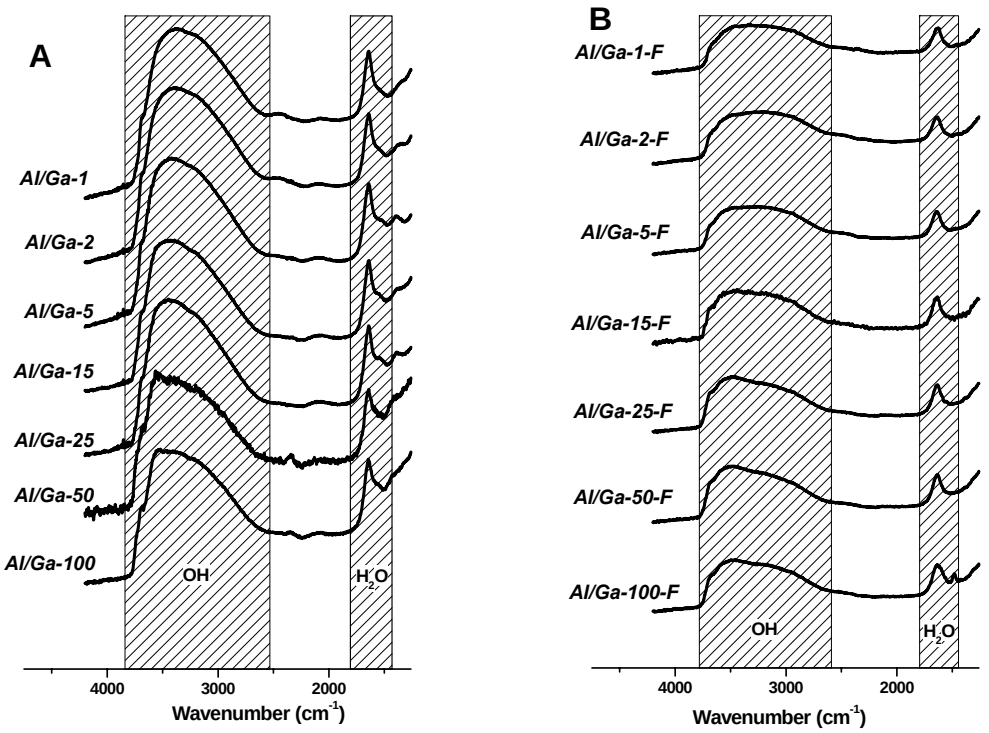

Figure 20: *Normalised PA-FTIR absorbance spectra of oxide precursors (A) and freshly fluorinated γ-Al_2O_3/γ-Ga_2O_3 xerogels (B).*

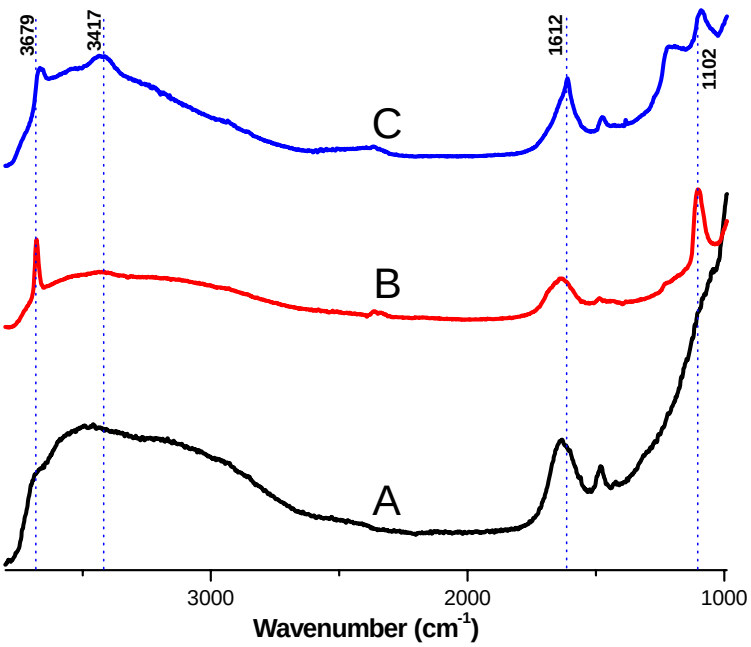

Figure 21: *Normalised PA-FTIR absorbance spectra of Al/Ga-100-F*; as prepared (A), aged for several months under limited contact with ambient air (B), aged material heated at 250 ºC under dynamic vacuum (C).

Intensity of the two bands at 3679 and 1102 cm^{-1} which are associated with the isolated bridging OH groups in the current pyrochlore $Al(F,OH)_3 \cdot nH_2O$ is considerably reduced after treatment under dynamic vacuum at 250 °C (Figure 21, trace C). This indicates that the structure of these hydroxyfluorides is thermally less stable and can be partially destroyed at relatively low temperatures. Such thermal behaviour is somehow in contrast with that of the above mentioned HTB $Al(F,OH)_3$ which shows just an opposite trend when activated at 300 °C [93].

4.1.3.5 Catalytic behaviour in isomerisation of CCl_2FCClF_2

Isomerisation of CCl_2FCClF_2 with subsequent dismutation reactions is frequently used as a model catalytic reaction to complement spectroscopic and other methodologies to evaluate the acidity of metal fluoride catalysts [35, 41, 42, 99, 100]. A number of such studies was carried out on AlF_3-based catalysts what allowed rather consistent comparisons between these solids, although their origin and characteristics varied significantly [41, 99]. Accumulated data strongly suggest that on these solids isomerisation of CCl_2FCClF_2 to the thermodynamically preferred isomer, CCl_3CF_3, is facile and occurs via an intramolecular mechanism on medium strong or strong Lewis acid sites (Eq. 10) [35, 81, 99, 100]. Isomerisation is accompanied by consecutive dismutation processes involving CCl_3CF_3 (Eq. 11) and CCl_2FCF_3 (Eq. 12) with the latter being less facile than the former. Formation of $CClF_2CF_3$ is therefore observed only with very active catalysts and at higher temperatures [41, 71], as observed also in this work (Table 3).

$$CCl_2FCClF_2 \rightarrow CCl_3CF_3 \quad (10)$$

$$2CCl_3CF_3 \rightarrow CCl_2FCF_3 + CCl_3CClF_2 \quad (11)$$

$$2CCl_2FCF_3 \rightarrow CClF_2CF_3 + CCl_3CF_3 \quad (12)$$

Results of CCl_2FCClF_2 isomerisation tests performed on fluorinated single oxides and two representative mixed oxides are summarised in Table 3. For both fluorinated Al-rich oxides, single Al#04-F, and mixed Al/Ga-100-F, catalytic behaviour is very similar indicating that catalytic functionality is not altered to a greater extent at low Ga levels. However, a slight reduction in catalytic activity, characterized by a slightly lower CCl_3CF_3 yields and considerably lower $CClF_2CF_3$ yields, is observed already with small Ga additions, *i.e.* in Al/Ga-100-F with Al/Ga ratio of 100/1. It should be noted that general catalytic behaviour of the two Al-rich materials is very similar to that exhibited by fluorinated commercial γ-Al_2O_3 with considerably higher fluorine content used as a reference in a previous comparative study [41]. On the other side, further increase of Ga content strongly reduces catalytic activity w.r.t. CCl_2FCClF_2 isomerisation, as observed for the mixed Al/Ga-2-F. In line with this trend, fluorinated γ-Ga_2O_3, Ga#04-F, was catalytically completely inactive over the whole temperature range tested. In analogy with similar γ-Al_2O_3 systems, this could be ascribed to the low extent of fluorination, *i.e.* 3.6 wt.% of F (see Table 1), that may be below the levels required to form sufficiently active surface sites. Namely, as found for fluorinated γ-Al_2O_3, approximately 10 atom% of anions must be replaced by F to achieve catalytic activity in dismutation of $CHClF_2$ [92]. However, this reason can be ruled out since a low catalytic activity was observed also for the fluorinated mixed oxide with considerably higher F content, *i.e.* Al/Ga-2-F with 16.9 wt.% of F. This strongly suggests that, in contrast to the Al-sites, the Ga-related Lewis acid sites are not strong enough to catalyse the isomerisation of CCl_2FCClF_2. Furthermore, these findings also indicate that with increasing Ga levels the catalytic functionality of strong Al-related sites drops considerably. Higher levels of Ga do not simply lower the concentration of strong Al-relates sites, but also obstruct their formation by preferential formation of Ga-sites, as suggested on the basis of PAS-py measurements mentioned above (see Sections 4.1.3.1 and 4.1.3.2).

Catalytic tests also show that all active materials examined, Al#04-F, Al/Ga-100-F and Al/Ga-2F, need a clear activation period in a stream of CCl_2FCClF_2 before they reach full catalytic activity. For the AlF_3-based catalysts, activation is associated with the removal of surface species that block Lewis acid sites. These species mostly originate from H_2O adsorption that besides blocking the Lewis acid sites leads to some hydrolysis and generates Brønsted acidity [78, 81]. Activation of AlF_3-based catalysts, most frequently performed in situ by diverse fluorocarbons, can therefore be regarded as a re-fluorination process in which surface OH species are replaced by F. For the current fluorinated γ-Al_2O_3, sample Al#04-F, onset of catalytic activity is observed already at 300 °C, while for the activation of both fluorinated mixed oxides, Al/Ga-100-F and Al/Ga-2-F, temperature of 350 °C is required. Observed behaviour during activation correlates very well with much higher Brønsted acidity of the fluorinated mixed oxides in comparison with the single ones, as evidenced by PAS-py investigations (see Figures 15A and 15B).

Observed differences in catalytic performance of fluorinated Al- and Ga-rich mixed oxides do however not correlate with PAS-py observations. As noted above, PAS-py spectra of fluorinated single and mixed oxides, Figures 15A and 15B, indicate the presence of Lewis acid sites that appear to be stronger in fluorinated mixed oxides. For the Al-rich mixed oxides these sites were associated with cus-Al^{3+} ions, which are replaced by cus-Ga^{3+} ions in Ga-rich materials. Lower catalytic activity of the latter would therefore suggest that catalytic isomerisation of CCl_2FCClF_2 is taking place only on cus-Al^{3+} sites and not on cus-Ga^{3+} sites. The corresponding redshifts in PAS-py spectra are however very low, 1–2 cm^{-1} for the band at 1626 cm^{-1} (see Figures 15A and 15B), that does not allow an unequivocal assignment of these bands to specific cationic sites. In addition, recent XPS and *ab initio* investigations of AlF_3 materials stressed that

Lewis acidity and catalytic activity can depend decisively on local geometric structure and stoichiometry, and not just on local coordination [78]. Furthermore, accessibility of active sites for both probe molecules, pyridine and CCl_2FCClF_2, may be different.

Table 3: *Reaction of CCl_2FCClF_2 in contact with fluorinated single and representative mixed oxides under steady flow conditions*; contact time 1 s, GC analyses done after 1 h equilibration at the temperature specified

Sample	Temp.[a], °C	Product distribution, relat. yield, %				
		$CClF_2CF_3$	CCl_2FCF_3 + $CClF_2CClF_2$[b]	CCl_2FCClF_2	CCl_3CF_3	CCl_3CClF_2
Ga#04-F	300*	0	0	100	0	0
	320*	0	0	100	0	0
	350*	0	0	100	0	0
Al/Ga-2-F	300*	0	0.5	99.5	0	0
	320*	0	1.5	98.2	0	0.4
	350*	0	7.2	84.0	3.3	5.5
	320	0	5.4	88.7	2.3	3.5
	300	0	3.5	94.8	0.4	1.4
	250	0	0.4	99.4	0	0.3
Al/Ga-100-F	300*	0	0	99.7	0	0.3
	320*	0	0.1	99.0	0	0.9
	350*	0.2	19.9	12.5	54.8	12.7
	320	0.3	19.5	3.4	70.6	6.2
	300	0.1	18.4	3.3	71.7	6.4
	250	0	18.4	18.6	55.5	7.5
Al#04-F	250*	0	0	100	0	0
	300*	0.3	22.4	2.9	71.3	3.1
	320*	0.3	19.7	3.2	71.4	5.3
	350*	0.6	24.0	3.9	67.1	4.3
	320	0.3	17.6	3.2	70.8	8.2
	300	0.2	16.5	2.8	73.6	6.8
	250	0	13.2	19.1	57.0	10.7

[a] Steps in the initial (activation) stage are marked with *.
[b] The two isomers could not be separated by GC. Previous studies showed that the asymmetric isomer, CCl_2FCF_3, largely prevails [35].

4.2 Interaction of CHF_3 with alkali hydroxides and alkali carbonates

4.2.1 Reaction under static conditions

Heterogeneous reactions between CHF_3 and different solid reactants under static isothermal conditions were studied in a batch reactor. Solid reactants used within this work, reaction conditions and compositions of the products are listed in Table 4. Majority of tests was performed with excess of CHF_3 to determine the fluorination end state achievable under the varying conditions. Extent of fluorination derived from the fluoride content of the solid products was used as a measure to compare the relative activities of various solids in the reaction with CHF_3.

Sodium hydroxide, NaOH, as the most common alkali hydroxide, was investigated in more details. Both temperature and the initial pressure of CHF_3 were varied to determine the influence of these two parameters on the CHF_3 decomposition reaction. Temperature was found to be a decisive factor in NaOH fluorination (tests NaOH-(1–7)). At temperatures up to 100 °C the extent of fluorination was very low. In the temperature range 100–150 °C an abrupt onset of the reaction was observed, afterwards the extent of fluorination increased steadily with increasing temperature. The highest extent of fluorination, corresponding to an almost complete (99 %) conversion to NaF, was achieved at the highest temperature investigated; 350 °C (sample NaOH-7, Table 4). This test was performed above the melting point of NaOH (323 °C). In contrast to temperature, fluorination was not significantly affected by pressure, at least within the pressure range investigated (tests NaOH-(9–13)). Behaviour of the investigated alkali hydroxides showed clear differences within the series. At the arbitrarily selected intermediate fluorination temperature of 250 °C, conversion to the corresponding fluorides was 51.8 % for LiOH, 71.8 % for NaOH and 93.3 % for KOH, suggesting that the activity of alkali hydroxides towards CHF_3 varied in the order KOH > NaOH > LiOH. It should be noted that these findings perfectly correlate with the results of temperature programmed flow experiments described in Section 4.2.2. For the only alkaline earth hydroxide investigated within this work, $Ca(OH)_2$, conversion to fluoride was similar to that found for LiOH.

Crystalline phases in samples after fluorination were determined by using powder XRD. Diffractograms of some NaOH samples treated by CHF_3 at different temperatures are shown in Figure 22. Products obtained at temperatures below 150 °C consist of the unchanged NaOH phase what is in line with the very low fluoride content determined by chemical analyses (see Table 4). Onset of fluorination at 150 °C results in the formation of crystalline NaF. Well crystallised NaF is observed in all highly fluorinated samples obtained at higher temperatures. In the intermediate temperature region, 150–250 °C, solid products are a mixture of NaF, minor quantities of sodium carbonate, Na_2CO_3, and non-reacted NaOH (see Figure 22, samples NaOH-3 and -5). Na_2CO_3 is formed from NaOH and CO_2, the latter is one of the gaseous side products that can be formed under the specific conditions encountered in the batch reactor (see Section 4.2.1.1). Gradual decrease of the Na_2CO_3 content at temperatures above 150 °C is the result of Na_2CO_3 fluorination. As mentioned above, separate experiments with carbonates indicated that fluorination of Na_2CO_3 with CHF_3 becomes relevant above 250 °C. In addition, experiment performed with excess of NaOH, *i.e.* under limited fluorination conditions, demonstrated that a considerable amount of Na_2CO_3 was also present after treatment at 250 °C (sample NaOH-8, Figure 23). XRD results of LiOH and KOH fluorination at 250 °C are consistent with chemical analyses (see Table 4) and indicate the formation of the corresponding well crystallised fluorides that are the main crystalline phases detected

(samples LiOH and KOH, Figure 24). Contrarily, no crystalline fluoride phases could be detected in CHF_3-treated carbonates (not shown). This can be associated with the relatively low extent of fluorination obtained with carbonates at 250 °C (see Table 4). It is very likely that at these levels the formed fluoride phase is highly dispersed and prevalently amorphous, and can therefore not be detected by XRD.

In contrast to hydroxides, alkali carbonates exhibited much lower activities towards CHF_3 at 250 °C with typical conversions to fluorides that are almost two orders of magnitude lower as those obtained by the corresponding hydroxides (see Table 4). Slightly higher conversions were obtained with some alkaline earth carbonates. As was the case with hydroxides, fluorination of carbonates was also strongly temperature dependent; for example, conversion of Li_2CO_3 to LiF increased from 0.12 % at 250 °C to 97.9 % at 400 °C (samples Li_2CO_3-1 and -2, Table 4). Reactions in the higher temperature range were however outside the scope of the present work and were not investigated in further details. Other salts tested, sodium sulphate, Na_2SO_4, and sodium oxalate, $Na_2C_2O_4$, were found to be practically inactive towards CHF_3 at 250 °C. Observed inactivity of $Na_2C_2O_4$ towards CHF_3 is in line with previous study [56] where it was found that $Na_2C_2O_4$ reacts with perhalocarbons (CFCs) but not with partially halogenated compounds. It was suggested that in the reaction between CFCs and $Na_2C_2O_4$ the latter acts as a two-electron transfer agent to the fluorocarbon while the cation acts as an acceptor for the fluoride ion. On the other side, partially halogenated compounds are insufficiently powerful electron acceptors and do therefore not react with $Na_2C_2O_4$.

SEM micrographs of some representative samples before and after fluorination with CHF_3 are shown in Figures 25 and 26. Fluorination of NaOH resulted in large morphological changes; initial NaOH (see Figure 25A) was converted to relatively uniformly shaped and loosely interconnected μm particles (see Figure 25B). According to chemical analyses and XRD measurements it can be concluded that these newly formed particles consist of crystalline NaF. Fluorination at higher temperatures that leads to an almost complete NaOH to NaF conversion is accompanied by a distinctive crystal growth; at 250 °C 1–3 μm particles prevail (see Figure 25B) while at 350 °C majority of particles exceeds 5 μm (see Figure 25C). SEM investigations of K_2CO_3 (Figure 26) show that changes in morphology are limited to the surface what is in line with low extent of fluorination determined by chemical analysis and XRD measurements.

Table 4: *Reaction conditions and composition of products for the interaction of CHF_3 with different solid reactants*

Solid reactant – Test №.	***Temperature, °C***	***Initial CHF_3 pressure, kPa***	***Molar ratio CHF_3 : Solid***	***CO content in gas products, vol. %***	***F^- content in solid products, wt. %***	***Metal fluoride in solid products, wt. %***
Hydroxides:						
LiOH-1	250	357	1.00 : 1.90	56	37.9	51.8
NaOH-1	50	357	1.00 : 2.08	3.6	0.04	0.09
NaOH-2	100	357	1.00 : 2.23	11	0.1	0.2
NaOH-3	150	357	1.00 : 2.30	25	25.0	55.3
NaOH-4	200	357	1.00 : 2.24	38	29.6	65.4
NaOH-5	250	357	1.00 : 2.24	49	32.5	71.8
NaOH-6	300	357	1.00 : 2.24	62	39.7	87.7
NaOH-7	350	357	1.00 : 2.20	69	44.8	99.0
NaOH-8	250	357	1.00 : 10.8	0	11.6	25.6
NaOH-9	250	13	1.00 : 2.14	97	31.4	69.4
NaOH-10	250	67	1.00 : 2.81	59	29.6	65.4
NaOH-11	250	133	1.00 : 2.86	55	31.5	69.6
NaOH-12	250	266	1.00 : 2.90	50	30.8	68.1
NaOH-13	250	399	1.00 : 2.90	55	33.5	74.0
NaOD-1	250	237	1.00 : 1.81	44	32.1	71.0
KOH-1	250	357	1.00 : 2.10	37	30.5	93.3
$Ca(OH)_2$	250	357	1.00 : 0.92	60	27.7	56.9
Carbonates:						
Li_2CO_3-1	250	357	1.00 : 1.15	2.3	0.09	0.12
Li_2CO_3-2	400	357	1.00 : 0.34	38	71.7	97.9
Na_2CO_3-1	250	357	1.00 : 0.89	2.9	0.23	0.51
K_2CO_3-1	250	357	1.00 : 1.03	2.4	0.3	0.9
$MgCO_3$	250	357	1.00 : 1.03	24	6.4	11.0
$CaCO_3$	250	357	1.00 : 1.00	13	2.1	4.3
$SrCO_3$	250	357	1.00 : 1.04	3.3	0.2	0.7
$BaCO_3$	250	357	1.00 : 1.03	40	6.3	29.0
Other salts:						
Na_2SO_4	250	357	1.00 : 0.58	1.80	0	0
$Na_2C_2O_4$	250	357	1.00 : 1.04	3.10	0.02	0.04

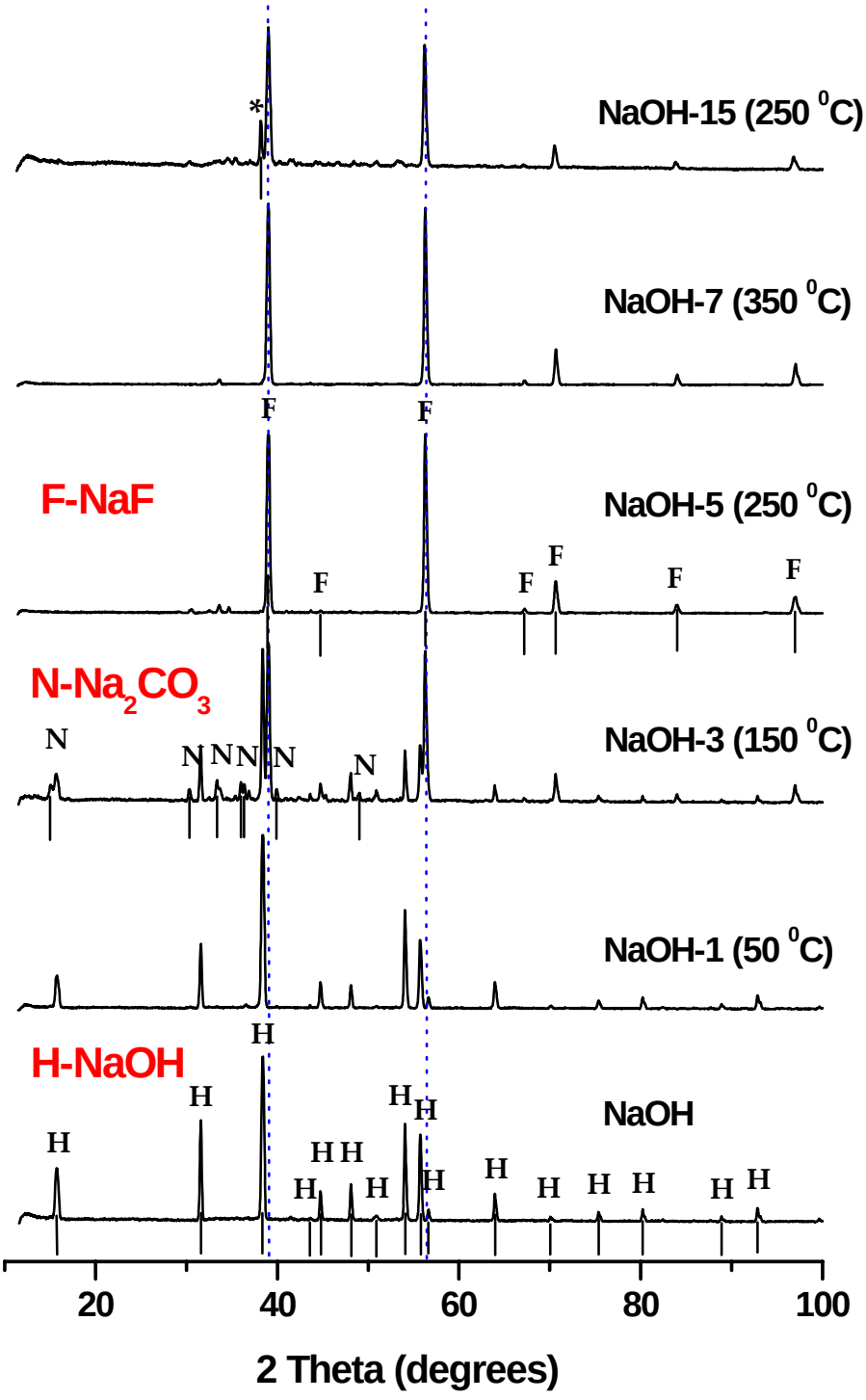

Figure 22: *X-ray powder diffractograms of NaOH after reaction with CHF_3*: NaOH fluorinated at different temperatures in the batch reactor (samples NaOH-1 to NaOH-7) and NaOH fluorinated at 250 °C in the flow reactor (sample NaOH-15; *- Ag from silver wool plug).

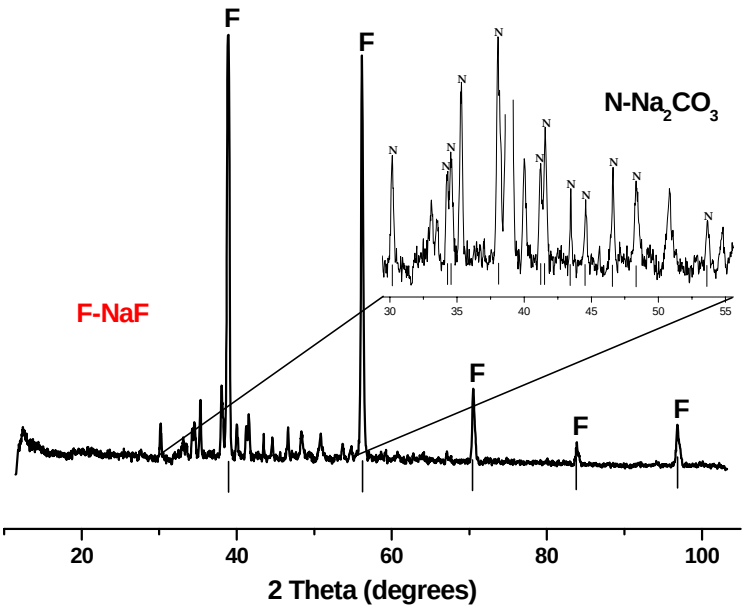

Figure 23: *X-ray powder diffractogram of a large excess of NaOH after reaction with CHF_3,* fluorination performed at 250 °C in the batch reactor (sample NaOH-8).

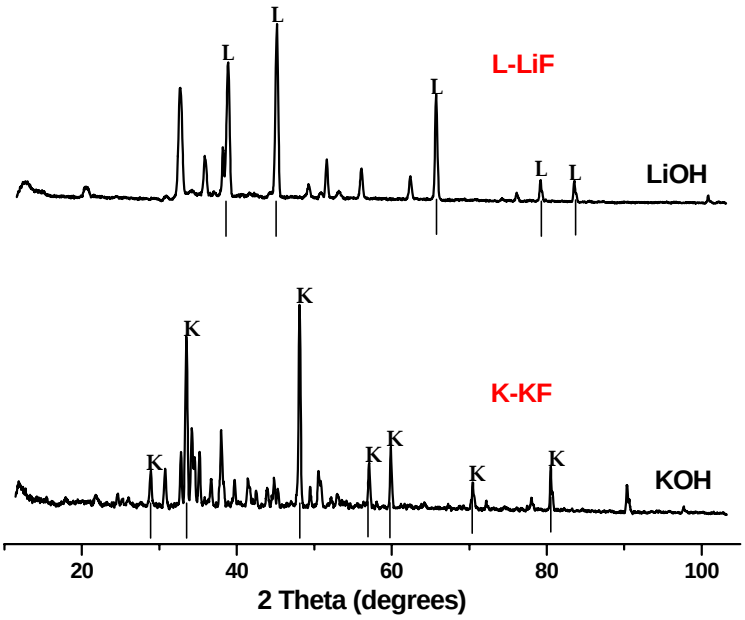

Figure 24: *X-ray powder diffractograms of LiOH and KOH after reaction with CHF_3 in a batch reactor at 250 °C.*

Reactive interaction of CHF_3 with solids containing oxygen results in the formation of

solid fluorides and gaseous products, mainly H_2O and CO [38], and in the case of carbonates also CO_2. The process can be therefore conventionally monitored by FTIR spectroscopy. Among the gaseous products, CO was found to be the most suitable since it can be clearly distinguished in the spectra of bulk gaseous products. On the other side, interferences with the background may considerably impair FTIR measurements of H_2O and CO_2, especially at lower concentrations. Amounts of CO formed in static tests with different solid reactants and determined by FTIR are summarised in Table 4. CO is formed in a number of dehalogenation processes, like in the interaction of haloforms with alkali hydroxides [15], in the decomposition of fluorine-containing ethers on strong metal hydroxides [58], or in the fluorination of various metal oxides with CHF_3 [38]. Our results are consistent with these findings; evolution of CO was observed in all reactions with the solid reactants used. CO contents correlate well with the extents of fluorination of the solid phases and can be used as an additional indicator for the activity of the solids to decompose CHF_3. Exact quantification of the fluorination processes in the batch reactor on the basis of CO data is however hampered by the occurrence of secondary reactions that may considerably alter the final CO contents (see Section 4.2.1.1).

In contrast to CO, formation of H_2O in the batch reactor could not be unequivocally determined by FTIR. Besides the already mentioned background interferences and secondary reactions, this can be also ascribed to the low relative vapour pressure of H_2O in gaseous products and possible H_2O retention in the solid products, either by strong adsorption or by formation of various hydrated phases. To obtain more definitive information about H_2O formation without interferences from the background H_2O, NaOD was fluorinated with CHF_3 in a batch reactor at 250 °C (sample NaOD, Table 4 and Figure 27). Gaseous products of this reaction were analysed by MS. It should be pointed out that even with MS H_2O or its deuterated analogues could not be unambiguously identified in the bulk gaseous phase. Bulk of the volatile products was therefore pumped off at room temperature and then the reactor was heated to 50 °C. The headspace gases were analysed by MS that confirmed the presence of all three forms of water, H_2O, HDO and D_2O (see Figure 27). These findings clearly confirm that H_2O is one of the main products in fluorinations with CHF_3 and that a considerable part of the H_2O formed may be strongly retained in the solid products.

The results confirm that the interaction of CHF_3 with alkali hydroxides or carbonates is consistent with the following primary fluorination reactions (M = Li, Na or K):

$$3MOH + CHF_3 \rightarrow 3MF + CO + 2H_2O \quad (13)$$

$$3M_2CO_3 + 2CHF_3 \rightarrow 6MF + 3CO_2 + 2CO + H_2O \quad (14)$$

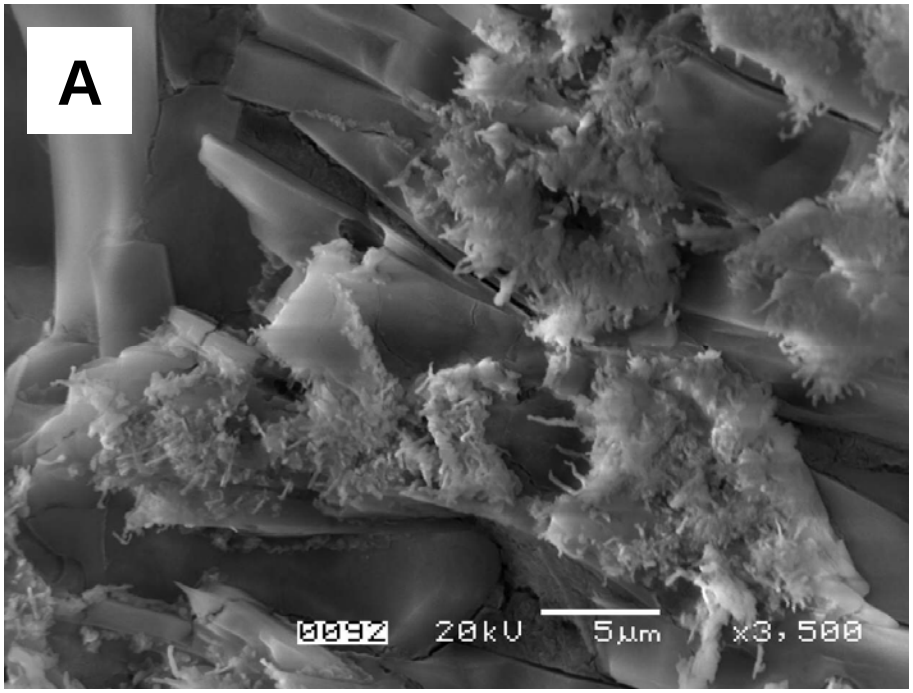
A
0092 20kV 5µm x3,500

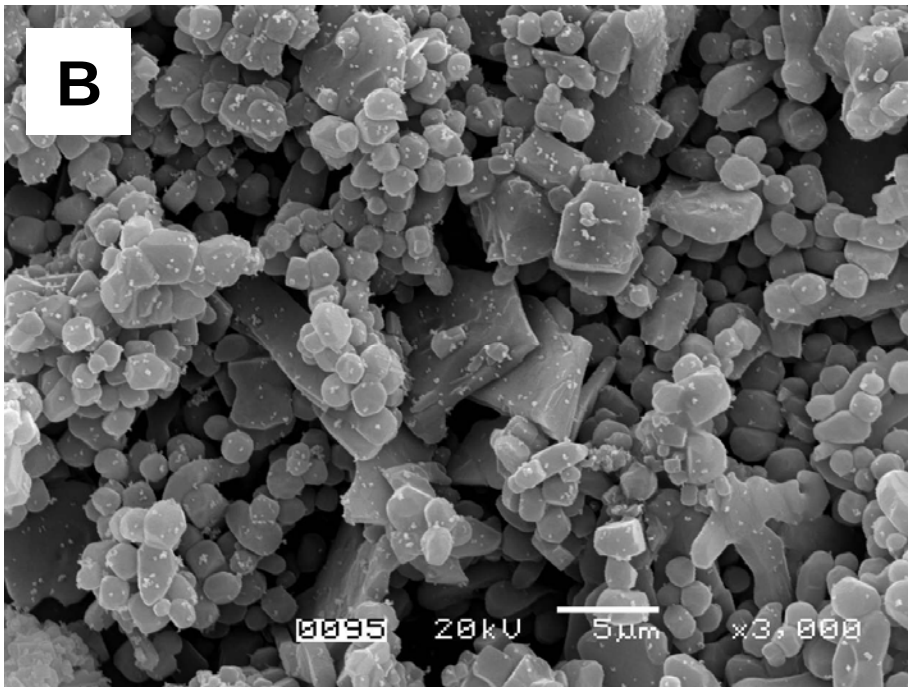
B
0095 20kV 5µm x3,000

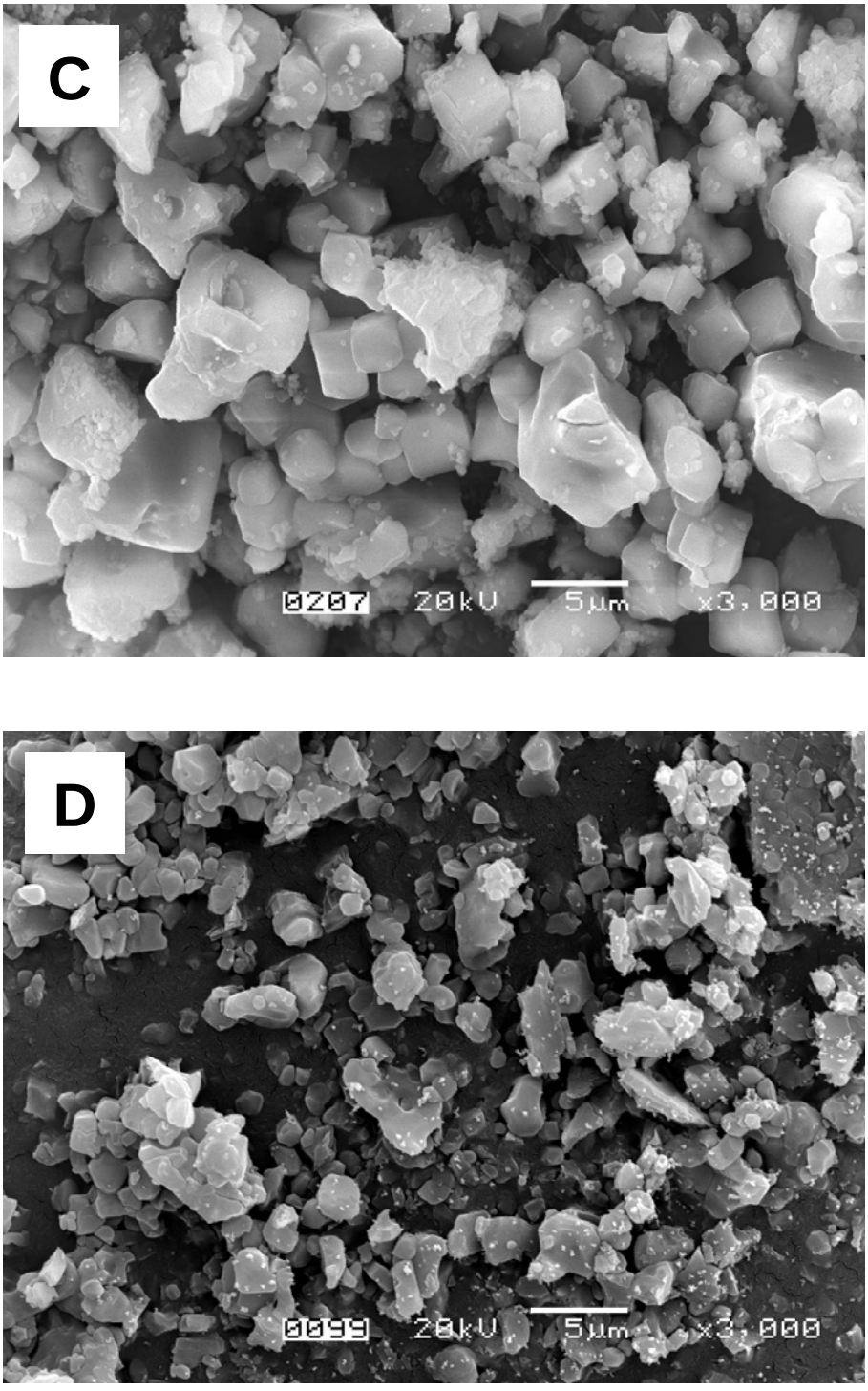

Figure 25: *SEM images of NaOH before and after reaction with CHF_3*: initial NaOH (A), NaOH treated at 250 °C in batch reactor (sample NaOH-5) (B), NaOH treated at 350 °C in batch reactor (sample NaOH-7) (C), NaOH treated at 250 °C in flow reactor (sample NaOH-15) (D).

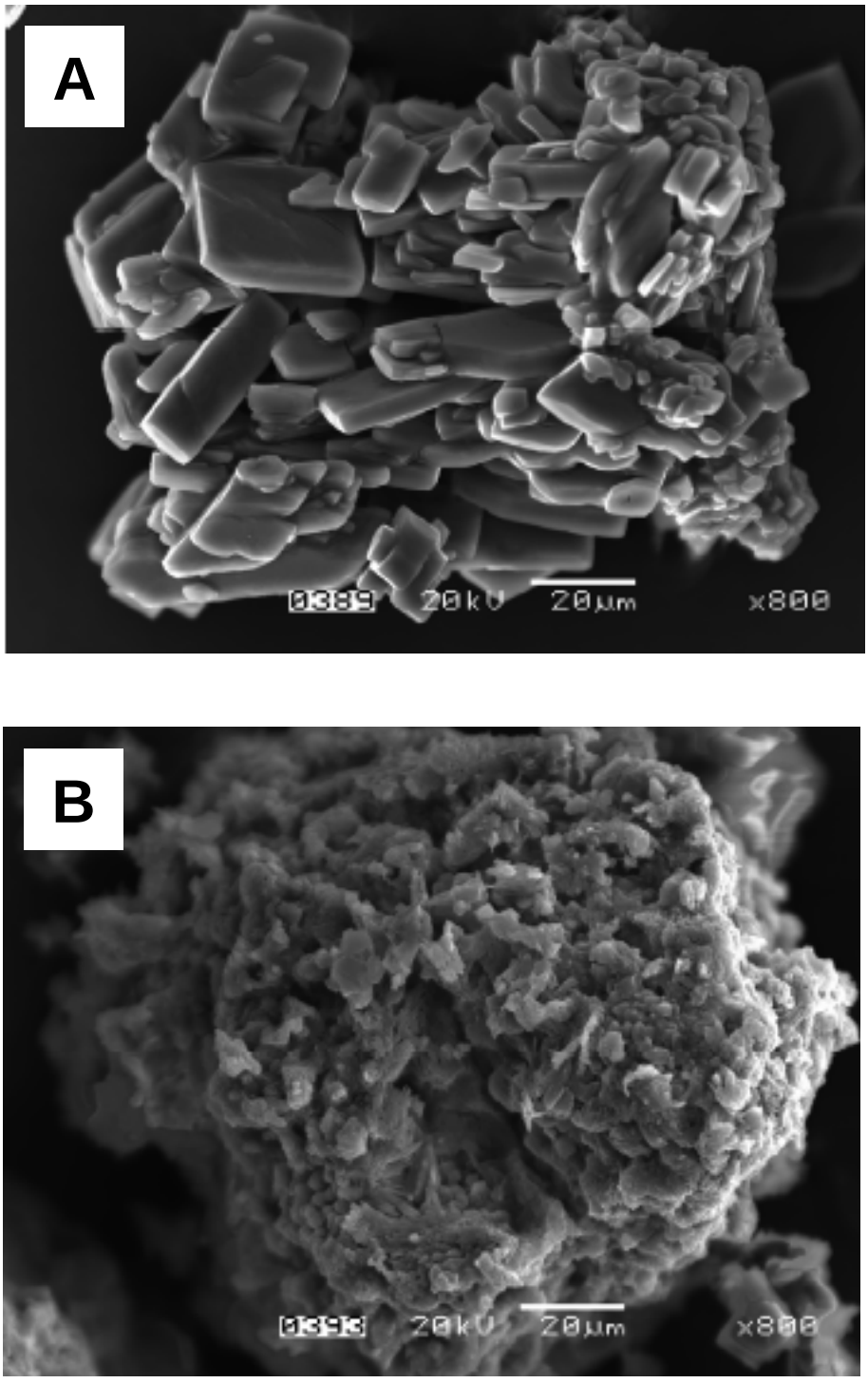

Figure 26: *SEM images of K_2CO_3 before and after reaction with CHF_3*: initial K_2CO_3 (A), K_2CO_3 treated at 523 K in batch reactor (sample K_2CO_3-1) (B).

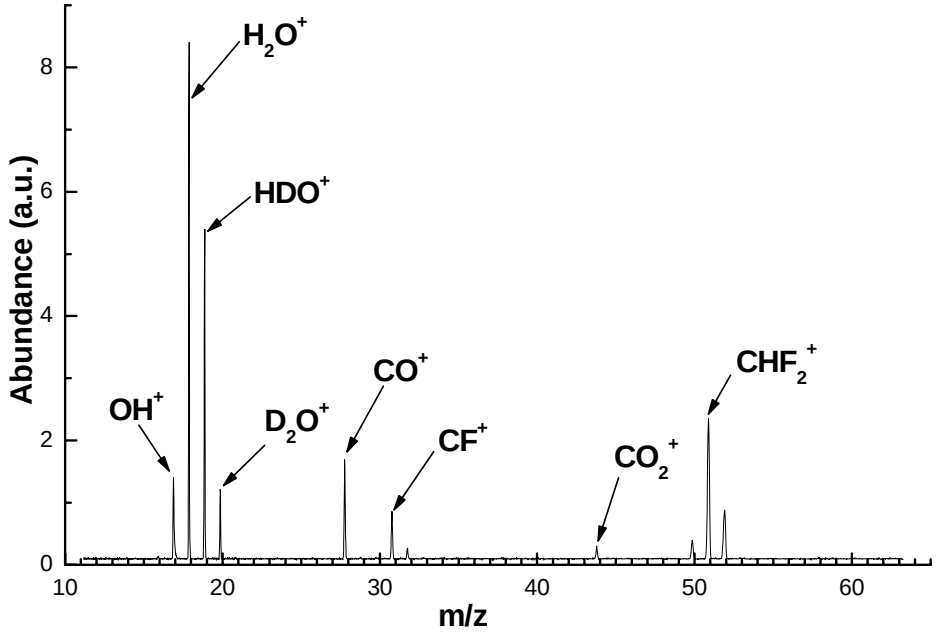

Figure 27: *Part of mass spectrum of the gas phase from the reaction between NaOD and CHF_3 at 250 °C in batch reactor confirming the presence of H_2O, HDO and D_2O.*

Table 5: *Composition of gas mixtures obtained in the reaction of CHF_3 with NaOH in the batch reactor at different temperatures*

T, °C	C(CO), vol.%	C(CHF_3), vol.%	C(CH_4), vol.%	C(H_2), vol.%
50	3.6	96	-	-
100	11	89	-	-
150	25	75	-	-
200	38	62	-	-
250	49	51	-	-
300	62	38	0.8	0
350	69	17	1.2	13

4.2.1.1 Side reactions with hydroxides

Closer examination of the gaseous products from some batch tests revealed that in the interaction of CHF_3 with alkali hydroxides H_2 and CH_4 are also formed. Formation of these two gaseous products was especially noticeable at higher temperatures (Table 5). Main reaction between CHF_3 and NaOH and likely side reactions that take place in the batch reactor at intermediate temperatures are represented in Scheme 2.

Formation of H_2/CO_2 and alkali carbonate: Formation of H_2 was confirmed by MS

in the products of some runs with NaOH or KOH at 250 and 350 °C (tests NaOH-5 and -7, and KOH, Table 4). In addition, H_2 and both of its deuterated analogues, HD and D_2, were detected by MS in the products of the reaction with NaOD at 250 °C (test NaOD, Table 4). Very likely, H_2 is the product of the equilibrium water-gas shift reaction (see Eq. 15) between CO and H_2O; the latter two are products of the primary fluorination reaction (see Eq. 13).

$$CO + H_2O \rightleftharpoons CO_2 + H_2 \quad (15)$$

In the transitional stage of fluorination, equilibrium of reaction (see Eq. 15) is shifted to the right due to the reaction of CO_2 with the non-reacted hydroxide and the consequent formation of the solid carbonate (see Eq. 16). Formation of carbonate at intermediate temperatures was clearly confirmed by XRD measurements.

$$CO_2 + 2MOH \rightarrow M_2CO_3 + H_2O \quad (16)$$

In experiments with excess of CHF_3, evolution of H_2 from reaction (see Eq. 15) stops when all hydroxide is converted to fluoride or a mixture of fluoride and carbonate. This means that when the hydroxide is the limiting reactant only part of the CO formed in reaction (see Eq. 13) can react further. Analyses of the gaseous phases after reaction, presented in Tables 4 and 5, are consistent with this, indicating that, besides the non-reacted CHF_3, CO is the main gaseous product detected. On the other side, experiment with excess of NaOH (test NaOH-8, Table 4) demonstrated that under such conditions CO can be quantitatively converted to carbonate, as confirmed by XRD (see Figure 23). In this specific case, *i.e.* excess of NaOH and long contact times, interaction between alkali hydroxides and CHF_3 can better be represented by the following overall equation:

$$5MOH + CHF_3 \rightarrow 3MF + M_2CO_3 + H_2 + 2H_2O \quad (17)$$

Formation of CH_4: Formation of CH_4 at levels detectable by FTIR was observed in some NaOH tests at higher temperatures (tests NaOH-6 and -7, Table 4). CH_4 is very likely formed by CO methanation (Eq. 18) that is strongly catalysed by nickel or nickel-based materials at 250–400 °C [101, 102].

$$CO + 3H_2 \rightleftharpoons CH_4 + H_2O \quad (18)$$

Our tests (see Section 3.4) confirmed that under the experimental conditions used within the current work, nickel from the reactor can act as an active methanation catalyst.

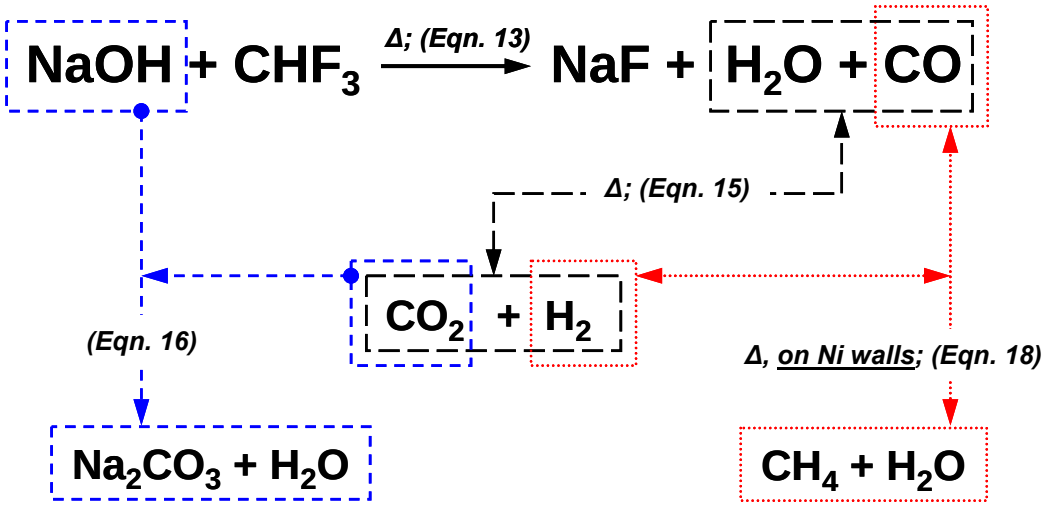

Scheme 2: *Schematic representation of the main reaction between NaOH and CHF_3 (top line) and the possible side reactions leading to the formation of CO_2/H_2, Na_2CO_3 and CH_4 (marked with dashed/dotted lines).* Scheme represents the likely situation in the temperature interval of 145–270 °C; above 270 °C Na_2CO_3 may react with CHF_3 (see Eq. 14, not shown in the scheme). Exact stoichiometry of the indicated reactions is given in the text.

4.2.1.2 Reactions with other halocarbons

Activity of CHF_3 towards NaOH was compared with that exhibited by some representative halocarbons. Experiments with these compounds were performed in the batch reactor under conditions similar to those used in the CHF_3/NaOH investigations. Reaction conditions and the corresponding fluorine contents are presented in Table 6.

Table 6: *Interaction of different halocarbons with NaOH in the batch reactor at 250 °C* (test duration 20 hours)

Compound	Molar ratio, Comp. : NaOH	Initial pressure, kPa	F^- content in solid products, wt.%
CCl_3F	1.00 : 9.71	100	0.60
CCl_2F_2	1.00 : 2.49	200	0.93
$C_6F_{11}CF_3$	1.00 : 10.0	100	0.11
$CHClF_2$	1.00 : 2.21	200	27.1

Results demonstrate that all investigated perhalogenated compounds, CCl_3F, CCl_2F_2, and $C_6F_{11}CF_3$, exhibit very low activities towards NaOH. In all cases, fluorine content in the NaOH treated at 250 °C is below 1 wt.%. On the other side, partially halogenated hydrocarbons, $CHClF_2$, and $CHCl_3$ (latter not included in Table 6), exhibit much higher

activities. Fluorine content of the $CHClF_2$-treated NaOH is comparable to that obtained with CHF_3. In line with the previously determined relative reactivities of haloforms in basic hydrolysis [15], the highest activity was exhibited by $CHCl_3$. In this case, almost complete chlorination of NaOH was achieved already at 50 °C. Activity towards NaOH is therefore inversely proportional to the stability of the molecule. Hydrogen-containing partially halogenated compounds (HFCs and HCFCs) are less stable and noticeably more active than the very stable fully halogenated compounds.

4.2.2 Reactions under flow conditions

Some of the tests in the batch reactor were complemented by investigations performed under flow conditions in a plug flow reactor with a fixed layer of the solid reactant. Representative data for a series of isothermal flow tests with NaOH are presented in Table 7. Although the whole duration of flow tests was 9–15 hours, the on–line FTIR monitoring of CO evolution showed that the reaction was virtually completed within the first hour on–stream.

Table 7: *Interaction of CHF_3 with NaOH in the flow reactor* (CHF_3 flow: 1 cm^3 min^{-1})

Test	NaOH, g	Temp., °C	Layer height, mm	Contact time, s	Overall test duration, h	F^- content in solid products, wt.%
NaOH-14	0.044	200	2	2.4	9	30.3
NaOH-15	0.048	250	2	2.4	15	28.0
NaOH-16	0.137	250	6	7.2	10	29.1
NaOH-17	0.307	250	16	18.8	10	31.3

Fluoride contents in the solid products obtained under flow conditions are similar to those obtained at same temperatures in the batch reactor (see Table 4). This indicates that in the interaction of CHF_3 with NaOH temperature is the dominant factor that determines the extent of fluorination. Although the overall reaction times for the two regimes differ considerably, they appear to be less significant at least within the time scales used in both sets of experiments.

XRD results are consistent with chemical analyses and indicate the formation of NaF as the main crystalline phase (sample NaOH-15, Figure 22). In contrast to batch tests, products obtained under flow conditions do not contain relevant levels of Na_2CO_3. SEM investigations showed that the basic morphology of the solid products is very similar to that observed in products from the batch reactor (sample NaOH-15 vs. NaOH-5, see Figure 25). Slightly smaller dimensions of the crystallites from the flow experiments can be associated with lower water concentration and shorter reaction time that are both characteristic for flow experiments.

FTIR analyses of the effluents from the flow reactor were consistent with the

formation of CO and H_2O as the main gaseous products. For the reasons mentioned before, evolution of CO was used to conveniently monitor the progress of fluorination. In a separate series of temperature programmed experiments, evolution of CO proved to be particularly suitable to determine the onset of fluorination for different alkali hydroxides and carbonates. Relevant data for these experiments are summarised in Table 8, with the corresponding CO evolution profiles shown in Figure 28A. Results clearly show that KOH is the most active solid that starts to react approximately at 100 ºC. For the hydroxides, the starting temperature of fluorination is increasing in the order KOH < NaOH < LiOH (see Figure 28A). Same trend is also observed for the carbonate series, although the corresponding temperatures are approximately 100–150 °C higher (Figure 28B). This confirms that the carbonates are less active than the hydroxides. Such behaviour can be correlated with lower basicity of carbonates in comparison to hydroxides. It should also be noted that the results of temperature programmed experiments for hydroxides correlate very well with the activities deduced from the experiments performed under static conditions in a batch reactor (see Section 4.2.1). On the other side, temperature programmed experiments show that for the investigated carbonates fluorination starts above the reference temperature used in comparative static experiments (250 °C). This is in accordance with the low extent of fluorination obtained with carbonates in the batch reactor.

Table 8: *Temperature programmed flow tests with alkali hydroxides and carbonates performed from room temperature to the indicated upper temperature* (heating rate: 1.8 °C min^{-1}; CHF_3/N_2 flow 11.0 cm^3 min^{-1}; 9.1 vol. % CHF_3)

Test	Upper temperature, °C	Layer height, mm	Start of CO evolution[a], °C
LiOH-2	300	1	211
NaOH-18	300	5	147
KOH-2	111	1	97
Li_2CO_3-3	400	5	292
Na_2CO_3-2	400	5	271
K_2CO_3-2	400	5	249

[a] – temperature at which a clear shift from the background could be established

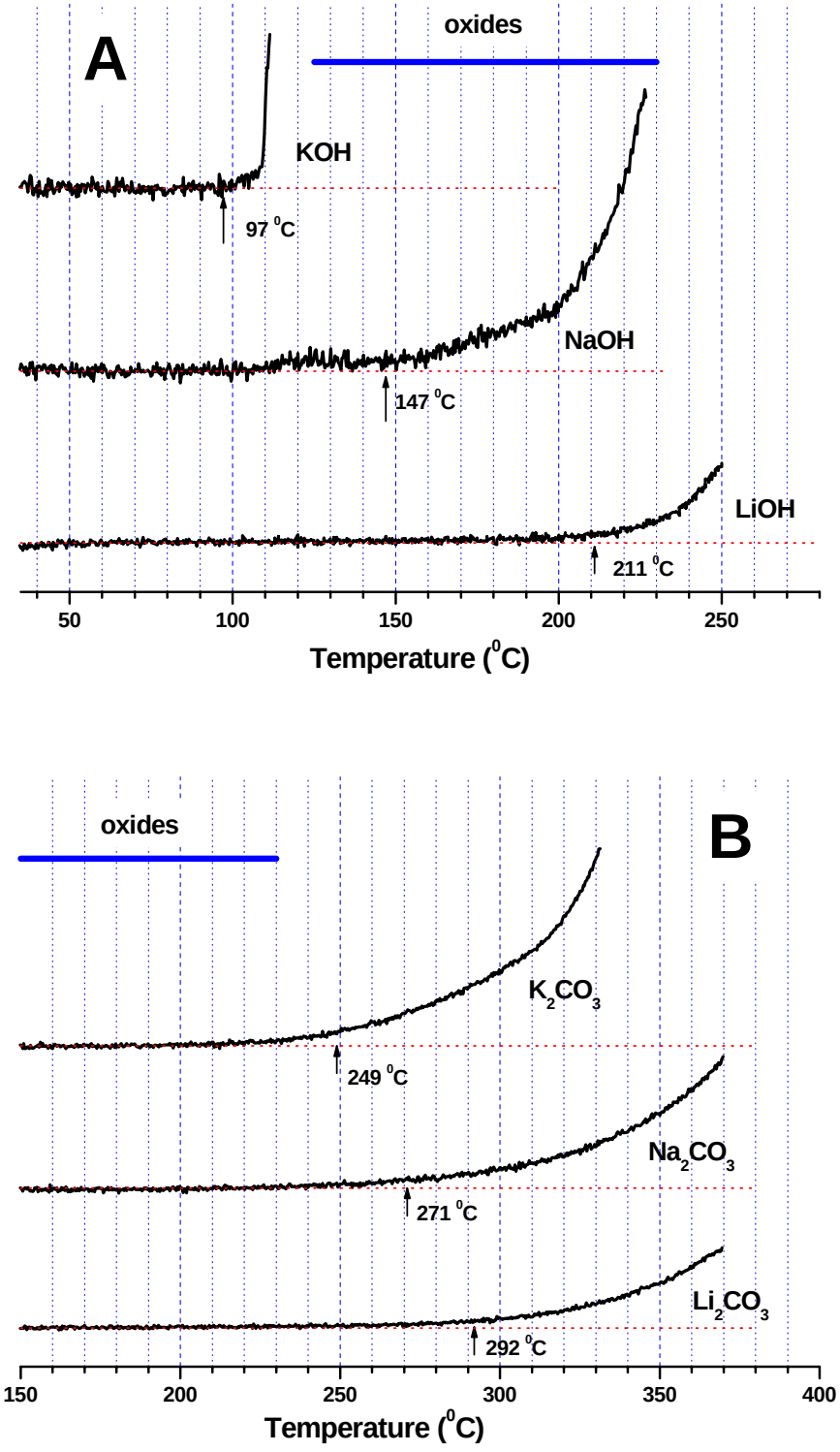

Figure 28: *CO-evolution profiles (offset) from temperature programmed experiments in the flow reactor*: A – reaction of CHF_3 with alkali hydroxides, B – reaction of CHF_3 with alkali carbonates. Inset horizontal lines show the range of fluorination onset temperatures for single and mixed Al/Ga-oxides (see Figure 11).

4.2.3 Comparison of CHF_3 reactions with hydroxides under static and dynamic conditions

Interaction of CHF_3 with alkali hydroxides under static or dynamic (flow) conditions yields solid product with remarkably similar morphologies and compositions. Under both reaction regimes, main reaction is fluorination and the hydroxide to fluoride conversion depends mainly on temperature. Similar conversions found under both reaction regimes indicate that hydroxide fluorination, although thermodynamically strongly favoured, is kinetically hindered by diffusion processes. Interaction of CHF_3 with alkali hydroxides can be regarded as a classical gas-solid reaction only in the initial stage when non-hydrated hydroxide is present. With the progress of reaction, hydroxide can be hydrated by H_2O formed during fluorination (see Eq.13). In the NaOH (or KOH)/H_2O systems melting temperatures are decreasing sharply with increasing H_2O contents; for example, respective hydroxide/hydroxide monohydrate melting points are 321/65 °C for NaOH and 404/145 ºC for KOH [103]. This implies that under the reaction conditions used in the present work, evolution of H_2O could be accompanied by partial melting of the residual hydroxide phase resulting in a rather complex gas-(liquid)-solid reaction system. This aspect is of particular importance in batch experiments where the H_2O/unreacted hydroxide ratio is increasing rapidly with the advancement of fluorination. On the other side, physical state of the hydroxide phase has apparently no decisive effect on the fluorination process as a whole, as demonstrated by the batch experiment conducted above the melting point of NaOH (test NaOH-7, Table 4). In the flow experiments, H_2O formed during fluorination is constantly removed from the reactor with the stream of effluents. H_2O levels within the reaction zone are therefore lower and more constant as in batch experiments. Occasional clogging of the flow reactor due the partial melting of the solid layer, observed mostly with KOH, indicated however that hydration may occur also under flow conditions. For these reasons, operation of the flow reactor with a fixed layer of solid reactant may become problematic already at temperatures that are considerably lower than the melting points of pure hydroxides. Pronounced susceptibility of KOH to melting can be associated with higher thermal stability of its hydrates in comparison with NaOH.

Experiments in the batch reactor with very long contact times allowed investigations at conditions that are close to the equilibrium state. As mentioned before (see Section 4.2.1.1), this allowed a clear identification of the main side reactions that may take place in these reaction systems. Due to technical limitations, occurrence of side reactions under flow conditions could not be studied in detail. However, it can be assumed that due to much shorter contact times that do not allow adequate equilibration and lower concentrations of gaseous products, extent of side reactions in flow experiments is likely to be much lower as under static conditions. This assumption is in part supported by the absence of measurable amounts of carbonate in the solid and the absence of methane in the gaseous products from the flow reactions.

4.2.4 Activation of CHF_3 by hydroxides or carbonates through acid-base interactions

CHF_3 is characterised by a remarkable thermal stability up to approximately 680 °C. Under homogeneous gas phase conditions, discernible thermal decomposition (pyrolysis) of CHF_3 starts above 700 °C [25, 27, 104]. Possible thermally induced decomposition processes for CHF_3 are presented by Eqs. 2", 19 and 20, with ΔH^0 values taken from

[105]. The kinetics of decomposition of different HFCs can be found in Appendix IV Table A-9.

$CHF_3 \rightarrow CF_2 + HF$ $\Delta H^0_{f,298} = 238$ kJ mol^{-1} (2")

$CHF_3 \rightarrow CF_3 + H$ $\Delta H^0_{f,298} = 448$ kJ mol^{-1} (19)

$CHF_3 \rightarrow CHF_2 + F$ $\Delta H^0_{f,298} = 529$ kJ mol^{-1} (20)

Among these processes, decomposition of CHF_3 through HF elimination and CF_2 formation is thermodynamically strongly favoured (see Eq. 2"). Numerous studies gave clear evidence that above 700 °C this is the main decomposition path for CHF_3. Homogeneous reactions with CHF_3 at high temperatures are, as a rule, rationalised on the basis of the initial thermally activated CHF_3 decomposition to CF_2 and HF [25, 28, 31, 32, 104]. On the other side, several heterogeneous reactions, either catalytic [30, 32, 106] or non-catalytic [31, 107], were investigated in order to elucidate the role of solid surfaces in the high temperature CHF_3 decomposition and following processes. Common feature of these investigations is that only carbon-based materials and solid metal fluorides exhibit sufficient initial chemical stability, other compounds, like metal oxides and salts, are converted to fluorides [30, 31, 107] due to severe fluorination conditions encountered during CHF_3 decomposition, *i.e.* high temperature and presence of very reactive fluorinating species, like HF, CF_2, CF_3 etc. In the presence of sufficiently stable solid catalysts, some reactions with CHF_3 could be performed at temperatures that were noticeably lower than those required by the non-catalysed reactions [29, 30]. It was concluded that in these cases CHF_3 was probably not activated thermally but chemically through the interaction with the solid. Although the mechanisms of these surface interactions remain largely unclear, it was suggested that KF-doped activated carbon catalyst may promote CHF_3 decomposition by lowering the energy required for C−F bond cleavage [30].

High temperature heterogeneous processes mentioned above are principally aimed to convert CHF_3 to valuable fluorocarbon products. In another class of heterogeneous reactions, usually performed at intermediate and lower temperatures, CHF_3 is completely decomposed. These reactions include catalytic hydrolysis [54, 55] and fluorinations with CHF_3 [35–40]. As is the case with high temperature heterogeneous reactions, mechanisms of the surface processes leading to CHF_3 decomposition are not entirely understood. For hydrolysis on zirconia-based catalysts it was proposed that CHF_3 decomposes in the reaction with surface OH groups, it is however unclear if CHF_3 reacts after adsorption or in the gas phase [54]. For phosphate catalysts, adsorption of CHF_3 on surface acid sites through the C−F···M^+ interaction was proposed [55]. As mentioned in the introduction, fluorination of metal oxides with CHF_3 was occasionally used as an alternative to conventional fluorinations. These studies were prevalently focused on the properties of fluorinated solid products; mechanisms of the basic fluorination reactions were not investigated in details. However, these studies clearly demonstrated that in these reactions CHF_3 decomposes at 300–500 °C. In the early work on γ-Al_2O_3 fluorination, CHF_3 fluorination activity was explained by the initial rupture of the relatively weak C−H bond that leads to the formation of active fluorinating species [38]. More recently, α-Al_2O_3 was fluorinated with CHF_3 to α-AlF_3 at temperatures above 750 °C. For this case, it was suggested that CHF_3 was initially thermally decomposed into HF and CF_2, and that both species acted as fluorinating agent for the α-Al_2O_3 phase [31]. Recently it was also found that above 550 °C $CaBr_2$ reacts with CHF_3 to form CaF_2 as a solid product. It was suggested that in this case interaction between $CaBr_2$ and CHF_3 is direct. Based on quantum chemical calculations, authors identified a stable complex of the type,

C−F···Ca^{2+}, as a possible intermediate in the formation of CaF_2 [107].

These precedents, although somehow controversial, indicate that in heterogeneous reactions CHF_3 can be activated thermally or chemically. Which of the two basic activation mechanisms prevails depends mainly on temperature and there is apparently a relatively narrow temperature limit between the two regions. Thermal activation with discernible CF_2 and HF formation is predominant above 700 °C. Below this temperature and especially below 500 °C, chemical activation predominates. In this case, activation is presumably achieved through direct interactions of the CHF_3 molecule with the solid.

As found in the present work, CHF_3 starts to react with alkali hydroxides and carbonates at approximately 100–210 °C and 250–310 °C (see Table 8), respectively. Fluorination onset temperatures for alkali hydroxides are, to the best of our knowledge, the lowest reported so far for bulk fluorinations with CHF_3. Alkali hydroxides show a remarkably higher activity towards CHF_3 than the corresponding carbonates. Reactivity of the latter is comparable or somewhat higher as that observed for some metal oxides that were usually fluorinated above 300 °C. It should be however noted that some of the mixed oxides investigated within this work exhibit very high activity, comparable to that of alkali hydroxides.

According to the argumentation given above, relatively very low reaction temperatures found in the present work suggest that activation of CHF_3 is probably chemical through a direct interaction with alkali hydroxides or carbonates, and some oxides. Some authors suggested that decomposition of CHF_3 on solid surfaces occurs by C−F bond activation through C−F···M^+ interactions [55, 107]. Such mechanisms do however not account for large difference in the activities towards hydroxides between hydrogen-containing HFCs and HCFCs, and fully halogenated fluorocarbons that were observed within this work (Section 4.2.1.2). Similar differences were also observed in TPD experiments with partially fluorinated γ-Al_2O_3. Authors of this study pointed out that some interaction with the solid via hydrogen in HFCs/HCFCs must occur, but no other details about the nature of the presumed interactions were given [39]. We therefore propose that in the initial stage CHF_3, as a weak C−H acid [23, 108], interacts with strong basic sites on the surface of the solids. In case of hydroxides and carbonates, basic sites correspond to oxygen atoms in hydroxide and carbonate ions. Possible acid-base interactions between CHF_3 and an alkali hydroxide are presented in Scheme 3.

Since the basicity of the oxygen in hydroxide ions is much higher than in carbonate ions, interaction of CHF_3 with hydroxides will be much stronger than with carbonates resulting in a higher activity of the former compounds. This correlates very well with current experimental findings and explains higher activity of hydroxides in comparison with carbonates. However, it should be noted that the proposed acid-base interaction of the type, C−H···O−M^+, is only one of the steps, although apparently a decisive one, in the process of complete CHF_3 decomposition. Other steps very probably include also interactions of the type, C−F···M^+, as intermediate stages in metal fluoride formation and in the decomposition of CF_x species that could also be formed as intermediates. Namely, FTIR investigations of CHF_3 adsorption on magnesia and alkali-exchanged Y-zeolites revealed that in the most probable adsorption complex CHF_3 binds to the solid simultaneously through C−H···O and C−F···M^+ interactions, with the latter being much stronger due to the small size and high electronegativity of the fluorine [109, 110]. It is reasonable to conclude that similar interactions are possible also in our systems although it is very likely that the relative strengths of the two interactions differ from those in oxide materials mentioned above. Namely, alkali cations in alkali oxides and related compounds exhibit very weak Lewis acidity [111] that probably results in much weaker C−F···M^+ interactions.

4.2.5 Comparison between the activity of alkali hydroxides and carbonates

Reactivity of the solid alkali hydroxides and carbonates towards fluorination with CHF_3 can be correlated with the strength of surface basic sites. Basicity of these sites is dictated by the basicity of the anion which is in turn regulated by the number of oxygen atoms attached to the central atom of the anion [112, 113]. For example, OH groups will be more basic than CO_3^{2-} or SO_4^{2-}. This was confirmed by fluorination of sodium sulphate, Na_2SO_4, and sodium oxalate, $Na_2C_2O_4$, under static conditions. Contrary to sodium hydroxide and carbonate the two salts were completely inactive towards fluorination with CHF_3 (see Table 4).

Under static and flow conditions, same trend in reactivity is exhibited within the series of alkali carbonates and hydroxides. Reactivity increases from lithium hydroxide (or carbonate) to potassium hydroxide (or carbonate). Alkali cation induces changes in the local electron density of hydroxyl groups or carbonate anions. Higher atomic number, *i.e.* larger diameter of a cation, leads to a higher effective charge of oxygen in hydroxyl groups of the corresponding hydroxides. In turn positive inductive effect, +I, caused by an alkali cation towards hydroxide group, indicates high impact of a covalent bonding between alkali cation and hydroxyl group in the mentioned alkali hydroxides. Similar cation-related effects are observed also in alkali carbonates.

As mentioned in Section 4.2.4, mechanisms of heterogeneous reactions of CHF_3 at temperatures below 700 °C are not entirely clear and are interpreted in a controversial manner. Some authors suggested that decomposition of CHF_3 on solid surfaces occurs by C−F bond activation through a C−F···M^+ type of interactions [109, 110]. Conversely, activity of CHF_3 in fluorination of γ-Al_2O_3 was interpreted by the initial rupture of the relatively weak C−H bond that leads to the formation of active fluorinating species [30, 38]. Some other studies of CHF_3 adsorption on magnesia and alkali-exchanged Y-zeolites revealed that in the most probable adsorption complex CHF_3 binds to the solid simultaneously through C−H···O and C−F···M^+ interactions [109, 110]. All three possible types of interactions are presented in Scheme 3. Current results strongly support the presumption that, at least when interactions of CHF_3 with solid alkali hydroxides are concerned, the most likely initial interaction is of the type C−H···O (see Scheme 3).

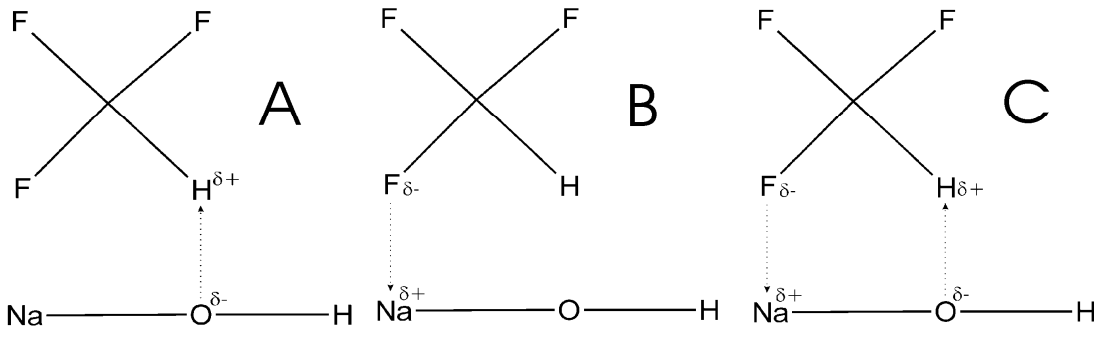

Scheme 3: *Possible initial contacts between the CHF_3 molecule and Na–OH surfaces*: A – hydrogen in CHF_3 bound to the oxygen of the OH group, B – fluorine in CHF_3 bound to the sodium cation of the NaOH, C – hydrogen and fluorine in CHF_3 simultaneously bound to oxygen and sodium cation of the NaOH.

In Scheme 4, different possible stages of the reaction between NaOH and CHF_3 are presented. Initial acid-base type of contact (C−H···O−Na^+) is followed by a gradual decomposition of CF_x (x = 1–3) species through C−F···Na^+ interactions yielding NaF, CO and H_2O as the final decomposition products.

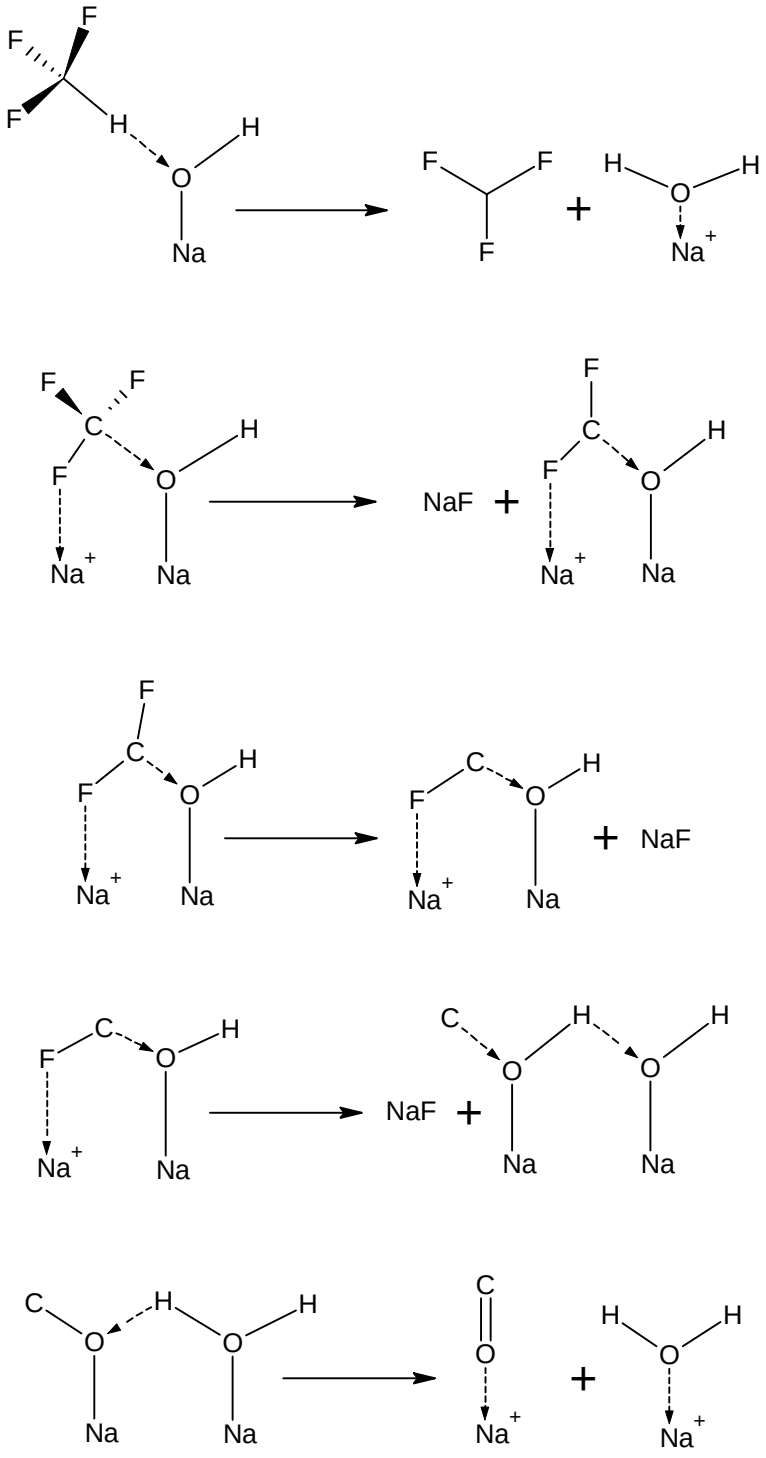

Scheme 4: *Proposed CHF_3 decomposition steps on NaOH.*

4.3 Possible technological and ecological implications of current findings

Research performed within the current work showed that CHF_3 can be an active fluorinating agent even at relatively mild conditions. This was associated with its weak acidic properties. Presumed acid-base interactions between CHF_3 and strongly basic surfaces lead to the fluorination of the solid and to complete decomposition of the CHF_3 molecule. To achieve the same effect, common thermal CHF_3 decomposition (incineration) processes require much more drastic conditions, *i.e.* temperatures of about 1200 °C. Hence, the reactivity of CHF_3 is mainly dictated by the nature the solid reactant. Three groups of materials were tested towards the destruction of CHF_3: alkali hydroxides, alkali carbonates, and single or mixed alumina-gallia xerogels. Alkali hydroxides and some of the mixed alumina-gallia xerogels exhibited similar activity and were fluorinated with CHF_3 already at medium temperatures. For example, optimal CHF_3 mineralisation activity of NaOH was observed in the temperature range of 200–300 ºC. In contrast to incineration, direct mineralisation with solid alkali hydroxides is achieved in one step at considerably lower temperatures and provides direct transformation of CHF_3 into a simple mineral salt which can be easily handled and can be stored or used. It should be also pointed out that with direct mineralisation the need for cleaning of effluent gases is practically eliminated. On the other side, alkali carbonates represent an economically more convenient alternative to hydroxides. However, effective mineralisation with carbonates requires higher temperatures in the range of 300–400 ºC. It is clear that for economic reasons decomposition of CHF_3 with solid alkali hydroxides or carbonates can not represent an equivalent alternative to the large scale incineration processes. It could be however used in some specific cases for the destruction of minor quantities of CHF_3 in situations where economics of the process is not of prime importance.

Although interactions of CHF_3 with single or mixed alumina-gallia materials could be regarded as alternative CHF_3 mineralisation processes, their main value is in the preparation of fluorinated solid products with modified characteristics. Among these characteristics, modification of surface acidity may for example lead to an improved catalytic behaviour in some acid-catalysed reactions. Treatment of an oxide with CHF_3 leads to the incorporation of fluorine due to the exchange of O/OH with F. In the initial stages incorporation of fluorine is limited to the surface and proceeds to the bulk in advanced stages of fluorination. Level of fluorination can be to some extent controlled by temperature. As found in this work, treatment of γ-Al_2O_3/γ-Ga_2O_3 with CHF_3 at 125–330 °C leads to partial fluorination that is limited mainly to the surface. In this way, amount of incorporated fluorine and the corresponding increase in Lewis acidity can be tailored with proper control of some preparation conditions. Another factor that can strongly affect Lewis acidity is the isomorphic incorporation of Ga^{3+} ions into the γ-Al_2O_3 structure, primarily due to the strong preference of Ga^{3+} ions to replace the most Lewis acidic Al^{3+} ions in tetrahedral environments. Partial fluorination of γ-Al_2O_3/γ-Ga_2O_3 with CHF_3 can thus be regarded as a promising method for the preparation of solids with tailored Lewis acidity, especially when acidic sites with medium strengths are required.

Heterogeneous reactions with CHF_3 at mild conditions investigated within this work open therefore some new possibilities for a clean decomposition or expedient conversion of this environmentally problematic compound.

5 Conclusions

Single γ-Al_2O_3 and γ-Ga_2O_3, and mixed γ-Al_2O_3/γ-Ga_2O_3, used as precursors within this work, exhibit very low crystallinity and have high surface areas. Bulk structure of the mixed oxides is consistent with the formation of γ-Al_2O_3/γ-Ga_2O_3 solid solutions. Comparative spectroscopic investigations of acidity, performed by means of pyridine adsorption, show that Lewis acidity of mixed γ-Al_2O_3/γ-Ga_2O_3 is higher than that of both single oxides. Such synergetic effects on acidity of mixed γ-Al_2O_3/γ-Ga_2O_3 are well-documented. Present findings do however give new evidence for the formation of additional strong Lewis acid sites in mixed oxides with higher Ga contents. Lewis acidity of mixed γ-Al_2O_3/γ-Ga_2O_3 is therefore associated with the presence of surface cus-Ga^{3+} ions, mainly due to their strong preference to occupy tetrahedral positions. Namely, coordinatively unsaturated (cus) cations in tetrahedral positions are commonly related with the strongest Lewis acid sites found on these types of oxides [86]. Increase in the number of acid sites and formation of additional strong Lewis acid sites are both an indication that heterogeneity of mixed γ-Al_2O_3/γ-Ga_2O_3 surfaces is considerably higher than that of single oxides and is increasing with increasing Ga content. On the other side, XPS shows that surfaces of mixed oxides are enriched with Al, very likely through some reconstruction processes. All these observations clearly indicate that both composition and structure of surfaces in real mixed oxides may deviate considerably from those expected for an ideal solid solution.

Treatment of single and mixed oxides with CHF_3 at 350 °C results in partial fluorination with concomitant reduction of surface areas. XPS confirms that under reductive conditions encountered during fluorination with CHF_3 Ga^{3+} is not reduced to lower oxidation states. Bulk structure of the oxide precursors is not affected by fluorination what indicates that fluoride phases initially formed are highly dispersed and amorphous. Appearance of distinctive $Al(F,OH)_3 \cdot nH_2O$ phases is correlated with slow post-crystallisation processes promoted by water adsorption. Preferential formation of Al–F based phases is additionally substantiated by XPS results which clearly showed that in fluorinated γ-Al_2O_3/γ-Ga_2O_3 F binds mainly to Al-atoms while Ga-atoms remain prevalently in O environments. XPS in addition showed that surfaces of fluorinated mixed oxides were enriched with Ga what is interpreted as formation of Al–F phases in the subsurface region what leads to the enrichment of Ga–O phases on the surface. These findings give strong evidence that fluorination of γ-Al_2O_3/γ-Ga_2O_3 surfaces is proceeding rather selectively what may lead to the formation of segregated (Al–F)-rich and (Ga–O)-rich regions.

As expected, partial fluorination of mixed γ-Al_2O_3/γ-Ga_2O_3 with CHF_3 increased the strength of Lewis acid sites due to the partial replacement of O/OH with F. Fluorination also reduced the heterogeneity of these acid sites probably due to some structural ordering. Similarly to the situation encountered with mixed oxides, number of acidic sites in fluorinated mixed oxides was higher than in fluorinated single oxides. Overall increase of Lewis acidity in fluorinated γ-Al_2O_3/γ-Ga_2O_3 observed by adsorption of pyridine was however not substantiated by catalytic activity w.r.t. isomerisation of CCl_2FCClF_2. Isomerisation activity was observed only for fluorinated oxides with lowest Ga contents. It is concluded that isomerisation is taking place only on cus-Al^{3+} sites that are stronger

Lewis acids than cus-Ga^{3+} sites. Isomerisation of CCl_2FCClF_2 can therefore be used as a sensitive test to differentiate between these sites and can in this respect complement pyridine adsorption that appears to be not selective enough to discriminate between various cationic acid sites present on the surfaces of fluorinated γ-Al_2O_3/γ-Ga_2O_3.

Fluorination of γ-Al_2O_3/γ-Ga_2O_3 with CHF_3 at intermediate temperatures is demonstrated to be a versatile approach for the preparation of solid materials with some specific characteristics. On one side, partial fluorination of oxide precursors yields materials with surface areas above 100 m^2 g^{-1}. On the other side, acidity is affected by both fluorination and preferential replacement of the most acidic cus-Al^{3+} ions with the less acidic cus-Ga^{3+} ions. All these aspect are important in the preparation of acidic materials with tailored characteristics for possible catalytic applications.

Metal hydroxides and carbonates investigated in the present work react with CHF_3 at moderate temperatures (below 300 °C). Basic reaction can be described as fluorination in which CHF_3 acts as a fluorinating agent. In this reaction, CHF_3 undergoes complete decomposition (mineralisation) with the formation of solid metal fluorides, and gaseous CO and H_2O. Under specific conditions, *i.e.* excess of hydroxide and sufficiently long contact times, water-gas shift reaction is an important side process in which CO is firstly converted to CO_2, and finally to solid metal carbonate. In this case, fluorine and carbon from CHF_3 are mineralised in the form of metal fluorides and carbonates.

Basicity of the solids is the key factor that determines their reactivity towards CHF_3. Alkali hydroxides, the most reactive solids within this work, start to react with CHF_3 at temperatures that are 100–150 °C lower than those determined for their carbonate counterparts. Oxides investigated within this work show intermediate activity. Reactions of CHF_3 with reactive solids are therefore rationalised on the basis of acid-base interactions between the weakly acidic hydrogen in CHF_3 and the basic oxygen species in the solids. Although the exact CHF_3 decomposition mechanisms remain unclear, it is reasonable to conclude that the acid-base interactions play an important role in the initial binding of CHF_3 molecule to the solid reactant. In this way they enable or facilitate other decomposition processes that lead to a complete destruction of the CHF_3 molecule.

With the two technically most relevant hydroxides, KOH and NaOH, decomposition of CHF_3 can be effectively accomplished in the temperature range 150–200 °C, *i.e.* at temperatures that are approximately 1000 °C lower than those usually used for incineration. Decomposition of CHF_3 with KOH or NaOH under relatively mild conditions could therefore represent a convenient and technically non-demanding process for the destruction of smaller amounts of CHF_3 in situations where economics of the process is not of prime importance.

6 Acknowledgements

Author is grateful to Slovenian Research Agency (ARRS) for funding this work through the young researcher programme (Contract No. 1000-08-310004).

Author is also grateful to Asst. Prof. Srečo D. Škapin and Asst. Prof. Evgeny Goreshnik for XRD measurements, to Asst. Prof. Maja Ponikvar-Svet and Mira Župančič for chemical analyses, to Aleš Štefančič for catalytical tests, to Asst. Prof. Danjela Kuščer for SEM investigations, to dr. Arkadij Popovič for MS measurements and to Asst. Prof. Janez Kovač for XPS measurements.

7 References

[1] Meslans, M. M. Recherches sur quelques fluorures organiques de la série grasse. *Annales de Chimie et de Physique* **7**, 346–423 (1894).

[2] Ruff, O.; Luchsinger, W.; Miltschitsky, G. Vom Jodoform zum Fluoroform. *Berichte der Deutschen Chemischen Gesellscheft* **69**, 299–308 (1936).

[3] Henne, A. L. Fluoroform. *Journal of the American Chemical Society* **59**, 1200–1202 (1937).

[4] Zanardi, A.; Novikov, M. A.; Martin, E.; Benet-Buchholz, J.; Grushin, V. V. Direct Cupration of Fluoroform. *Journal of the American Chemical Society* **133**, 20901–20913 (2011).

[5] Tomashenko, O. A.; Grushin, V. V. Aromatic Trifluoromethylation with Metal Complexes. *Chemical Reviews* **111**, 4475–4521 (2011).

[6] Han, W.; Li, Y.; Tang, H.; Liu, H. Treatment of the potent greenhouse gas, CHF_3 – An overview. *Journal of Fluorine Chemistry* **140**, 7–16 (2012).

[7] Lide, D. R. *Handbook of Chemistry and Physics, 84th edition* (CRC Press, New York, 2003–2004).

[8] Nakamoto, K. *Infrared and Raman Spectra of Inorganic and Coordination Compounds, Part A, 5th edition* (John Wiley & Sons, New York, 1997).

[9] Solomon, S. et al. *Climate Change 2007: The Physical Science Basis. Contribution of Working Group I to the Fourth Assessment Report of the Intergovernmental Panel on Climate Change* (Cambridge University Press, Cambridge, 2007) http://www.ipcc.ch/publicationsanddata/ar4/wg1/en/ch2.html. (accessed December 2011).

[10] McCulloch, A.; Lindley, A. A. Global emissions of HFC-23 estimated to year 2015. *Atmospheric Environment* **41**, 1560–1566 (2007).

[11] Miller, B. R. et al. HFC-23 (CHF_3) emission trend response to HCFC-22 ($CHClF_2$) production and recent HFC-23 emission abatement measures. *Atmospheric Chemistry and Physics* **10**, 7875–7890 (2010).

[12] Sekiya, A.; Okamoto, S. Evaluation of carbon dioxide equivalent values for greenhouse gases: CEWN as a new indicator replacing GWP. *Journal of Fluorine Chemistry* **131**, 364–368 (2010).

[13] McCulloch, A. Fluorocarbons in the global environment: a review of the important interactions with atmospheric chemistry and physics. *Journal of Fluorine Chemistry* **123**, 21–29 (2003).

[14] McCulloch, A. CFC and Halon replacements in the environment. *Journal of Fluorine Chemistry* **100**, 163–173 (1999).

[15] Hine, J.; Dowell, A. M.; Singley, J. E. Carbon Dihalides as Intermediates in the Basic Hydrolysis of Haloforms. IV. Relative Reactivities of Haloforms. *Journal of the American Chemical Society* **78**, 479–482 (1956).

[16] Hine, J.; Burske, N. W. The Kinetics of the Base-catalyzed Deuterium Exchange of Dichlorofluoromethane in Aqueous Solution. *Journal of the American Chemical Society* **78**, 3337–3339 (1956).

[17] Hine, J.; Burske, N. W.; Hine, M.; Langford, P. B. The Relative Rates of Formation of Carbanions by Haloforms. *Journal of the American Chemical Society* **79**, 1406–1412 (1957).

[18] Hine, J.; Butterworth, R.; Langford, P. B. The Hydrolysis and Deuterium Exchange of Dibromofluoromethane and Fluorodiiodomethane. *Journal of the American Chemical Society* **80**, 819–824 (1958).

[19] Hine, J.; Langford, P. B. Methylene Derivatives as Intermediates in Polar Reactions. XIV. The Effect of pH on the Rate of Hydrolysis of Chloroform. *Journal of the American Chemical Society* **80**, 6010–6013 (1958).

[20] Hine, J.; Ehrenson, S. J. The Effect of Structure on the Relative Stability of Dihalomethylenes. *Journal of the American Chemical Society* **80**, 824–830 (1958).

[21] Hine, J.; Wiesboeck, R.; Ghirardelli, R. G. The Kinetics of the Base-catalyzed Deuterium Exchange of 2,2-Dihalo-1,1,1-trifluoroethanes. *Journal of the American Chemical Society* **83**, 1219–1222 (1961).

[22] Hine, J.; Ketley, A. D.; Tanabe, K. Methylene Derivatives as Intermediates in Polar Reactions. XIX. The Reaction of Potassium Isopropoxide with Chloroform, Bromoform and Dichlorofluoromethane. *Journal of the American Chemical Society* **82**, 1398–1401 (1960).

[23] Symons, E. A.; Clermont, M. J. Hydrogen isotope exchange between fluoroform (CF_3H) and water. 1. Catalysis by hydroxide ion. *Journal of the American Chemical Society* **103**, 3127–3130 (1981).

[24] Symons, E. A.; Clermont, M. J.; Coderre, L. A. Hydrogen isotope exchange between fluoroform (CF_3H) and water. 2. Catalysis by hydroxide ion in the presence of added dimethyl sulfoxide. *Journal of the American Chemical Society* **103**, 3131–3135 (1981).

[25] Tschuikow-Roux, E.; Marte, J. E. Thermal Decomposition of Fluoroform in a Single-Pulse Shock Tube. *Journal of Chemical Physics* **42**, 2049–2056 (1965).

[26] Olsen, D. A.; Osteraas, A. J. Difluorocarbene modification of polymer and fiber surfaces. *Journal of Applied Polymer Science* **13**, 1523–1535 (1969).

[27] Romelaer, R.; Kruger, V.; Baker, J. M.; Dolbier, W. R. Pyrolyses of Chlorodifluoromethane and Trifluoromethane in the Presence of Hydrogen. Mechanism and Optimization of Reaction Conditions. *Journal of the American Chemical Society* **123**, 6767–6772 (2001).

[28] Moon, D. J.; Chung, M. J.; Kim, H.; Kwon, Y. S.; Ahn, B. S. Pyrolysis of Trifluoromethane to Procedure hexafluoropropylene. *Industrial & Engineering Chemistry Research* **41**, 2895–2902 (2002).

[29] Yang, G.-C.; Lei, S.; Pan, R.-M.; Quan, H.-D. Investigation of CF_2 carbene on the surface of activated charcoal in the synthesis of trifluoromethane via vapor-phase catalytic reaction. *Journal of Fluorine Chemistry* **130**, 231–235 (2009).

[30] Han, W. et al. Catalytic pyrolysis of CHF_3 over activated carbon and activated carbon supported potassium catalyst. *Journal of Fluorine Chemistry* **131**, 698–703 (2010).

[31] Yu, H.; Kennedy, E. M.; Mackie, J. C.; Dlugogorski, B. Z. Studies of the Reaction of CHF_3 with methane. *Environmental Science & Technology* **40**, 5778–5785 (2006).

[32] Han, W. et al. Experimental and chemical kinetic study of the pyrolysis of trifluoromethane and the reaction of trifluoromethane with methane. *Journal of Fluorine Chemistry* **131**, 751–760 (2010).

[33] Han, W.; Kennedy, E. M.; Mackie, J. C.; Dlugogorski, B. Z. Conversion of a CFCs, HFCs and HCFCs waste mixture via reaction with methane. *Journal of Hazardous Materials* **184**, 696–703 (2010).

[34] Kemnitz, E.; Winfield, J. M. Fluoride Catalysts: Their Application to Heterogeneous Catalytic Fluorination and Related Processes. In: Nakajima T.; Žemva B.; Tressaud A. (Eds.) *Advanced Inorganic Fluorides: Synthesis, Characterization and Applications*. 367–401 (Elsevier Science S. A, Amsterdam, 2000).

[35] Bozorgzadeh, H.; Kemnitz, E.; Nickkho-Amiry, M.; Skapin, T.; Winfield, J. M. Catalytic reactions of chlorofluoroethanes at fluorinated alumina and chromia aerogels and xerogels. A comparison of reaction pathways in alumina- and chromia-based catalysts. *Journal of Fluorine Chemistry* **110**, 181–189 (2001).

[36] Skapin, T.; Kemnitz, E. Fluorinated γ-alumina aerogels and xerogels: characterization and catalytic behaviour. *Catalysis Letters* **40**, 241–247 (1996).

[37] Skapin, T. Preparation and Properties of Highly Fluorinated Alumina prepared from Boehmite Aerogels or Commercial γ-Al_2O_3. *Journal of Materials Chemistry* **5**, 1215–1222 (1995).

[38] McVicker, G. B.; Kim, C. J.; Eggert, J. J. Properties of Aluminium-Fluoride Catalysts Prepared by the Fluoridation of Aluminium Oxide with Trifluoromethane. *Journal of Catalysis* **80**, 315–327 (1983).

[39] Hegde, R. I.; Barteau, M. A. Preparation, Characterization, and Activity of Fluorinated Aluminas for Halogen Exchange. *Journal of Catalysis* **120**, 387–400 (1989).

[40] Bozorgzadeh, H.; Kemnitz, E.; Nickkho-Amiry, M.; Skapin, T.; Winfield, J. M. Dynamic behaviour of chlorofluoroethanes at fluorinated chromia aerogels and fluorinated zinc(II) or magnesium(II) doped chromia aerogels. *Journal of Fluorine Chemistry* **121**, 83–92 (2003).

[41] Skapin, T. et al. Aluminium(III) fluoride originating from decomposition of hydrazinium fluoroaluminate(III) under oxidative conditions: Syntheses, X-ray photoelectron spectroscopy and some catalytic reactions. *Journal of Fluorine Chemistry* **132**, 703–712 (2011).

[42] El-Bahy, Z. M.; Ohnishi, R.; Ichikawa, M. Hydrolytic decompositions of CF_4 over alumina-based binary metal oxide catalysts: high catalytic activity of Gallia-alumina catalyst. *Catalysis Today* **90**, 283–290 (2004).

[43] El-Bahy, Z. M.; Ohnishi, R.; Ichikawa, M. Hydrolysis of CF_4 over alumina-based binary metal oxide catalysts. *Applied Catalysis B-Environmental* **40**, 81–91 (2003).

[44] Areán, C. O.; Bellan, A. L.; Mentruit, M. P.; Delgado, M. R.; Palomino, G. T. Preparation and characterization of mesoporous γ-Ga_2O_3. *Microporous and Mesoporous Materials* **40**, 35–42 (2000).

[45] Vimont, A. et al. Infrared Spectroscopic Study on the Surface Properties of γ-Gallium Oxide as Compared to Those of γ-Alumina. *Journal of Physical Chemistry B* **109**, 9656–9664 (2005).

[46] Haneda, M.; Kintaichi, Y.; Mizushima, T.; Kakuta, N.; Hamada, H. Structure of Ga_2O_3-Al_2O_3 perpared by sol-gel method and its catalytic performance for NO reduction by propene in the presence of oxygen. *Applied Catalysis B-Environmental* **31**, 81–92 (2001).

[47] Nakatani, T. et al. Characterization of γ-Ga_2O_3-Al_2O_3 Prepared by Solvothermal Method and Its Performance for Methane-SCR of NO. *Journal of Physical Chemistry A* **113**, 7021–7029 (2009).

[48] Takahashi, M.; Inoue, N.; Takeguchi, T.; Iwamoto, S.; Inoue, M. Synthesis of γ-Ga_2O_3-Al_2O_3 Solid Solutions by the Glycothermal Method. *Journal of the American Ceramic Society* **89**, 2158–2166 (2006).

[49] Shimizu, K. –I. et al. Alumina-Supported Gallium Oxide Catalysts for NO Selective Reduction: Influence of the Local Structure of Surface Gallium Oxide Species on the Catalytic Activity. *Journal of Physical Chemistry B* **103**, 1542–1549 (1999).

[50] Chen, M. et al. Dehydrogenation of propane over spinel-type gallia-alumina solid solution catalysts. *Journal of Catalysis* **256**, 293–300 (2008).

[51] Olorunyolemi, T.; Kydd, R. A. Gallium-Aluminium Mixed Oxides as Supports for Ni-Mo Catalysts: Characterization and Reactivity for Cumene Cracking and Thiophene HDS Reactions. *Journal of Catalysis* **158**, 583–586 (1996).

[52] Olorunyolemi, T.; Kydd, R. A. The effect of fluoride addition on the catalytic activity of gallium-aluminium mixed oxides and Ni-Mo supported on them. *Catalysis Letters* **63**, 173–178 (1999).

[53] McCulloch, A. Incineration of HFC-23 Waste Streams for Abatement of Emissions from HCFC-22 Production: A Review of Scientific, Technical and Economic Aspects, Prepared for UNFCCC. http://cdm.unfccc.int/methodologies/Background240305.pdf. (accessed December 2011).

[54] Feaver, W. B.; Rossin, J. A. The catalytic decomposition of CHF_3 over ZrO_2-SO_4. *Catalysis Today* **54**, 13–22 (1999).

[55] Onoda, H.; Ohta, T.; Tamaki, J.; Kojima, K. Decomposition of trifluoromethane over nickel pyrophosphate catalysts containing metal cation. *Applied Catalysis A-General* **288**, 98–103 (2005).

[56] Burdeniuc, J.; Crabtree, R. H. Mineralization of Chlorofluorocarbons and Aromatization of Saturated Fluorocarbons by a Convenient Thermal Process. *Science* **271**, 340–341 (1996).

[57] Bourlinos, A. B. et al. Reaction of graphite fluoride with NaOH–KOH eutectic. *Journal of Fluorine Chemistry* **129**, 720–724 (2008).

[58] Baxter, P. J.; Garton, K. ; Kharasch, E. D. Mechanistic Aspects of Carbon Monoxide Formation from Volatile Anesthetics. *Anesthesiology* **89**, 929–941 (1998).

[59] Reutov, O. A.; Butin, K. P.; Beletskaya, I. P. *CH-kysloty* (Nauka, Moscow, 1980).

[60] Reutov, O. A.; Butin, K. P.; Beletskaya, I. P. Ravnovestnaya Kislotnost CH-svyazej v Organicheskih Soedineniyah. *Uspekhi Khimii* **43**, 35–63 (1974).

[61] Andreades, S. Fluorocarbanions. Rates of Base-Catalyzed Hydrogen-Deuterium Exchange, Isotope Effects, and Acidity of Monohydrofluorocarbons. *Journal of the American Chemical Society* **86**, 2003–2010 (1964).

[62] Hine, J. *Physical Organic Chemistry* (McGraw-Hill, New York, 1962).

[63] Hill, V. G.; Roy, R.; Osborn, E. F. The system Alumina-Gallia-Water. *Journal of the American Ceramic Society* **35**, 135–142 (1952).

[64] Escribano, V. S. et al. Solid state characterization of coprecipitated alumina-gallia mixed oxide powders. *Journal of Materials Science* **40**, 2013–2021 (2005).

[65] Roy, R.; Hill, V. G.; Osborn, E. F. Polymorphism of Ga_2O_3 and the system Ga_2O_3-H_2O. *Journal of the American Chemical Society* **74**, 719–722 (1952).

[66] Ponikvar, M.; Sedej, B.; Pihlar, B.; Žemva, B. Determination of fluoride in $M(SbF_6)_x$ compounds. *Analitica Chimica Acta* **418**, 113–118 (2000).

[67] Liebman, J. F.; Ponikvar, M. Ion Selective Electrode Determination of Free Versus Total Fluoride Ion in Simple and Fluoroligand Coordinated Hexafluoropnictate (PnF_6 −, Pn = P, As, Sb, Bi) Salts. *Structural Chemistry* **16**, 521–528 (2005).

[68] Hess, A.; Kemnitz, E. Characterization of catalytically Active Sites on Aluminium Oxides, Hydroxyfluorides, and Fluorides in correlation with Their Catalytic Behaviour. *Journal of Catalysis* **149**, 449–457 (1994).

[69] Pejov, L.; Skapin, T. Adsorption of pyridine on the Lewis acid sites of microcrystalline γ-alumina: a quantum chemical cluster model study. *Chemical Physics Letters* **400**, 453–461 (2004).

[70] Nastova, I.; Skapin, T.; Pejov, L. Effect of partial fluorination on the Lewis sites of

microcrystalline γ-alumina studied by adsorption of pyridine as a probe molecule: A quantum chemical cluster model study. *Surface Science* **605**, 1525–1536 (2011).

[71] Bozorgzadeh, H.; Kemnitz, E.; Nickkho-Amiry, M.; Skapin, T.; Winfield, J. M. Conversion of 1,1,2-trichlorotrifluoroethane to 1,1,1-trichlorotrifluoroethane and 1,1-dichlorotetrafluoroethane over aluminium-based catalysts. *Journal of Fluorine Chemistry* **107**, 45–52 (2001).

[72] Lavalley, J. C. et al. Unexpected similarities between the surface chemistry of cubic and hexagonal gallia polymorphs. *Physical Chemistry Chemical Physics* **5**, 1301–1305 (2003).

[73] Areán, C. O.; Delgado, M. R.; Montouillout, V.; Massiot, D. Synthesis and Characterization of Spinel-Type Gallia-Alumina Solid Solutions. *Zeitschrieft für Anorganische und Allgemeine Chemie* **631**, 2121–2126 (2005).

[74] JCPDS PDF-files: 41-0381, 18-0024 and 4-0196.

[75] König, R.; Scholz, G.; Bertram, R.; Kemnitz, E. Crystalline aluminium hydroxyl fluorides-Suitable reference compounds for ^{19}F chemical shift trend analysis of related amorphous solids. *Journal of Fluorine Chemistry* **129**, 598–606 (2008).

[76] Hajime, E. K. L. Y.; Delattre, J. L.; Stacy, A. M. Temperature-Dependent Halogen-Exchange Activity Studies of Zeolite-derived Aluminium Trifluoride. *Chemistry of Materials* **19**, 894–902 (2007).

[77] Skapin, T.; Tavčar, G.; Benčan, A.; Mazej, Z. Recent developments in the preparation of high surface area metal fluorides. *Journal of Fluorine Chemistry* **130**, 1086–1092 (2009).

[78] Makarowicz, A. et al. Electronic structure of Lewis acid sites on high surface area aluminium fluorides: a combined XPS and ab initio investigation. *Physical Chemistry Chemical Physics* **11**, 5664–5673 (2009).

[79] Bailey, C. L.; Mukhopadhyay, S.; Wander, A.; Searle, B. G.; Harrison, N. M. Structure and Stability of α-AlF_3 Surfaces. *Journal of Physical Chemistry C* **113**, 4976–4983 (2009).

[80] Francke, L. et al. Synthesis and characterization of Al^{3+}, Cr^{3+}, Fe^{3+} and Ga^{3+} hydroxyfluorides: correlations between structural features, thermal stability and acidic properties. *Journal of Materials Chemistry* **13**, 2330–2340 (2003).

[81] Krahl, T.; Vimont, A.; Eltanany, G.; Daturi, M.; Kemnitz, E. Determination of the Acidity of High Surface AlF_3 by IR Spectroscopy of Adsorbed CO Probe Molecules. *Journal of Physical Chemistry C* **111**, 18317–18325 (2007).

[82] Zhang, W.; Sun, M.; Prins, R. Multinuclear MAS NMR Identefication of Fluorine Species on the Surface of Fluorinated γ-Alumina. *Journal of Physical Chemistry B* **106**, 11805–11809 (2002).

[83] Petre, A. L.; Auroux, A.; Gélin, P.; Caldararu, M.; Ionescu, N. I. Acid-base properties of supported gallium oxide catalysts. *Thermochimica Acta* **379**, 177–185 (2001).

[84] Michorczyk, P.; Sikora, E.; Ogonowski, J. Study of the acid-base properties of Ga_2O_3/Al_2O_3 by using test reactions. *Reaction Kinetics and Catalysis Letters* **94**, 243–252 (2008).

[85] Farber, M.; Frisch, M. A.; Ko, C. H. Thermodynamic properties of CF and CF_2 from molecular flow effusion and mass spectrometer investigations. *Transactions of the Faraday Society* **65**, 3202–3209 (1969).

[86] Morterra, C.; Magnacca, G. A case study: surface chemistry and surface structure of catalytic aluminas, as studied by vibrational spectroscopy of adsorbed species. *Catalysis Today* **27**, 497–532 (1996).

[87] Winfield, J. M. Investigating acidity of metal fluoride surfaces by spectroscopic and chemical methods. *Journal of Fluorine Chemistry* **130**, 1069–1079 (2009).

[88] Pushkar, Yu. N.; Sinitsky, A.; Parenago, O. O.; Kharlanov, A. N.; Lunina, E.V. Structure and Lewis acid properties of gallia-alumina catalysts. *Applied Surface Science* **167**, 69–78 (2000).

[89] Tanabe, K.; Sumiyoshi, T.; Shibata, K.; Kiyoura, T.; Kitagawa, J. A New Hypothesis Regarding the Surface Acidity of Binary Metal Oxides. *Bulletin of the Chemical Society of Japan* **47**, 1064–1066 (1974).

[90] Busca, G. The surface acidity of solid oxides and its characterization by IR spectroscopic methods. An attempt at systematization. *Physical Chemistry Chemical Physics* **1**, 723–736 (1999).

[91] a) Sohlberg, K.; Pennycook, S. J.; Pantelides, S. T. Explanation of the Observed Dearth of Three-Coordinated Al on γ-Alumina Surfaces. *Journal of the American Chemical Society* **121**, 10999–11001 (1999); b) Sohlberg, K.; Pantelides, S. T.; Pennycook, S. J. Surface Reconstruction and the Difference in Surface Acidity between γ- and η-Alumina. *Journal of the American Chemical Society* **123**, 26–29 (2001).

[92] Boese, O.; Unger, W. E. S.; Kemnitz, E.; Schroeder, S. L. M. Active sites on an oxide catalyst for F/Cl-exchange reactions: X-ray spectroscopy of fluorinated γ-Al_2O_3. *Physical Chemistry Chemical Physics* **4**, 2824–2832 (2002).

[93] Dambournet, D. et al. The use of multiple probe molecules for the study of the acid-base properties of aluminium hydroxyfluoride having the hexagonal tungsten bronze structure: FTIR and [^{36}Cl] radiotracer studies. *Physical Chemistry Chemical Physics* **11**, 1369–1379 (2009).

[94] Vimont, A. et al. Infrared Study of the Surface Properties of HTB-Type Al-, Cr-, Fe-Hydroxyfluorides. *Journal of Physical Chemistry B* **108**, 3246–3255 (2004).

[95] Kemnitz, E.; Zhu, Y.; Adamczyk, B. Enhanced Lewis acidity by aliovalent cation doping in metal fluorides. *Journal of Fluorine Chemistry* **114**, 163–170 (2002).

[96] Moulder, J. F.; Stickle, W. F.; Sobol, P. E.; Bomben, K. D. *Handbook of X-Ray Photoelectron Spectroscopy* (Physical Electronics Inc., Minnesota, 1995).

[97] a) Serykh, A. I.; Amiridis, M. D. *Surface Science* **603**, 2037–2041 (2009); b) Serykh, A. I.; Amiridis, M. D. In-situ X-ray photoelectron spectroscopy study of supported

gallium oxide. *Surface Science* **604**, 1002–1005 (2010).

[98] Murthy, J. K.; Groß, U.; Rüdiger, S.; Ünveren, E.; Kemnitz, E. *Journal of Fluorine Chemistry* **125**, 937–949 (2004).

[99] Murthy, J. K. et al. Aluminium Chloride as a Solid is not a Strong Lewis Acid. *Journal of Physical Chemistry B* **110**, 8314–8319 (2006).

[100] Nickkho-Amiry, M.; Winfield, J. M. Investigation of fluorinated surfaces by means of radio-labelled probe molecules. *Journal of Fluorine Chemistry* **128**, 344–352 (2007).

[101] Inui, T.; Funabiki, M.; Takegami, Y. Simultaneous Methanation of CO and CO_2 on Supported Ni-Based Composite Catalysts. *Industrial & Engineering Chemistry Production Research and Development* **19**, 385–388 (1980).

[102] Sehested, J.; Dahl, S.; Jacobsen, J.; Rostrup-Nielsen, J. R. Methanation of CO over Nickel: Mechanism and Kinetics at High H_2/CO Ratios. *Journal of Physical Chemistry B* **109**, 2432–2438 (2005).

[103] Kirgintsev, A. N.; Trushnikova, L. N.; Lavrent'eva, V. G. *Rastvorimost neorganicheskih veshchestv v vode* (Izd. Khimiya, Leningrad, 1972).

[104] Han, W.; Kennedy, E. M.; Mackie, J. C.; Dlugogorski, B. Z. Mechanistic study of the reaction of CHF_3 with CH_4. *Chemical Engineering Journal* **166**, 822–831 (2011).

[105] Burgess, Jr. D. R.; Zachariah, M. R.; Tsang, W.; Westmoreland, P. R. Thermochemical and chemical kinetic data for fluorinated hydrocarbons. *Progress in Energy and Combustion Science* **21**, 453–529 (1996).

[106] Yang, G.-C.; Jia, X.-Q.; Pan, R.-M.; Quan, H.-D. The disproportionation of CF_2 carbene in vapor-phase pyrolysis reaction over activated carbon and porous aluminium fluoride. *Journal of Molecular Catalysis A-Chemical* **309**, 184–188 (2009).

[107] Han, W.; Yu H.; Kennedy, E. M.; Mackie, J. C.; Dlugogorski, B. Z. Conversion of CHF_3 to CH_2=CF_2 via Reaction with CH_4 and $CaBr_2$. *Environmental Science & Technology* **42**, 5795–5799 (2008).

[108] Ma, N. L.; Lau, K.-C.; Chien, S.-H.; Li, W.-K. Thermochemistry of hydrochlorofluoromethanes revisited: a theoretical study with the Gaussian-3 (G3) procedure. *Chemical Physics Letters* **311**, 275–280 (1999).

[109] Huber, S.; Knözinger, H. Adsorption of CH-acids on magnesia. An FTIR-spectroscopic study. *Journal of Molecular Catalysis A-Chemical* **141**, 117–127 (1999).

[110] Bosch, E.; Huber, S.; Weitkamp, J.; Knözinger, H. Adsorption of trichloro- and trifluoromethane in Y-zeolites as studied by IR spectroscopy and multinuclear solid-state NMR. *Physical Chemistry Chemical Physics* **1**, 579–584 (1999).

[111] Busca, G. Bases and Basic Materials in Chemical and Environmental Processes. Liquid versus Solid Basicity. *Chemical Reviews* **110**, 2217–2249 (2010).

[112] Greenwood, N. N.; Earnshaw, A. *Chemistry of the Elements, 2nd Edition* (Butterworth-Heinemann, Oxford, 1997).

[113] Pearson, R. G. Chemical hardness and density functional theory. *Journal of Chemical Sciences* **117**, 369–377 (2005).

[114] Crystallography Open Database. http://www.crystallography.net/search.html (accessed August 2012).

Index of Figures and Schemes

Figure 1: *Schematic representation of the symmetry (C_{3v}) of the CHF_3 molecule (a view along the third order axis).* 4
Figure 2: *Transmittance FTIR spectrum of gaseous CHF_3.* 5
Figure 3: *Scheme of the flow reactor combined with the FTIR monitoring of the effluent gases.* 13
Figure 4: *Batch reactor.* 14
Figure 5: *Static gas IR cell.* 16
Figure 6: *Gas flow IR cell.* 16
Figure 7: *Scheme of the applied mass spectrometer.* 18
Figure 8: *Representative powder diffractograms (offset) for mixed oxide precursors and products of fluorination with CHF_3 at 350 °C.* 25
Figure 9: *SEM images of oxide precursor Al/Ga-2 (A), and its fluorinated product Al/Ga-2-F (B).* 27
Figure 10: *H_2O and HF evolution profiles obtained with a temperature programmed heating of Al/Ga-100-F in a flow of N_2.* 28
Figure 11: *Temperature programmed reaction of single and mixed oxides with CHF_3 under flow conditions.* 30
Figure 12: *Typical CO-evolution profile for the reaction of oxide precursors with CHF_3 under flow conditions.* 32
Figure 13: *Evolution of CF_4 and CO during the fluorination of the γ-Al_2O_3 xerogel with CHF_3 at 500 °C in the flow reactor.* 32
Figure 14: *Evolution of CF_4 and CO during the fluorination of the γ-Al_2O_3 xerogel with CHF_3 at 550 °C in the flow reactor.* 33
Figure 15: *Normalized PAS-py absorbance spectra (offset) of oxide precursors (A) and products after fluorination with CHF_3 at 350 °C (B).* 36
Figure 16: *Normalized PAS-py absorbance spectra (offset) of representative mixed oxide precursors.* 37
Figure 17: *Normalized PAS-py absorbance spectra (offset) of representative mixed oxides fluorinated with CHF_3 at 350 °C.* 37
Figure 18: *XPS spectra of Ga 2p (a), Ga 3d (b), O 1s (c) and F 1s (d) for γ-Ga_2O_3 (Ga#0) and its fluorinated product (Ga#04-F).* 42
Figure 19: *XPS spectra of Ga 2p (a), Ga 3d (b), O 1s (c), F 1s (d) and Al 2p (e) for mixed oxide (Al/Ga-1) and its fluorinated product (Al/Ga-1-F).* 43
Figure 20: *Normalised PA-FTIR absorbance spectra of oxide precursors (A) and freshly fluorinated γ-Al_2O_3/γ-Ga_2O_3 xerogels (B).* 45
Figure 21: *Normalised PA-FTIR absorbance spectra of Al/Ga-100-F.* 46
Figure 22: *X-ray powder diffractograms of NaOH after reaction with CHF_3.* 52

Figure 23: *X-ray powder diffractogram of a large excess of NaOH after reaction with CHF_3.* 53
Figure 24: *X-ray powder diffractograms of LiOH and KOH after reaction with CHF_3 in a batch reactor at 250 °C.* 53
Figure 25: *SEM images of NaOH before and after reaction with CHF_3.* 56
Figure 26: *SEM images of K_2CO_3 before and after reaction with CHF_3.* 57
Figure 27: *Part of mass spectrum of the gas phase from the reaction between NaOD and CHF_3 at 250 °C in batch reactor confirming the presence of H_2O, HDO and D_2O.* 58
Figure 28: *CO-evolution profiles (offset) from temperature programmed experiments in the flow reactor.* 63

Scheme 1: *Resonance structures of the haloform radicals* (X = Cl, Br or I). 10
Scheme 2: *Schematic representation of the main reaction between NaOH and CHF_3 (top line) and the possible side reactions leading to the formation of CO_2/H_2, Na_2CO_3 and CH_4 (marked with dashed/dotted lines).* 60
Scheme 3: *Possible initial contacts between the CHF_3 molecule and M–OH surfaces.* 67
Scheme 4: *Proposed CHF_3 decomposition steps on NaOH.* 68

Scheme A-1: *Possible structures of pyridine adsorbed on the surface of γ-Al_2O_3.* 99

Index of Tables

Table 1: *Denomination and properties of single and mixed oxide precursors, and corresponding fluorinated products after treatment with CHF_3.* 23
Table 2: *Surface concentration (in at.%) determined by XPS for the analysed oxide precursors and fluorinated products* 41
Table 3: *Reaction of CCl_2FCClF_2 in contact with fluorinated single and representative mixed oxides under steady flow conditions* 48
Table 4: *Reaction conditions and composition of products for the interaction of CHF_3 with different solid reactants* 51
Table 5: *Composition of gas mixtures obtained in the reaction of CHF_3 with NaOH in the batch reactor at different temperatures* 58
Table 6: *Interaction of different halocarbons with NaOH in the batch reactor at 250 °C* 60
Table 7: *Interaction of CHF_3 with NaOH in the flow reactor* 61
Table 8: *Temperature programmed flow tests with alkali hydroxides and carbonates performed from room temperature to the indicated upper temperature* 62

Table A-1: *Selected physical properties of CHF_3* 90
Table A-2: *Calibration of the static gas IR cell with CHF_3* 92
Table A-3: *Calibration of the static gas IR cell with CO* 93
Table A-4: *Calibration of the static gas IR cell with CH_4* 93
Table A-5: *V_s/V_p ratios for the conversion of relevant oxides and hydroxides to the corresponding fluorides* 94
Table A-6: *Crystal structure data for alkali hydroxides.* 95
Table A-7: *Crystal structure data for alkali fluorides.* 95
Table A-8: *Crystal structure data for alkali carbonates.* 95
Table A-9: *Arrhenius parameters of some relevant decomposition processes involving different HFCs.* 96
Table A-10: *pK_a values for different fluorocarbons* 97
Table A-11: *Assignation of the main bands in the IR spectrum of pyridine adsorbed on the surface of γ-Al_2O_3* 98

Appendices

Appendix I

Table A-1: *Selected physical properties of CHF_3 [7]*

Property	**Value**
Molecular mass, M_r	70.01 g mol^{-1}
Density of liquid CHF_3 (@ 25 ºC), ρ	0.673 g cm^{-3}
Boiling point	–82.1 ºC
Melting point	–155.2 ºC
Critical temperature, T_C	25.83 ºC
Critical pressure, P_C	4.82 MPa
Dipole moment, D	1.65 C m
pK_a	26÷28
Enthalpy of burning, $\Delta_{fus}H^{118}$	4.06 kJ mol^{-1}
Enthalpy of formation, $\Delta_f H^0$	–695.4 kJ mol^{-1}
Entropy, S^0	259.7 J mol^{-1}
Heat capacity, C_p	51.069 J K^{-1} mol^{-1}
Van der Waals, **a**	5.378 bar L^2 mol^{-2}
Van der Waals, **b**	0.0640 L mol^{-1}
Molar volume, V_c	133 cm^3 mol^{-1}
Bond strength H–CF_3	449.5 kJ mol^{-1}
Dielectric constant, ε^{294}	5.2

Appendix II

Calibration of the static gas cell: Static gas cell (see Figure 5) was calibrated with different pressures of CHF_3, CO and CH_4. In all cases whole FTIR spectra were recorded in the region from 4400 to 350 cm^{-1}. Calibration was performed with lines characteristic for each compound. From the recorded spectra, extinction coefficient, $\varepsilon_{\bar{\nu}}$, at the compound-specific wavenumber, $\bar{\nu}$, was calculated using the formula (F-1) where T is transmittance, C is concentration and l is width of absorption layer.

$$\varepsilon_{\bar{\nu}} = -\frac{\ln(T/100\%)}{C \cdot l} \tag{F-1}$$

Calibration of the static gas cell with CHF_3: Corresponding calibration data are presented in Table A-2. Calibration was done with the line at 2519 cm^{-1}; average value of ε_{2519} for CHF_3 was 0.55 m^2 mol^{-1}. The following pressure-transmittance dependence for CHF_3 was obtained:

$$P_{CHF_3} = -t_1 \cdot \ln\left[\left(T - y_0\right)\Big/ A_1\right] \tag{F-2}$$

where t_1 is (3928.4 ± 115.1), A_1 is (91.73 ± 1.83), y_0 is (7.9 ± 1.9).

Calibration of the static gas cell with CO: Corresponding calibration data are presented in Table A-3. Calibration was done with the line at 2120 cm^{-1}; average value of ε_{2120} for CHF_3 was 2.4 m^2 mol^{-1}. The following pressure-transmittance dependence for CO was obtained:

$$P_{CO} = -t_1 \cdot \ln\left[\left(T - y_0\right)\Big/ A_1\right] \tag{F-3}$$

where t_1 is (931.78 ± 9.33), A_1 is (103.03 ± 0.75), y_0 is 0.

Calibration of the static gas cell with CH_4: Corresponding calibration data are presented in Table A-4. Calibration was done with the line at 2958 cm^{-1}; average value of ε_{2958} for CHF_3 was 5.0 m^2 mol^{-1}. The following pressure-transmittance dependence for CH_4 was obtained:

$$P_{CH_4} = -t_1 \cdot \ln\left[\left(T - y_0\right)\Big/ A_1\right] \tag{F-4}$$

where t_1 is (179.54 ± 22.35), A_1 is (48.07 ± 1.62), y_0 is (52.45 ± 2.61).

Corresponding concentrations of CHF_3, CO and CH_4 formed in the static reactor were calculated by using these formulae and are presented in Tables 4 and 5.

Table A-2: *Calibration of the static gas IR cell with CHF_3*

$P(CHF_3)$, kPa	**$C(CHF_3)$, mol m^{-3}**	**T_{2519}, %**	**ε_{2519}, m^2 mol^{-1}**
0	0	-	-
13	5	97.50	0.63
27	11	95.07	0.58
40	16	92.64	0.60
53	22	90.73	0.55
67	27	88.42	0.57
80	33	86.72	0.54
93	38	84.68	0.55
107	43	82.98	0.54
120	49	80.87	0.54
133	54	78.95	0.55
147	60	76.94	0.55
160	65	75.67	0.54
173	70	74.10	0.54
187	76	72.34	0.53
200	81	70.33	0.54
213	87	68.89	0.54
227	92	67.29	0.54
240	98	65.92	0.53
253	103	64.66	0.53
267	108	62.85	0.54
280	114	61.50	0.53
293	119	60.26	0.53
307	125	58.78	0.53
320	130	57.72	0.53
333	135	56.49	0.53
347	141	55.21	0.53
360	146	54.22	0.52

Table A-3: *Calibration of the static gas IR cell with CO*

$P(CHF_3)$, kPa	$C(CHF_3)$, mol m^{-3}	T_{2120}, %	ε_{2120}, m^2 mol^{-1}
0	0	-	-
13	5.4	91.3	2.1
27	11	82.6	2.2
40	16	73.6	2.4
53	22	67.6	2.2
67	27	60.8	2.3
80	33	55.4	2.2
93	38	49.5	2.3
107	43	44.6	2.4
120	49	40.3	2.3
133	54	35.9	2.4
147	60	32.3	2.4
160	65	28.6	2.4
173	70	25.4	2.5
187	76	23.1	2.4
200	81	20.5	2.5
213	87	18.0	2.5
227	92	18.2	2.3
240	98	14.5	2.5
253	103	12.8	2.5
267	108	11.3	2.5
280	114	9.90	2.5
293	119	8.61	2.6
307	125	7.50	2.6
320	130	6.60	2.6
333	136	5.64	2.6
347	141	4.79	2.7
360	146	4.14	2.7

Table A-4: *Calibration of the static gas IR cell with CH_4*

$P(CH_4)$, kPa	$C(CH_4)$, mol m^{-3}	T_{2958}, %	ε_{2958}, m^2 mol^{-1}
8	3	87.00	5.8
13	5.3	79.66	5.4
20	8.1	73.48	4.8
28	11	67.53	4.5
33	13	64.25	4.3

Appendix III

1) Changes in molar volumes for the conversion of some metal oxides and hydroxides to the corresponding fluorides:

Table A-5 contains the calculated V_s/V_p ratios (where V_s is a molar volume of the starting oxides/hydroxides and V_p is a molar volume of the fluoride; corresponding stoichiometries are taken into consideration). V_s/V_p ratios allow the estimation of the permeabilities of the formed fluoride layers. For example, if $V_s/V_p<1$ the layer is expected to be dense; *i.e.* impermeable to gaseous reactants/products while for $V_s/V_p>1$ the layer is expected to be less compact with higher permeability for gaseous reactants/products.

Table A-5: *V_s/V_p ratios for the conversion of relevant oxides and hydroxides to the corresponding fluorides [7]*

Compound		Density of hydroxide/ oxide, g cm^{-3}	Density of fluoride, g cm^{-3}	Molar mass of hydroxide/oxide, g mol^{-1}	Molar mass of fluoride, g mol^{-1}	V_s/V_p
Al_2O_3	AlF_3	3.97	3.10	101.961	83.977	0.47
Ga_2O_3	GaF_3	~6.00	4.47	187.444	126.718	0.55
LiOH	LiF	1.45	2.640	23.95	25.939	1.68
NaOH	NaF	2.13	2.78	39.993	41.989	1.24
KOH	KF	2.044	2.48	56.106	58.097	1.17
RbOH	RbF	3.2	3.2	102.475	104.466	0.98
CsOH	CsF	3.68	4.64	149.912	151.90	1.24
$Mg(OH)_2$	MgF_2	2.37	3.148	58.320	62.302	1.24
$Ca(OH)_2$	CaF_2	~2.2	3.18	74.093	78.07	1.37
$Sr(OH)_2$	SrF_2	3.625	4.24	121.63	125.62	1.13
$Ba(OH)_2$	BaF_2	4.5	4.893	171.34	175.34	1.06

2) Basic crystallographic information: In Tables A-6, A-7 and A-8 basic crystallographic information for the relevant alkali fluorides, hydroxides and carbonates are summarised.

Table A-6: *Crystal structure data for alkali hydroxides [114].*

Name	**LiOH**	**NaOH**	**KOH**
Space group	$P4/nmm$	$Cmcm$	$Fm\bar{3}m$
Coordination number of cation	4	5	6
Cation radius (C.N. = 6), Å	0.60	0.95	1.33
Type of structure	Layers of tetrahedra, $(LiOH)_n$	Layers of tetragonal pyramids, $(NaOH)_n$	NaCl type

Table A-7: *Crystal structure data for alkali fluorides [114].*

Name	**LiF**	**NaF**	**KF**
Space group		$Fm\bar{3}m$	
Coordination number of cation		6, octahedral	
Cation radius (C.N. = 6), Å	0.60	0.95	1.33
Type of structure		Ionic, NaCl type of packaging	

Table A-8: *Crystal structure data for alkali carbonates [114].*

Name	**Li_2CO_3**	**Na_2CO_3**	**K_2CO_3**
Space group	$C2/c$	$C2/m$	$P2_1/c$
Coordination number of cation	4	6	6
Cation radius (C.N. = 6), Å	0.60	0.95	1.33
Type of structure	Covalent 3-D network	Layered packaging of anions and cations	Potassium carbonate 3-D network

Appendix IV

1) Arrhenius parameters for some decomposition and other reactions: In Table A-9, Arrhenius parameters for some relevant reactions with HFCs or HF are summarized. Parameters demonstrate the ability of HFCs to form HF at higher temperatures.

Table A-9: *Arrhenius parameters of some relevant decomposition processes involving different HFCs [105].*

Reaction	A^*	b^*	$E\,R^{-1*}$
$CHF_3 + M \rightarrow CF_2 + HF + M$	$2.39 \cdot 10^{30}$	–4.00	34.751
$HF + M \rightarrow H + F + M$	$3.12 \cdot 10^{13}$	0.00	49.985
$CH_3–CH_2F \rightarrow C_2H_4 + HF$	$2.63 \cdot 10^{13}$	0.00	30.146
$CH_3–CHF_2 \rightarrow CH_2=CHF + HF$	$7.94 \cdot 10^{13}$	0.00	31.152
$CH_3–CF_3 \rightarrow CH_2=CF_2 + HF$	$1.00 \cdot 10^{14}$	0.00	34.575
$CH_2F–CH_2F \rightarrow CH_2=CHF + HF$	$2.50 \cdot 10^{13}$	0.00	31.656
$CH_2F–CHF_2 \rightarrow CHF=CHF + HF$	$1.26 \cdot 10^{14}$	0.00	34.776

* - $k = A\,T^{b} \cdot exp(-ER^{-1}T^{-1})$, A prefactor (mol cm^3 s^{-1}), b temperature dependence (dimensionless) and $E\,R^{-1}$ activation energy (K).

2) pK_a values: In Table A-10, pK_a values for some representative HFCs and related compounds are given. Acidity correlates with the low-temperature activity of these compounds.

Table A-10: *pK_a values for different fluorocarbons [59, 60]*

Compound	pK_a
CF_3–H	26÷28
$(CF_3)_2CF$–H	22.5
$(CF_3)_2CH$–H	22.0
$(CF_3)_3C$–H	7.0
EtO_2C–CF_2–H	25.0
EtO_2C–CHF–H	21.0
EtO_2C–CFCl–H	18.0
EtO_2C–$CH(CF_3)$–H	16.0
EtO_2C–$CF(CF_3)$–H	14.0
EtO_2C–$C(CF_3)_2$–H	14.0
CF_2=CF–H	20.0
C_6F_5–H	23.0

Appendix V

Table A-11: *Assignation of the main bands in the IR spectrum of pyridine adsorbed on the surface of γ-Al_2O_3 [68–70]*

Band, cm^{-1}	Assignation	Probable structure (see Scheme A-1)
1261	Possibly N=O vibration of pyridine N-oxide	B,C
1435	19b pyridine, gaseous, 20 °C, (very strong)	-
1438	19b pyridine, liquid 20 °C, (very strong)	-
1445–1455	19b pyridine coordinately bonded to Lewis acid sites **LPy**	D
1449	19b pyridine, gaseous, 20 °C (very strong)	-
1482	19a pyridine, liquid, 20 °C (medium)	-
1492	19a pyridine, gaseous, 20 °C (weak)	-
1493	19a pyridine coordinately bonded to Lewis acid sites **LPy**	D
1450–1550	19b pyridine hydrogen bonded to quasi-Brønsted acid site **BPy**	A
1570	8b pyridine, gaseous and liquid, 20 °C (medium)	-
1578	8b pyridine coordinately bonded to Lewis acid sites **LPy**	D
1580	Possibly N–H deformation mode of $Py–H^+$	A
1581	8a pyridine, liquid, 20 °C (very strong)	-
1586	8a pyridine, gaseous, 20 °C (very strong)	-
1590	8a pyridine hydrogen bonded to quasi-Brønsted acid sites **BPy**	A
1595	8a pyridine coordinately bonded to octahedral aluminium Lewis acid sites (calcination temperatures > 377 ºC) **LPy**	D
1598	Pyridine, liquid, 20 °C, combination mode (medium)	-
1615	8a pyridine, coordinately bonded to Lewis acid sites of lower strength **LPy**, assigned them to tetrahedral aluminium vacancies	D
1620	8a pyridine coordinately bonded to Lewis acid sites of higher strength **LPy**, assigned them to tetrahedral aluminium vacancies	D
1634	Possibly pyridone C=O mode	-
1639	8a $Py–H^+$ pyridinium cation **BPy**	A
2450	Possibly N–H stretching vibration	A

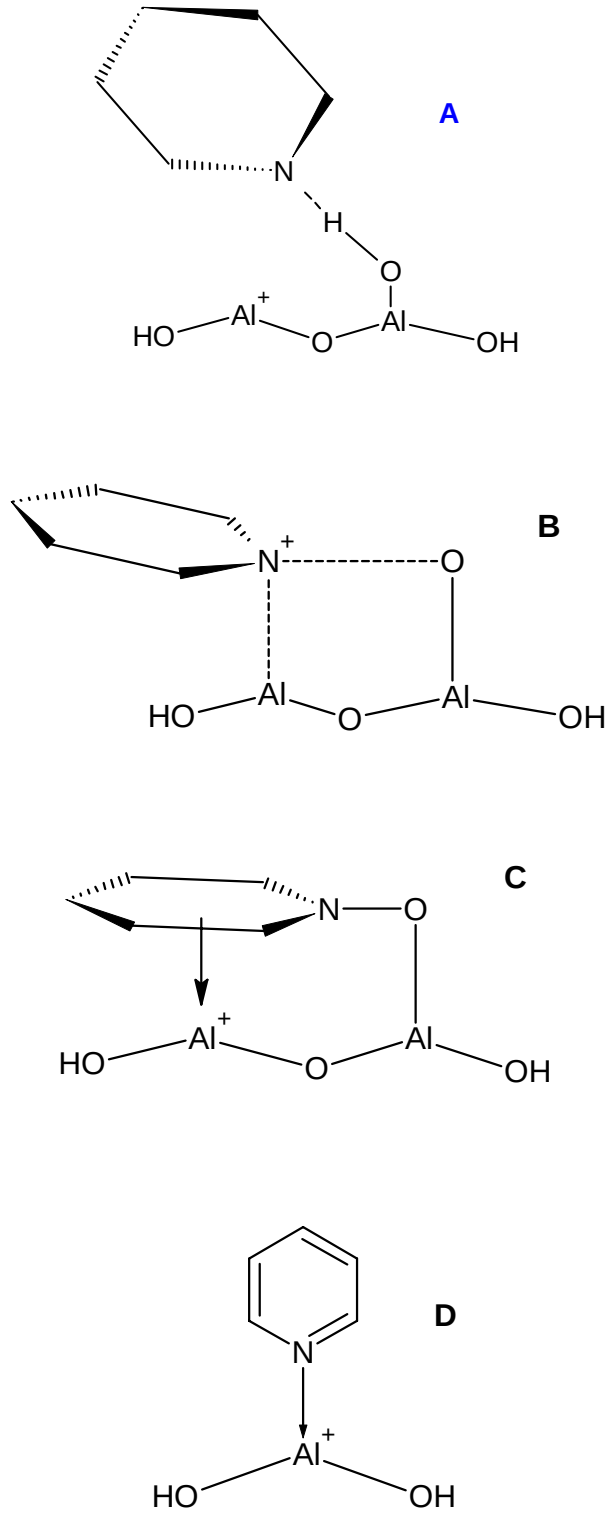

Scheme A-1: *Possible structures of pyridine adsorbed on the surface of γ-Al_2O_3*: A - pyN^+–H, B and C - pyridinium oxide, and D - σ-bonding to a Lewis acid site ($Al^{\delta+}$) [90].

Appendix VI

List of publications related to this dissertation:

1) Papers:

[1] Vakulka, A.; Tavčar, G.; Skapin, T. Interaction of trifluoromethane (CHF_3) with alkali hydroxides and carbonates, *Journal of Fluorine Chemistry* **142**, 52–59 (2012).

[2] Vakulka, A.; Kovač, J.; Tavčar, G; Skapin, T. Fluorination of mixed γ-alumina/γ-gallia xerogels with trifluoromethane: some effects on bulk and surface characteristics, *Acta Chimica Slovenica* (Accepted, August 2012).

2) Contributions at meetings:

[1] Vakulka, A.; Skapin, T. Preparation and characterization of alumina, gallia and alumina/gallia xerogels and their reaction with trifluoromethane, 4th Dan mladih raziskovalcev KMBO, Ljubljana, Slovenija, 11. 2. 2010.

[2] Vakulka, A.; Skapin, T. Al_2O_3-Ga_2O_3 xerogels: the surface acid-base effects of their fluorination with trifluoromethane, 16th ESFC – European Symposium on Fluorine Chemistry, Ljubljana, Slovenia, 18. 7. 2010.

[3] Vakulka, A.; Skapin, T. Mineralisation of trifluoromethane by sodium hydroxide, 5th Dan mladih raziskovalcev, Ljubljana, Slovenia, 17. 2. 2011.

[4] Vakulka, A.; Skapin, T. Acid-Base nature of the reaction between trifluoromethane and different hydroxides and carbonates, Slovenski kemijski dnevi 2011, Portorož, Slovenia 14. 9. 2011.

[5] Vakulka, A.; Skapin, T. Investigation of surface acidity of fluorinated and non-fluorinated alumina-gallia xerogels by pyridine adsorption, 6th Young Researcher's Day 2012, Ljubljana, Slovenia, 27. 2. 2012.

[6] Vakulka, A.; Skapin, T. Reactions of trifluoromethane with some reactive inorganic solids under moderate conditions, 20th International Symposium on Fluorine Chemistry 2012, Kyoto, Japan, 22. 7. 2012.